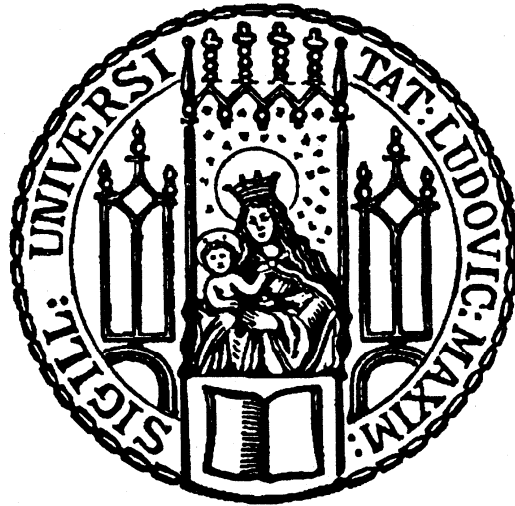


Functionalization of bacterial magnetic nanoparticles by genetic engineering and encapsulation with inorganic coatings



Dissertation zur Erlangung des Doktorgrades
der Fakultät für Biologie
der Ludwig-Maximilians-Universität München

vorgelegt von

Sarah Denise Borg

aus Herdecke

München, November 2014

Die vorliegende Doktorarbeit wurde im Zeitraum von Januar 2011 bis November 2014 an der Ludwig-Maximilians-Universität München in Martinsried durchgeführt.

1. Gutachter: Prof. Dirk Schüler (Universität Bayreuth)

2. Gutachter: PD Dr. Ralf Heermann (Ludwig-Maximilians Universität München)

Tag der Abgabe: 05.11.14

Tag der mündlichen Prüfung: 16.01.15

Publications and manuscripts originating from this thesis

Publication 1

Borg S., Hofmann J., Pollithy A., Lang C. and Schüler D.

New vectors for chromosomal integration enable high-level constitutive or inducible magnetosome expression of fusion proteins in *Magnetospirillum gryphiswaldense* in Appl Environ Microbiol

Status: published | Year: 2014 | DOI: 10.1128/AEM.00192-14

Publication 2

Roda A., Cevenini L., Borg S., Michelini E., Calabretta MM. and Schüler D.

Bioengineered bioluminescent magnetotactic bacteria as a powerful tool for chip-based whole-cell biosensors in Lab Chip

Status: published | Year: 2013 | DOI: 10.1039/c3lc50868d

Manuscript 1

Borg S.^{*}, Popp F.^{*}, Hofmann J., Rothbauer U., Leonhardt H., and Schüler D.

An intracellular nanotrap re-directs proteins and organelles in live bacteria in mBio

Status: submitted | Year: 2014 | DOI: NN

^{*} These authors contributed equally to this study.

Manuscript 2

Borg S.^{*}, Rothenstein D.^{*}, Bill J. and Schüler D.

Generation of magnetic hybrid nanoparticles by encapsulation of magnetosomes with ZnO and SiO₂

Status: in preparation | Year: 2014 | DOI: NN

^{*} These authors contributed equally to this study.

Co-authored publications and manuscripts originating during this thesis

I) Li Y., Sabaty M., Borg S., Silva KT., Pignol D. and Schüler D.

The oxygen sensor MgFnr controls magnetite biomineralization by regulation of denitrification in *Magnetospirillum gryphiswaldense* in BMC Microbiol

Status: published | Year: 2014 | DOI: 10.1186/1471-2180-14-153

II) Lohße A., Borg S., Raschdorf O., Kolinko I., Tompa E., Pósfai M., Faivre D., Baumgartner J. and Schüler D.

Genetic dissection of the *mamAB* and *mms6* operons reveals a gene set essential for magnetosome biogenesis in *Magnetospirillum gryphiswaldense* in J Bacteriol

Status: published | Year: 2014 | DOI: 10.1128/JB.01716-14

III) Kolinko I., Lohße A., Borg S., Raschdorf O., Jogler C., Tu Q., Pósfai M., Tompa E., Plitzko J., Brachmann A., Wanner G., Müller R., Zhang Y., and Schüler D.

Biosynthesis of magnetic nanostructures in a foreign organism by transfer of bacterial magnetosome gene clusters in Nat Nano

Status: published | Year: 2014 | DOI: 10.1038/nnano.2014

IV) Li Y., Bali S., Borg S., Katzmann E., Ferguson SJ. and Schüler D.

Cytochrome *cd1* nitrite reductase NirS is involved in anaerobic magnetite biomineralization in *Magnetospirillum gryphiswaldense* and requires NirN for proper d1 heme assembly in J Bacteriol

Status: published | Year: 2013 | DOI: 10.1128/JB.00686-13

V) Li Y., Katzmann E., Borg S. and Schüler D.

The periplasmic nitrate reductase *nap* is required for anaerobic growth and involved in redox control of magnetite biomineralization in *Magnetospirillum gryphiswaldense* in J Bacteriol

Status: published | Year: 2012 | DOI: 10.1128/JB.00903-12

VI) Lohsse A., Ullrich S., Katzmann E., Borg S., Wanner G., Richter M., Voigt B., Schweder T. and Schüler D.

Functional analysis of the magnetosome island in *Magnetospirillum gryphiswaldense*: The *mamAB* operon is sufficient for magnetite biomineralization in PLoS One

Status: published | Year: 2011 | DOI: 10.1371/journal.pone.0025561

Contributions to publications

Publication 1:

S.B. and D.S. designed the study. S.B., J.H., A.P. and C.L. constructed the mutant strains and performed experiments. S.B. took transmission electron micrographs and S.B. analyzed the data. S.B. and D.S. wrote the manuscript.

Publication 2:

S.B. constructed the expression system for expression of luciferase in *M. gryphiswaldense*. S.B. created luciferase expressing mutants and performed transmission electron microscopy analysis of the generated strains. S.B. and L.C. performed luciferase assays. L.C. wrote the manuscript and S.B. contributed to the manuscript.

I hereby confirm the above statements:

Sarah Borg

Prof. Dirk Schüler

Contributions to co-authored publications and manuscripts originating during this thesis

Manuscript 1:

S.B. and D.S. designed the study. S.B. and J.H. constructed the mutant strains and S.B. and F.P. performed experiments. S.B. took transmission electron micrographs and S.B. analyzed the data. S.B., F.P. and D.S. wrote the manuscript.

Manuscript 2:

S.B. and D.S. designed the study. S.B. constructed mutant strains and cultivated *M. gryphiswaldense* cells in an oxystat fermenter for large scale production and isolation of magnetosomes. S.B. and D.R. performed experiments. S.B. controlled purity of magnetosomes by transmission electron microscopy and quantified amount of magnetosomes by iron assays. S.B. analyzed the data. S.B., D.R. and D.S. wrote the manuscript.

Publications I-IV & VI-VII:

S.B. performed transmission electron microscopy analysis of all generated strains.

I hereby confirm the above statements:

Sarah Borg

Prof. Dirk Schüler

Index

Publications and manuscripts originating from this thesis	I
Co-authored publications and manuscripts originating during this thesis.....	III
Contributions to publications.....	V
Contributions to co-authored publications and manuscripts originating during this thesis .	VI
Index	VII
Abbreviations.....	IX
Summary	1
Zusammenfassung.....	3
1. Introduction	5
1.1 Magnetic nanoparticles.....	5
<i>Coating of inorganic magnetic nanoparticles</i>	<i>6</i>
1.2 Biosynthesis of magnetosomes in <i>Magnetospirillum gryphiswaldense</i>	7
<i>Characteristics of M. gryphiswaldense.....</i>	<i>7</i>
<i>Characteristics of magnetosomes: The mineral core</i>	<i>8</i>
<i>Characteristics of magnetosomes: The magnetosome membrane</i>	<i>9</i>
<i>Function of MMPs in magnetosome synthesis.....</i>	<i>10</i>
<i>The magnetosome anchor protein MamC.....</i>	<i>12</i>
<i>Functionalization of magnetosomes</i>	<i>12</i>
<i>a) Chemical functionalization.....</i>	<i>12</i>
<i>b) Functionalization of magnetosomes by genetic engineering.....</i>	<i>14</i>
1.3 Use of camelid nanobodies in biomedical and biotechnological applications	15
1.4 Tools for expression of heterologous gene fusions in <i>M. gryphiswaldense</i>	17
1.5 Scope of this thesis	20
2. Publications and manuscripts	21
Publication 1:.....	21

Index

Publication 2:	39
Manuscript 1:	49
Manuscript 2:	82
3. Discussion	114
3.1 Expression of genetic fusions in <i>M. gryphiswaldense</i>	114
<i>Construction of an inducible expression system in M. gryphiswaldense</i>	115
<i>Chromosomal insertion of expression systems for display of single and multiple genetic fusions on magnetosomes results in super-fluorescent magnetic nanoparticles</i>	117
<i>Construction of luciferase producing M. gryphiswaldense cells for application in biosensors</i>	119
3.2 Construction of a nanotrap by display of nanobodies on magnetosomes	120
3.3 Nanobodies as nanotrap for rearrangement of cellular structures and resulting chemotaxis knockdown	122
3.4 First attempts for the generation of magnetic hybrid nanoparticles	125
3.5 Open questions and future directions	130
4. References	132
<i>Curriculum vitae</i>	148
Danksagung	149
Eidesstattliche Erklärung	150

Abbreviations

Atet	Anhydrotetracycline
CM	Cytoplasmic membrane
CSNs	Core-shell nanoparticles
EGFP	Enhanced green fluorescent protein
Fab	Antigen-binding fragment
GBP	GFP-binding protein
GFP	Green fluorescent protein
HCAb	Heavy-chain antibodies
IPTG	Isopropylthiogalactoside
MAI	Magnetosome island
MD	Multi domain
MM	Magnetosome membrane
Mam	Magnetosome membrane proteins
MHC II	Class II major histocompatibility complex
MMPs	Magnetosome membrane proteins
MNPs	Magnetic nanoparticles
Mms	Magnetic particle membrane-specific proteins
MTB	Magnetotactic bacteria
OATZ	Oxic anoxic transition zone
ORFs	Open reading frames
PCR	Polymerase chain reaction
PEG	Polyethylene glycol
PVP	Polyvinylpyrrolidone
RBP	RFP-binding protein
RBS	Ribosomal binding site
RFP	Red fluorescent protein
SBE A	Starch branching enzyme A
SD	Single domain
SEM	Scanning electron microscope
SP	Superparamagnetic
SPION	Superparamagnetic iron oxide nanoparticles

Abbreviations

STV	Streptavidin
Sulfo-LC-SPDP	Sulfosuccinimidyl 6-(3'-(2-pyridyldithio)propionamido)hexanoate
Sulfo-SMCC	Sulfosuccinimidyl 4-(N-maleimidomethyl)cyclohexane-1-carboxylate
TEM	Transmission electron microscope
TSHR	Thyroid-stimulating hormone receptor
XMCD	X-ray magnetic circular dichroism

Summary

Magnetic nanoparticles have great potential in biomedical applications such as targeted drug delivery, hyperthermia, bioimaging or as biosensors. However, generation of synthetic magnetic nanoparticles requires toxic reactants and high energy consumption and it is difficult to control shape and size of the generated particles. The magnetotactic bacterium *Magnetospirillum gryphiswaldense* naturally produces bacterial magnetic nanoparticles (so called magnetosomes) for magnetic orientation. Magnetosomes offer several advantages over synthetic magnetic nanoparticles. For example bioproduction can be achieved by sustainable approaches. Moreover, magnetic cores of magnetosomes are naturally enveloped by a biocompatible membrane that can be easily targeted for functionalization. In this thesis, magnetosomes were functionalized via genomic engineering using an optimized expression system or in first attempts by chemical encapsulation with inorganic coatings to generate inorganic-organic magnetic hybrid nanoparticles.

In the first part, chromosomally insertable expression systems for high constitutive or inducible expression of heterologous fusion genes were developed. To this end, the combination of a truncated version of the strong native P_{mamDC} promoter from the *mamGFDC* operon and an engineered ribosomal binding site and the codon-optimized reporter gene *magegfp*, resulted in increased gene expression. Additionally, the inducible tetracycline P_{tet} promoter was introduced into the optimized expression cassette. Determination of promoter strength was achieved using the reporter genes *egfp* and *gusA* and the copy number of MamC-magEGFP targeted to a single magnetosome was estimated between 80 and 250 per magnetosome by quantitative Western blot, which correlates with previous estimations of native MamC anchor proteins present on the magnetosome surface.

The new system was used in the second part of this thesis for functionalization of magnetosomes with multivalent GFP-binding nanobodies. Display of the nanobodies on magnetosomes led to efficient recruitment of GFP-tagged chemotaxis proteins, ectopic retargeting within the cell and, consequently aero/chemotaxis knockdown by depletion from their native polar environment. Concurrently, entire magnetosome chains and clusters could be ectopically tethered to the chemoreceptors at the cell pole.

Finally, MagEGFP functionalized magnetosomes were used in first attempts for the generation of inorganic-organic hybrid materials consisting of the magnetic core and

Summary

inorganic coating with silica or zinc oxide. Chemical coating of the bacterial magnetic nanoparticles resulted in core-shell nanoparticles with defined shell thickness. The generated nanoparticles were characterized with respect to surface charge and particle size. Silica encapsulated MagEGFP functionalized magnetosomes exhibited increased resistance against proteases and detergents, which makes these new magnetic hybrid nanoparticles an interesting potential tool for biomedical applications.

Zusammenfassung

Magnetische Nanopartikel besitzen großes Potenzial in biomedizinischen Anwendungen, wie zum Beispiel für gezielte Wirkstoffabgabe, bildgebende Verfahren oder in Biosensoren. Das magnetotaktische Bakterium *Magnetospirillum gryphiswaldense* produziert natürlicherweise magnetische Nanopartikel, so genannte Magnetosomen, welche es zur Orientierung am Magnetfeld der Erde nutzt um so schnellstmöglich seine biologische Nische zu finden. Magnetosomen haben viele Vorteile gegenüber synthetischen magnetischen Nanopartikeln, zum Beispiel können sie nachhaltig durch Fermentation der magnetotaktischen Bakterien gewonnen werden, während synthetische Nanopartikel unter Verbrauch toxischer Ausgangsstoffe und hohem Energieverbrauch hergestellt werden müssen. Darüber hinaus sind Magnetosomen von einer Magnetosomenmembran umgeben, welche Biokompatibilität gewährleistet und leicht durch genetische Manipulation zu funktionalisieren ist. In dieser Dissertation sollten Magnetosomen mit Hilfe eines neu entwickelten, optimierten Expressionssystems, unter anderem mit Nanobodies funktionalisiert und schließlich mit einer inorganischen Hülle versehen werden, um neue funktionale Hybridmaterialien zu generieren.

Im ersten Teil dieser Arbeit wurden zwei Expressionssysteme für eine starke konstitutive und induzierbare Expression von heterologen Fusionsproteinen entwickelt. Eine trunkierte Version des starken nativen P_{mamDC} Promotors des *mamGFDC* Operons wurde mit einer optimierten Ribosomenbindestelle und dem Codon-optimierten Reporter gen „MagEGFP“ kombiniert, um die Genexpression des Reporters zu steigern. Zusätzlich wurde der induzierbare P_{tet} Promotor in das Expressionssystem integriert. Beide Systeme wurden in transponierbare Vektoren kloniert, um sie in das Chromosom von *M. gryphiswaldense* zu inserieren. Die Promotorstärke wurde mit Hilfe der Reporter gene *egfp* und *gusA* bestimmt und die Anzahl der Fusionsproteine auf einem Magnetosom wurde mit Hilfe der quantitativen Western Blot Analyse auf 80 bis 250 Kopien pro Magnetosom geschätzt.

Im zweiten Teil dieser Arbeit wurden die neuen Expressionssysteme für die Funktionalisierung der Magnetosomen mit multivalenten Nanobodies eingesetzt. Die Verankerung der Nanobodies auf der Oberfläche der Magnetosomen führte dazu, dass Fluoreszenz-markierte Chemotaxisproteine zu den Magnetosomen rekrutiert und somit zu ektopischen Kompartimenten innerhalb der Zelle umgeleitet wurden. Die damit verbundene

Zusammenfassung

Abnahme der Chemotaxisproteine an ihrem Bestimmungsort führte zu einem Chemotaxis-defizienten Phänotypen. Gleichzeitig konnten Chemorezeptor-gebundene Proteine ganze Magnetosomenketten an den Zellpol rekrutieren.

Schließlich konnten Fluoreszenz-markierte Magnetosomen für die Produktion von magnetischen Hybridmaterialien, bestehend aus einem magnetischen Kern und einer inorganischen Hülle aus Zinkoxid oder Siliciumdioxid, genutzt werden. Ursprünglich sollte die Präzipitation der inorganischen Hülle mit Hilfe von biologischen Peptiden auf den Magnetosomen erreicht werden. Da dies aber in *M. gryphiswaldense* nicht möglich war, wurden chemische Ansätze für die Verkapselung herangezogen. Die daraus resultierenden Nanopartikel wurden hinsichtlich ihrer Oberflächenladung und Größe charakterisiert. Interessanterweise weisen Siliciumdioxid verkapselte, mit EGFP funktionalisierte Magnetosomen eine höhere Resistenz gegenüber Proteasen und Tensiden auf. Dies macht die neuen Hybridmaterialien äußerst interessant für biomedizinische Anwendungen.

1. Introduction

1.1 Magnetic nanoparticles

Magnetic nanoparticles (MNPs) have been used in numerous biomedical applications, such as drug delivery, hyperthermia, cell separation or as contrast agent for magnetic resonance imaging [1, 2]. Most studies have been conducted using magnetite (Fe_3O_4) because of its proven biocompatibility [3]. Magnetite is a mixed-valence oxide and has a cubic inverse spinel structure where oxygen is forming fcc closed packing and Fe cations occupy the interstitial tetrahedral and octahedral sites [4]. Electrons can hop between Fe^{2+} and Fe^{3+} ions in the octahedral sites at room temperature, which is responsible for conductivity and making magnetite an important class of half-metallic material [5]. The main factor responsible for magnetic properties of magnetic nanoparticles is crystal size. Three different domain states can be distinguished for increasing size of magnetite nanoparticles: i) superparamagnetic (for ideal particles, <35 nm, SP), ii) single domain (<100 nm, SD) and iii) multi domain (>100 nm, MD) [2]. Small SP particles cannot retain SD magnetization at room temperature and are only magnetic in presence of an external magnetic field [2], while SD and MD particles are ferrimagnetic and remain their magnetization even in the absence of a magnetic field. Typical size ranges of MNPs are 5-100 nm [1], which means they are superpara- to ferrimagnetic and the magnetization of the particles ranges between 10-50 emu/g [1].

Man-made magnetite nanoparticles are commonly produced by aqueous or organic solution synthesis [6]. Three main synthesis routes can be distinguished for the production of synthetic magnetite nanoparticles: i) Co-precipitation of Fe^{2+} and Fe^{3+} with NH_4OH [7], ii) thermal decomposition of iron(III)acetylacetonate ($\text{Fe}(\text{acac})_3$) in tri-ethyleneglycol [8] and iii) sonochemical decomposition of hydrolyzed Fe(II) salt [9]. Although production of synthetic Fe_3O_4 nanoparticles can be achieved at high yields, there are still obstacles to overcome in order to obtain uniform and pure nanoparticles. It remains difficult to synthesize particles with a small size distribution and to control the morphology of the particles. Moreover, some of the processes require long synthesis times to produce desired yields and high energy consumption or toxic compounds. Additionally, chemical synthesis demands surface modification of the particles during or subsequent to the process [10]. However, it remains challenging to achieve uniform size and morphology of magnetic nanoparticles with aqueous or organic solution synthesis.

1. Introduction

Coating of inorganic magnetic nanoparticles

Special forms of magnetic nanoparticles are core-shell nanoparticles (CSNs). They are of particular interest because these particles consist of layers of different materials which can add further properties, or passivate the core particle and thereby confer biocompatibility [11]. For example, coating of magnetite with silica or zinc oxide yields inorganic-inorganic CSNs (Figure 1a) [11]. Magnetite-silica CSNs (Figure 1b) have been synthesized following different synthesis routes e.g., layer-by-layer assembly [12], co-precipitation [13] or reverse microemulsion approach [14] and meant to be used in a variety of applications as biocatalysts [15] or drug delivery systems [16]. In contrast there is little information available about Fe_3O_4 -ZnO CSNs. One of the few studies describes seed-mediated grown Fe_3O_4 -ZnO CSNs consisting of a 8-13 nm Fe_3O_4 core surrounded by a 4.45-5.15 nm ZnO layer, which could be used as recyclable catalyst [17]. In a similar approach Wan and co-workers generated Fe_3O_4 -ZnO nanoparticles (Figure 1c) of about the same size, as spintronic devices [18].

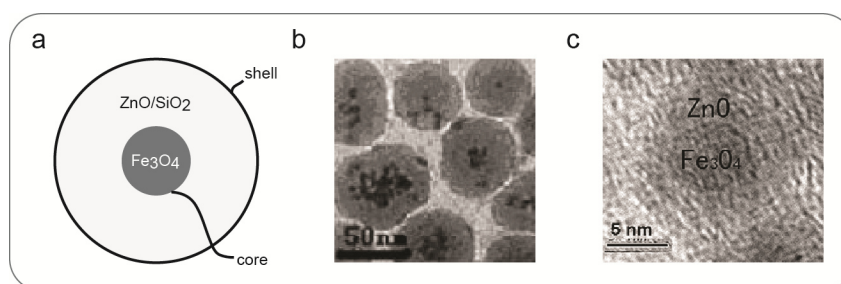


Figure 1: Core-shell nanoparticles a) Schematic of a spherical core-shell nanoparticle, consisting of a magnetite core and a silica or zinc oxide shell; b) TEM micrograph of silica magnetite core-shell nanoparticles, adapted from [14] and c) high resolution TEM micrograph of zinc oxide magnetite core-shell nanoparticle, adapted from [18].

Inorganic cores like magnetite can also be coated with organic materials to enhance functionality and biocompatibility, these materials belong to the inorganic-organic CSNs. For many applications, surface modification of magnetite nanoparticles is of major importance to ensure proper dispersion in different media by avoiding agglomeration [19]. Surfactants can also be chosen according to the desired application, e. g. polyethylene glycol (PEG), polyvinylpyrrolidone (PVP) and dextran enhance the blood circulation time [20-22], whereas fatty acids enhance the colloidal stability in organic solvents [23], while coating with peptides is suitable for cell biology applications like targeting to cells [24]. Moreover, various

1. Introduction

functional groups can be attached to coated magnetic nanoparticles, such as fluorescence tags [25], transferrin for targeted drug delivery [26] or chitosan to trace pollutants in environmental samples [27]. General requirements for application of magnetic nanoparticles and CSNs are high magnetization, uniform size distribution, colloidal stability and the possibility of functionalization [1], but meeting these criteria is difficult by chemical synthesis approaches. However, magnetite nanoparticles meeting these criteria that are naturally enveloped by a lipid-bilayer, can also be produced by bacteria.

1.2 Biosynthesis of magnetosomes in *Magnetospirillum gryphiswaldense*

Characteristics of M. gryphiswaldense

Naturally occurring biogenic core-shell nanoparticles with a size of 35-120 nm [28] and superior characteristics, consisting of a magnetic Fe_3O_4 core and an organic outer layer, are so called magnetosomes. These special organelles are synthesized by magnetotactic bacteria (MTB). MTB were already discovered by Salvatore Bellini in 1963 [29] but gained attention in 1975, when Blakemore rediscovered the magnetic response of environmental bacteria [30]. Although MTB are highly abundant and ubiquitous, only few strains can be cultivated in the lab. The best characterized MTB are two alphaproteobacteria species of the genus *Magnetospirillum*, *M. magneticum* AMB-1 [31] and *M. gryphiswaldense* MSR-1. *M. gryphiswaldense* was isolated by Dirk Schüler from mud of the river Ryck near Greifswald, Germany [32, 33]. It is a spiral-shaped, bi-polar monotrich flagellated bacterium that produces up to 50 magnetic nanoparticles (Figure 2a). The magnetosomes are arranged in chains, which causes the bacteria to align to the earth magnetic field, thereby facilitating migration to their preferred habitat in the oxic anoxic transition zone (OATZ) [33, 34]. Therefore, magnetotaxis is thought to be a reliable mean to keep *M. gryphiswaldense* close to growth favoring conditions and offer an advantage by reducing 3D biased walk to 1D directed swimming [35]. Recently, Popp and co-workers found that aerotaxis is mainly responsible for controlling swimming reversals and that both aerotaxis as well as swimming polarity are determined by only one of the four operons encoding chemotaxis proteins [36].

1. Introduction

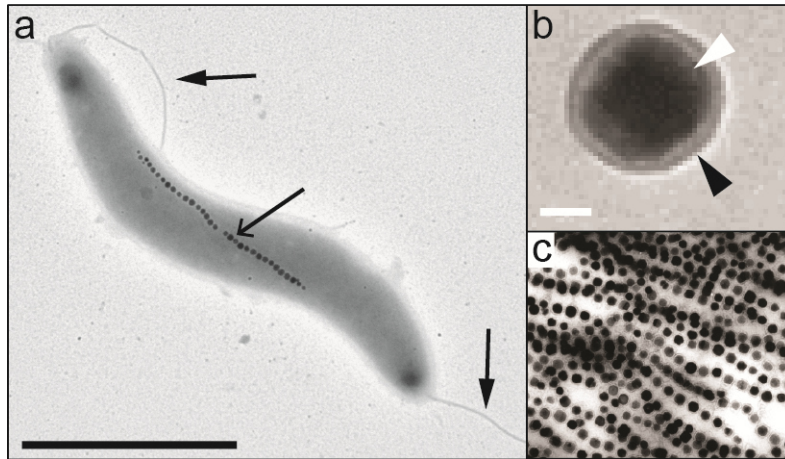


Figure 2: *M. gryphiswaldense* wild type cell and isolated magnetosomes. TEM micrograph of a bipolar flagellated (filled arrows) *M. gryphiswaldense* wild type cell with magnetosome chain (arrow); b) TEM micrograph of an isolated magnetosome of *M. gryphiswaldense*, with intact MM (black arrow head) and magnetite crystal (white arrow head); c) TEM micrograph of isolated magnetosomes of *M. gryphiswaldense*, dried in a magnetic field (adapted from [37]). Black scale bar represents 2 μm , white scale bar 20 nm.

Characteristics of magnetosomes: The mineral core

The physic-chemical characteristics of the magnetic core of magnetosomes are determined by composition, shape and size. In contrast to greigite (Fe_3S_4) producing MTB [38, 39], the core of magnetosomes of *M. gryphiswaldense* consists of magnetite, even under reducing conditions that are favoring the biomineralization of the magnetic iron Fe_3S_4 [2]. High purity of magnetite crystals with an average 10 emu/g magnetization [40] and without even minor impurities is preserved even if *M. gryphiswaldense* is cultured with high amounts of other metal ions, such as copper, zinc, nickel or manganese [2]. The only exception with enhanced magnetic properties are cobalt-doped magnetosomes reported in 2008, which presumably could be produced by cultivation of different strains with varying cobalt concentrations, resulting in an increase of the coercive field by 36-45% [41]. However, it is important to note that these results could never be reproduced by our lab. Even cultivation with exceptional high cobalt concentrations did not yield magnetosomes with any impurities (Damien Faivre, unpublished results). Apart from high chemical purity, magnetosomes exhibit a high degree of structural perfection. X-ray magnetic circular dichroism (XMCD) revealed that magnetosomes have nearly the same structure as calculated for stoichiometric magnetite. Only the ratio of Fe^{2+} to Fe^{3+} was slightly increased in comparison to

1. Introduction

stoichiometric magnetite, also the ratio of tetrahedral to octahedral iron was slightly lower [42]. Magnetic properties of magnetosomes are largely determined by their crystal morphology [43], which is under genetic control [44-46]. Magnetosomes of *M. gryphiswaldense* are cubooctahedral (Figure 3a), while other magnetotactic strains can produce pseudo-hexagonal prismatic or tooth-shaped magnetosomes, which cannot be produced by chemical approaches [2]. Mature magnetosomes from *M. gryphiswaldense* wild type cells are typically about 37-42 nm in diameter and therefore ferrimagnetic (Figure 3a) [47-49]. However, in mutant cells, lacking specific genes or entire operons, it is possible to synthesize superparamagnetic magnetosomes with a size range of 18-25 nm [50]. As morphology, size of magnetosomes is species-specific and determined by genetics. For different MTB, crystals from 35 nm to 120 nm can be found [44, 51-53]. Therefore magnetosomes fall into the SD domain state, which provides maximal magnetization for magnetite [2].

Characteristics of magnetosomes: The magnetosome membrane

The magnetite core of magnetosomes is enveloped by the magnetosome membrane (MM) (Figure 3b). The MM is a lipid bilayer, which contains a specific set of more than 20 proteins (Figure 3b) [54]. Magnetosome vesicles originate from the cytoplasmic membrane (CM) [55] and develop prior to magnetite biomineralization (Figure 3c) [50, 56]. They serve as “nanoreactors” to ensure biological control of physico-chemical conditions, such as redox potential and pH as well as super saturating iron concentrations, for the crystallization of magnetite [37]. The MM remains intact even after isolation and purification of magnetosomes from disrupted cells (Figure 1b&c). For isolation of magnetosomes, cells can be harvested, washed and mechanically disrupted by sonication, with a french press or use of a cell homogenizer. Afterwards magnetosomes can be extracted with a magnetic column and purified by centrifugation through a sucrose cushion to avoid contamination with other cellular components [57]. After purification of magnetosomes the MM can be solubilized and analyzed with respect to its composition. Biochemical analysis of the isolated MM revealed that phosphatidylethanolamine and phosphatidylglycerol are the most abundant lipids associated with magnetosome crystals [54]. Lipid and fatty acid patterns of the MM are similar to that of other subcellular compartments, which supports the ultrastructural observation of invagination of the CM for vesicle formation [54, 58]. In contrast, the set of magnetosome membrane proteins (MMP) is very distinct from other subcellular compartments in *M. gryphiswaldense* [37, 59]. A specific set of more than 30 proteins,

1. Introduction

described as magnetosome membrane (Mam) proteins and magnetic particle membrane-specific proteins (Mms), is required for the formation of mature magnetosomes [54, 60]. Many of these proteins are typically hydrophobic with transmembrane domains that are tightly integrated in the MM and exhibit higher resistance against proteases and detergents (e. g. MamG, MamF, MamD and MamC). In contrast, proteins like MamJ or MamA are hydrophilic and predicted to have magnetosome associated localization with rather accessory function for magnetosome synthesis [54, 58].

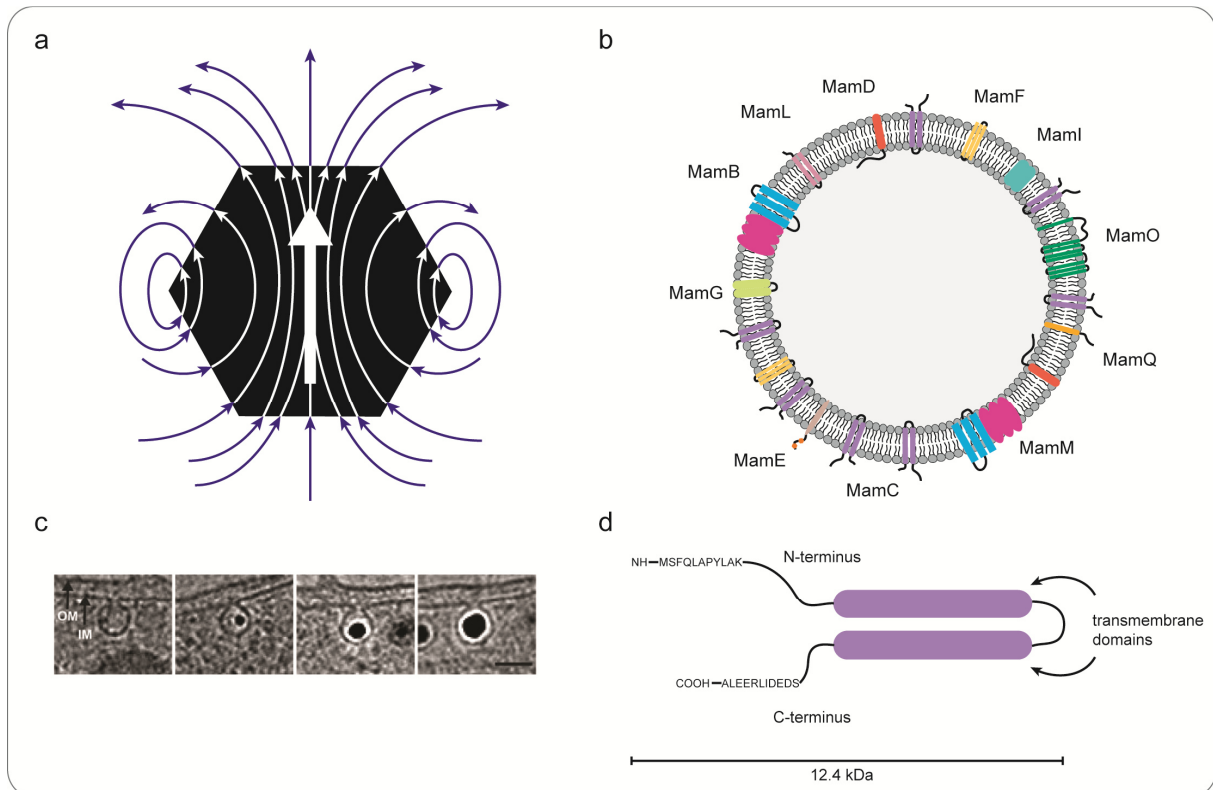


Figure 3: Structure of a magnetosome particle, the magnetosome vesicle and the MamC protein
a) Single-domain magnetosome crystal with indicated magnetic field lines; b) magnetosome membrane with magnetosome anchor proteins (MamG, MamF, MamD, MamC) and MMPs (MamE, MamL, MamM, MamO, MamQ, MamB and MamI) essential for magnetosome biomineralization; c) electron cryotomographs of invaginating cytoplasmic membrane and consequent biomineralization of magnetite particles in *M. magneticum* AMB-1 (adapted from [55]); d) predicted structure of the 12.4 kDa MMP MamC, consisting of two transmembrane domains, the aa sequence of C- and N-terminus are indicated.

Function of MMPs in magnetosome synthesis

The biosynthesis of magnetosomes is assumed to occur in five sequential steps: i) vesicle formation, ii) recruitment of MMPs to the vesicle, iii) iron uptake and crystal

1. Introduction

nucleation, iv) crystal maturation and v) chain assembly and positioning within the cell. Formation of the magnetosome vesicle in *M. gryphiswaldense* occurs prior to magnetite biomineralization [61] and is assumed to be induced by the proteins MamQ, MamL and MamB that are essential for vesicle formation [62, 63]. In the next step MamA forms a multiprotein complex, enveloping the magnetosome vesicle [64], while MamE is involved in recruitment of other MMPs [65]. Uptake of ferrous iron is mediated by a heterodimer of the cation diffusion facilitators (CDF) MamB and MamM [63], while MamH and MamZ assure transport of ferric iron into the vesicle [66]. Alternatively magnetite could be formed by co-precipitation of ferrous iron from the phosphate-rich ferritins (nanometric ferric (oxyhydr)oxides) by a highly disordered ferric hydroxide phase within the vesicle [67]. Precipitation of iron oxide is speculated to be catalyzed by MamO [65], and crystal maturation is then controlled by several different proteins. The proteins MamE, MamT, MamP and MamX share a conserved CXXCH heme-binding motif, which is assumed to form complexes for electron transport and the proteins might therefore participate in redox control [66, 68]. MamN is regulating the intramagnetosomal pH, the protein exhibits similarities to H⁺-translocation proteins and might control intravesicle conditions and regulate crystal maturation [37]. The only protein known so far to interact directly with the magnetite crystal is Mms6 [69, 70], which presumably assembles in a monolayer templating crystal growth [71]. During crystal maturation Mms36 and Mms48 inhibit crystal growth by an unknown mechanism [62], while the small hydrophilic MamG, MamF, MamD and MamC proteins cumulatively control growth of the magnetite crystal [48]. Finally, chain assembly and positioning is mediated by attachment of the magnetosomes via the acidic MamJ protein to the actin-like MamK filament [72] that is responsible for chain positioning [61, 73]. Genes encoding all proteins involved in magnetosome biosynthesis are clustered in a 115 kb magnetosome island (MAI) [50, 74]. Four major operons within this MAI are responsible for the strictly defined synthesis of magnetosomes. The *mamAB* operon, containing 17 genes, is the only one essential for biomineralization of magnetic crystals, deletion of the operon leads to non-magnetic cells with normal morphology and growth [75]. Recently it was shown that only seven genes from this operon (*mamE*, *mamL*, *mamM*, *mamO*, *mamQ*, *mamI* and *mamB*) are essential for formation of magnetite [62]. Residual genes of the *mamAB* operon and those of other operons have accessory functions for magnetosome synthesis. Cells with deletion of the *mamXY* operon produce fewer fully grown magnetite crystals, which are flanked by smaller irregular flake-like structures which are positioned randomly within the cell [50, 66].

1. Introduction

Similar, deletion of the *mms6* operon causes a less magnetic phenotype with smaller, fewer magnetosomes that were poorly aligned [50]. The *mamGFDC* operon is not essential for magnetosome synthesis, but responsible for crystal size, since deletion led to 25% smaller crystals [48].

The magnetosome anchor protein MamC

The MamC protein (Mms13 in *M. magneticum* AMB-1), encoded in the *mamGFDC* operon, is the most abundant protein within the MM with a relative abundance of 16.3% of the proteins of the entire MM [54]. Deletion of MamC has no significant effect on magnetosome synthesis, and causes only slightly diminished crystal size [48]. Therefore, no disturbance of the MM after fusion of heterologous genes to *mamC* is expected. The small 12.4 kDa protein, with a calculated isoelectric point of 4.9 [37], consists of two helical transmembrane domains (Figure 3d) [54, 57], which theoretically allows for functionalization of both the C- and the N-terminal end, but in practice the C-terminus is commonly used for construction of fusion proteins [57]. It was shown that MamC is stably inserted into and exclusively localized in the MM [57]. Therefore, MamC was used as anchor protein for functionalization of magnetosomes in various approaches, for instance with the enhanced-fluorescent protein (EGFP) [57, 76, 77]. MamC-EGFP fusions proved to be stable for neutral to basic pH and temperatures between -20 and 50°C [57]. Moreover sodium chloride concentrations up to 4 M and guanidinium chloride of 100 mM could not abolish fluorescence of the functionalized particles [57]. Moreover, MamC-EGFP fusions were resistant against 0.01% of detergents like sodium dodecyl sulfate (SDS) and triton X-100 [57]. The resistance of MamC against abiotic factors as well as proteases and detergents and the distinct localization of the protein qualify MamC as perfect anchor protein within the MM.

Functionalization of magnetosomes

a) Chemical functionalization

Functionalization with respect to nanoparticles means attaching functional moieties to the particle. In early approaches functionalization of magnetosomes was achieved by chemical coupling of functional groups, such as antibodies or nucleic acids to the magnetosome surface via cross-linking [78, 79]. Glucose oxidase was immobilized on magnetosomes from the related bacterium *M. magneticum* AMB-1 by incubation with γ -aminopropyltriethoxysilane prior to enzyme attachment. Functionalized magnetosomes

1. Introduction

exhibited a 40-times higher enzyme activity than synthetic magnetite or Zn-ferrite nanoparticles that were treated the same way [80]. For immobilization of antibodies, magnetosomes of *M. magneticum* AMB-1 were incubated with sulfosuccinimidyl 6-(3'-(2-pyridyldithio)propionamido)hexanoate (sulfo-LC-SPDP) that reacted with sulfosuccinimidyl 4-(N-maleimidomethyl)cyclohexane-1-carboxylate (sulfo-SMCC)-modified anti-mouse IgG antibodies. The functionalized particles were then used for immunoassaying of mouse immunoglobulin G (IgG) (Figure 4) [81]. Biotin functionalized magnetic nanoparticles were prepared using the same principle and could be captured with streptavidin immobilized on a glass surface [82]. For *M. gryphiswaldense* chemical functionalization of magnetosomes was achieved by incorporation of the biotinylated lipid biotin-DPPE and covalent modification of MMPs by using NHS-biotin to generate biotinylated magnetic nanoparticles [83]. The functionalized particles could then bind streptavidin (STV), leading to STV-functionalized magnetosomes with biotin-binding capacity, which allows for attachment of biotinylated DNA fragments or antibodies for specific detection of proteins and nucleic acids. Functionalized magnetosomes were applied to capture oligonucleotide conjugated gold nanoparticles (Figure 4) and immobilization on DNA or antibody coated surfaces [83]. In a different approach, biotin-STV functionalized magnetosomes [83] were applied for magneto immuno-PCR (Figure 4) [84]. Therefore the STV-functionalized magnetosomes were coupled with biotinylated anti-Hepatitis B surface Antigen (HBsAg) antibodies for detection of recombinant HBsAg. Functionalized magnetosomes were incubated with HBsAg and with DNA conjugated anti-HBsAg antibodies for real-time immuno-PCR. Magneto immuno-PCR proved to be 25-fold more sensitive with magnetosomes as carrier material in comparison to commercial magnetic microbeads [84].

1. Introduction

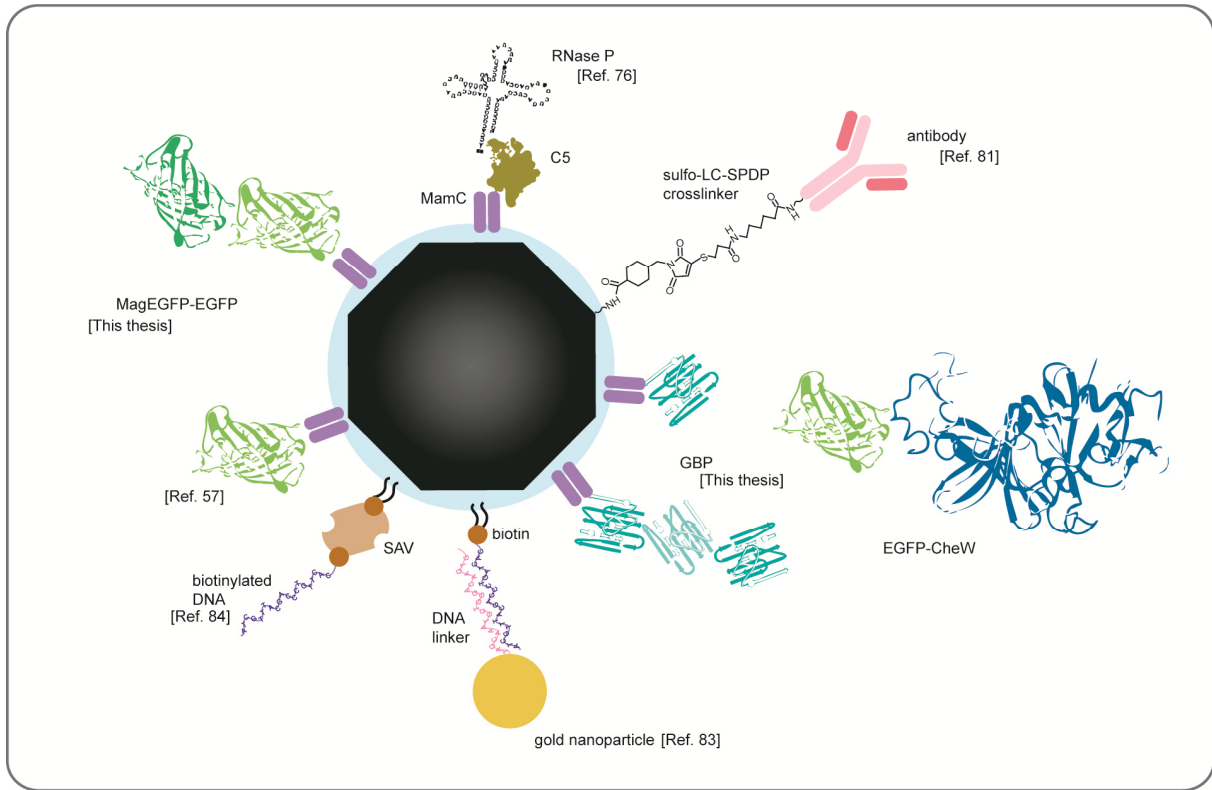


Figure 4: Summary of realized functionalization approaches of magnetosomes with various functional groups. Chemical functionalization of magnetosomes with antibodies via crosslinkers [81] or biotinylation [83, 84]. Functionalization via genetic engineering was achieved by fusion of MamC with enhanced green fluorescent protein (EGFP) [57] and a *Magnetospirillum*-optimized version (MagEGFP) [this thesis], a multisubunit enzyme complexes [76] or GFP-binding protein (GBP) nanobodies capturing the EGFP-tagged chemotaxis protein CheW [this thesis].

b) Functionalization of magnetosomes by genetic engineering

A more elegant and powerful approach for functionalization of magnetosomes uses the anchor protein MamC for generation of genetic fusions, securing stable and controlled expression of fusion proteins targeted to the magnetosome surface. Genetic engineering is a more favorable approach than chemical engineering of magnetosomes, because no harsh reaction conditions are needed, which might degrade proteins present on the magnetosome surface. Most importantly, modification can be achieved in a defined manner with higher specificity. Moreover, functionalized magnetosomes with precisely tailored characteristics can be produced and thereby synthesized particles can be isolated in a single step from disrupted cells without further modifications and loss of material, which cannot be achieved by chemical synthesis approaches. For example, the MamC protein was used as anchor in *M.*

1. Introduction

magneticum AMB-1, for immobilization of biotin accepting peptides or biotin carboxyl carrier proteins on the magnetosome surface to generate biotinylated magnetosomes [85]. Functionalization of magnetosomes from *M. magneticum* AMB-1 was also achieved by expression of a phosphohydrolase fused to MamC, which produced a recyclable nanobiocatalyst for organophosphate pesticide biodegradation [86] or by genetic fusion of luciferase or the immunoglobulin G-binding domain of protein A (ZZ) to MamC (Mms13) [87]. In a recent study the $\Delta mms13$ strain was used for higher expression of two human proteins (thyroid-stimulating hormone receptor, TSHR) and the class II major histocompatibility complex (MHC II molecules) as MamC (Mms13) fusions [88]. One of the first studies in *M. gryphiswaldense* was utilizing the MamC protein as anchor for immobilization of EGFP (Figure 4) [57]. Following this example many MamC fusions were constructed, e.g. producing magnetosomes displaying multisubunit enzyme complexes (Figure 4) [76]. The protein subunit (C5) of *Escherichia coli* RNase P is known to interact with RNA subunits from a wide variety of bacteria [89]. Therefore, a fusion of the gene encoding the C5 protein with *mamC* was constructed in *M. gryphiswaldense* and expressed to recruit the active endogenous RNA subunit [76]. This strategy can be employed for construction of a variety of similar multisubunit enzyme complexes. In a different study, the gene encoding staphylococcal protein A from *Staphylococcus aureus* was fused to *mamC*, expressed on magnetosomes of *M. gryphiswaldense* and used in combination with mammalian antibodies to capture pathogenic bacteria [90]. Recently, Pollithy and co-workers were able to immobilize so called red-fluorescent protein (RFP)-binding nanobodies (RBP) on magnetosomes via fusion of *rbp* to *mamC*. The RBP conjugated magnetosomes were able to capture cytoplasmic RFP *in vivo* and were used for immunoprecipitation of RFP-tagged proteins from complex soluble mammalian cell extracts *in vitro* [77].

1.3 Use of camelid nanobodies in biomedical and biotechnological applications

Among various functional moieties displayed on magnetosomes, so called nanobodies are of particularly high interest. They represent nanometer sized fragments of camelid heavy-chain antibodies (HCAb), which lack the light chains present in conventional IgG antibodies (Figure 5a) and recognize their target by interaction with single VHH domains. The VHH in an HCAb is the equivalent of the antigen-binding fragment (Fab) of conventional antibodies (Figure 5a&b) [91]. Due to their small size of about 15 kDa (~117 aa) (Figure 5c) [92], the

1. Introduction

genes of nanobodies against fluorescent proteins, like the GFP-binding nanobody (called GFP-binding protein, GBP), can be directly cloned into expression systems and expressed in various organisms [93]. Because of their special topology, nanobodies preferentially bind to concave surfaces of antigens which are often inaccessible to conventional antibodies [94]. Examples for nanobody-based applications comprise inhibition of enzyme activity for instance through specific binding to the active site of bovine erythrocyte carbonic anhydrase and porcine pancreatic α -amylase [95] or the potato starch branching enzyme A (SBE A) [96].

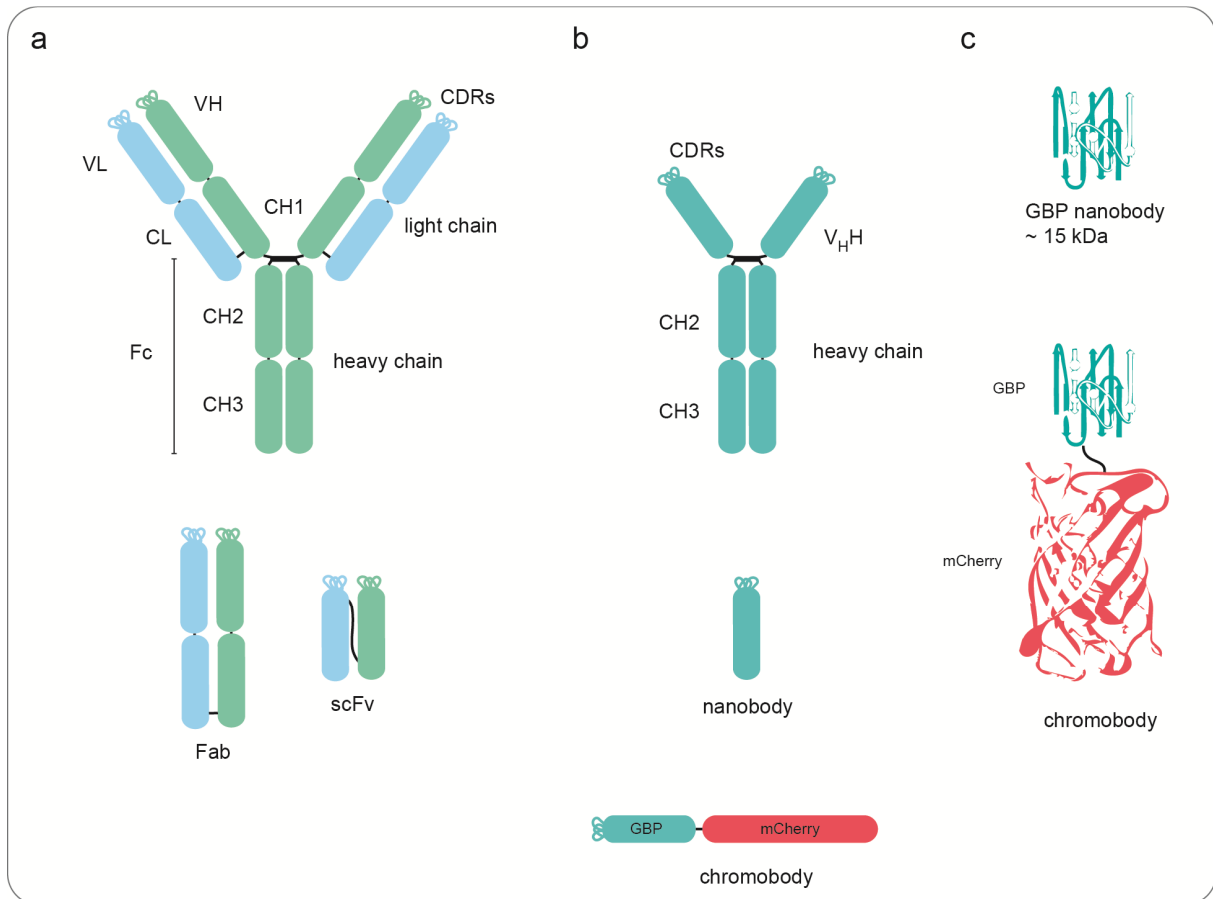


Figure 5: Characteristics of conventional, heavy-chain antibodies and antibody fragments (nanobodies). a) Conventional antibody consisting of heavy and light chains. The constant domain is responsible for recruitment of immune cells, while the variable region and the CDR loops recognize the antigen. The antigen binding fragment (Fab) and single chain variable fragment (scFv) are used in various applications for antigen recognition; b) Camelid heavy-chain antibodies are devoid of light chains, therefore recognition of the antigen is mediated by the V_HH fragment exclusively. Nanobodies are the V_HH domain of camelid heavy-chain antibodies and are termed chromobody, if conjugated with a fluorescence protein; c) abstracted ribbon-band structure of the GBP nano- and chromobody.

1. Introduction

Furthermore, different strategies for nanobody-mediated protein knockdowns have been developed in eukaryotes, either by targeting nanobody-bound proteins to degradation pathways [97], or by artificially retargeting interaction partners to specific intracellular localizations, e.g. distinct cellular compartments by use of nanobodies as intracellular “nanotraps” [92, 98, 99]. Coupling of nanobodies with fluorescence proteins generated so called chromobodies, which allows tracking of nanobody localization and interaction via fluorescence microscopy [100]. Nanobodies are also tested for applications in medical approaches against neurological disorders, like Parkinson’s or Alzheimer’s [101]. Functional production of nanobodies in bacterial cells has been restricted to only very few studies. Recently nanobodies have been produced in bacteria to inhibit enzyme function, such as dioxygenase activity [102], and in *M. gryphiswaldense* on magnetosomes coupled to MamC for recruitment of cytoplasmic fluorescent proteins [77].

1.4 Tools for expression of heterologous gene fusions in *M. gryphiswaldense*

For stable and high expression of gene fusions in *M. gryphiswaldense* functional expression systems are needed. Expression of heterologous genes in other bacteria has been widely used for scientific and biotechnological applications. Development of expression systems aims on high and inducible production of the protein of interest. General requirements for expression systems are strong and tunable promoters for control on the transcriptional level as well as for instance optimization of ribosomal binding sites (RBS) for efficient translation of the gene of interest. Additionally, it is favorable to include antibiotic resistances for phenotypic selection [103]. Preferentially, expression systems should be constructed with tunable promoters, since over-expression of proteins in a foreign host could challenge the metabolic load of the organism [104], or compartments could restrict the number of proteins that can be produced. Many features have to be optimized such as promoter strength, terminator sequences, elements affecting translational initiation, translation enhancers [103] or codon usage of the gene of interest [105]. While many powerful expression systems are available for *E. coli* and other model organisms [106], very few systems are developed for alphaproteobacteria such as *M. gryphiswaldense*. Well-characterized promoter systems are e.g. the *lac*, *tac* and *trc* promoters. The *lac* promoter from the operon controlling lactose utilization in *E. coli* was already used 1976 in a vector system expressing eukaryotic DNA in bacteria, by induction with isopropylthiogalactoside (IPTG)

1. Introduction

[107]. To increase promoter strength of this rather weak promoter, the *tac* hybrid promoter containing the -35 region of the strong *trp* promoter and the -10 region of the weak *lac* promoter was constructed, which proved to be inducible 3-times higher than the *trp* promoter [108]. Further modification resulted in the *trc* promoter that differs only in one base pair (bp) length from the *tac*, which increased activity by 90% [109]. In alphaproteobacteria best characterized expression systems can be found for model organisms like *Caulobacter crescentus*. Xylose and vanillate inducible expression systems are well established and commonly used in *C. crescentus* [110, 111]. Another inducible expression system, which can be tightly controlled but delivers strong expression at the same time is the *tet* promoter/operator system [112, 113]. Instead of tetracycline it is common practice to use anhydrotetracycline (Atet) as inducer, since it binds to the promoter 35-fold higher and its antibiotic activity is 100-fold lower than for tetracycline [114]. In *C. crescentus* P_{tet} could be applied for the expression of the DNA-partitioning protein ParB after induction with Atet [115].

Genetic systems in MTB are poorly developed and only recently a limited tool set was established. In previous approaches, Yoshino and co-workers identified the *msp13* and *mms16* promoters as presumably strong promoters in *M. magneticum* AMB-1 and used them for magnetosome display of fusion proteins [116, 117], but promoters of the homologous genes exhibit only weak expression in *M. gryphiswaldense* [118]. An inducible tetracycline [112, 113] hybrid expression system was used for expression of tetraspanin CD81 in *M. magneticum* AMB-1 [119]. However, it is not possible to estimate the real strength of the hybrid promoter in comparison to other established promoters. Recently Topp and co-workers synthesized a riboswitch expression system, which responds to the inducer theophylline and allows expression of a MamK-EGFP fusion in *M. magneticum* ABM-1 [120].

In *M. gryphiswaldense*, only recently genetic systems were available and tools for expression are poorly developed. Expression of heterologous genes in *M. gryphiswaldense* can be achieved either cytoplasmic or specifically targeted to the magnetosome membrane by fusion to MamC. Expression systems for magnetosome display of foreign proteins need to meet special requirements, such as specific targeting to the MM, controlled copy number and stable attachment of the fusion proteins. *M. gryphiswaldense* is one of the few cultivated magnetotactic bacteria with established genetic systems for transfer and expression of heterologous genes [121]. Transfer of plasmids into MTB can be achieved by conjugation

1. Introduction

from *E. coli* [121, 122]. Recently, Kolinko and co-workers constructed a *recA* deficient strain, which is incapable of homologous recombination and facilitates production of heterologous proteins or multiple copies of proteins [123]. This strain could be used to successfully introduce additional copies of the same gene without risking homologous recombination and excision of the genes [123]. For markerless chromosomal insertion of heterologous genes or deletion of genes of interest a *galK*-based counterselection method was developed [124].

However, although many genetic tools for genetic manipulation of MTB have been developed, expression of magnetosome targeted fusion proteins is still cumbersome and inefficient in *M. gryphiswaldense*. Only few promoters were functional in *M. gryphiswaldense*. The P_{mamDC} promoter, which is the native promoter of the *mamGFDC* operon yielded high constitutive expression, while other native promoters like the P_{mamAB} promoter of the *mamAB* operon and the widely used *E. coli* P_{lac} promoter resulted in significant weaker transcription [118, 125]. Even native *M. gryphiswaldense* promoters from ribosomal operons, which were expected to ensure high expression, yielded unexpectedly only weak expression of the reporter gene *egfp* [118]. First attempts to optimize P_{mamDC} driven expression included optimization the RBS of *mamG* with regard to spacing between the Shine-Dalgarno sequence and the start codon of *mamG*. A spacing of 8 bp was found to increase *egfp* expression in combination with a 45 bp truncated version of the P_{mamDC} promoter [126]. All approaches for expression in *M. gryphiswaldense* used a replicative system based on a medium copy number plasmid of the pBBR family. However, this has the disadvantage of segregational instability and growth phase dependent artificial expression levels [127] and resulted in non-uniform expression in cell populations [118]. This is unfavorable for genetic engineering of magnetosomes for biotechnological applications, as gene expression will be reflected by heterogeneously modified magnetosomes [118]. Moreover, inducible expression systems for display of toxic fusion proteins, expression of proteins that may interfere with magnetosome biomineralization or cellular processes [119], or the generation of conditional mutants, are still missing. Promoter analysis showed that the urease promoter (P_{ure}) from the *Enterobacteriaceae* family [128] is not inducible in *M. gryphiswaldense* [129]. In contrast, the P_{tet} promoter from the *E. coli* *Tn10* Tc^R gene can be induced with Atet [129] and repression of the promoter could be improved by expression of the TetR repressor protein under the control of the neomycin promoter (P_{neo}) [126]. However, appropriate tools for high yield and magnetosome specific expression of heterologous proteins are still missing in *M. gryphiswaldense*.

1.5 Scope of this thesis

The general goal of this thesis was to establish strategies for biosynthesis of innovative magnetic nanoparticles by generation of functionalized magnetosomes in *M. gryphiswaldense*. Due to the lack of suitable tools for protein expression that is targeted to the MM, the first part of this thesis was devoted to the construction of expression systems yielding high and inducible expression in *M. gryphiswaldense*. This required extensive testing of established promoters as well as the generation of new hybrid promoters. In addition to optimization of promoter strength, codon optimized genes were tested to investigate if adapting the codon usage of heterologous genes to the codon bias of *M. gryphiswaldense* is improving expression of the protein. The copy number of MamC-fusions on a single magnetosome was estimated by quantitative Western blot analysis of single and tandem fusions of EGFP to the magnetosomes.

In the second part, the optimized expression system was then used for the generation of functionalized magnetosomes. As an example, nanobodies were chosen and their intracellular expression was optimized, since nanobodies are able to recruit specific targets *in vivo* and *in vitro*. Magnetosomes displaying GBP and expression of an EGFP-tagged version of the chemotaxis protein CheW₁ were tested for artificial recruitment of membrane bound proteins or even whole organelles and consequent chemotaxis knock-down.

Finally, the third part of this work focused on approaches for development of hybrid MNPs. As examples, coating of magnetosomes with inorganic layers was achieved by chemical approaches. Thereby produced fluorescent silica and ZnO magnetosome hybrid MNPs were subsequently characterized.

2. Publications and manuscripts

Publication 1:

New vectors for chromosomal integration enable high-level
constitutive or inducible magnetosome expression of fusion proteins
in *Magnetospirillum gryphiswaldense*

Sarah Borg, Julia Hofmann, Anna Pollithy,* Claus Lang* and Dirk Schüler

Applied and Environmental Microbiology 2014, 80(8):2609

Ludwig Maximilian University Munich, Department of Biology I, Martinsried, Germany

* Present address: Anna Pollithy, Department of Gene Vectors, Helmholtz Center
Munich, German Research Center for Environmental Health GmbH, Munich,
Germany; Claus Lang, Department of Biology, Stanford University, Stanford,
California, USA.

New Vectors for Chromosomal Integration Enable High-Level Constitutive or Inducible Magnetosome Expression of Fusion Proteins in *Magnetospirillum gryphiswaldense*

Sarah Borg, Julia Hofmann, Anna Pollithy,* Claus Lang,* Dirk Schüler

Ludwig Maximilian University Munich, Department of Biology I, Martinsried, Germany

The alphaproteobacterium *Magnetospirillum gryphiswaldense* biomineralizes magnetosomes, which consist of monocrystalline magnetite cores enveloped by a phospholipid bilayer containing specific proteins. Magnetosomes represent magnetic nanoparticles with unprecedented magnetic and physicochemical characteristics. These make them potentially useful in a number of biotechnological and biomedical applications. Further functionalization can be achieved by expression of foreign proteins via genetic fusion to magnetosome anchor peptides. However, the available genetic tool set for strong and controlled protein expression in magnetotactic bacteria is very limited. Here, we describe versatile vectors for either inducible or high-level constitutive expression of proteins in *M. gryphiswaldense*. The combination of an engineered native P_{mamDC} promoter with a codon-optimized *egfp* gene (*Mag-egfp*) resulted in an 8-fold increase in constitutive expression and in brighter fluorescence. We further demonstrate that the widely used P_{tet} promoter is functional and tunable in *M. gryphiswaldense*. Stable and uniform expression of the EGFP and β -glucuronidase (*GusA*) reporters by single-copy chromosomal insertion via Tn5-mediated transposition. In addition, gene duplication by *Mag-EGFP-EGFP* fusions to MamC resulted in further increased magnetosome expression and fluorescence. Between 80 and 210 (for single MamC–*Mag-EGFP*) and 200 and 520 (for MamC–*Mag-EGFP-EGFP*) GFP copies were estimated to be expressed per individual magnetosome particle.

For magnetic orientation, magnetotactic bacteria (MTB) biomineralize bacterial (ferri)magnetic nanoparticles. In the model organism *Magnetospirillum gryphiswaldense* and other MTB, these organelles consist of magnetite (Fe_3O_4) cores enveloped by the magnetosome membrane (MM) (1, 2). Because of their unprecedented material properties, such as high crystallinity, strong magnetization, uniform shapes and sizes, and biocompatibility, the use of isolated magnetosome particles has been suggested for a number of biotechnological and biomedical applications, such as using them as nanocarriers in magnetic drug targeting, magnetosome-based immunoassays and as reporters for magnetic resonance imaging (MRI) (3). Many of these applications require further functionalization, for instance, by displaying additional functional moieties on the magnetosome surface such as antibodies, oligonucleotides, fluorophores, or enzymes (3, 4). It was shown that in *M. gryphiswaldense*, in addition to chemical functionalization of isolated particles *in vitro* (5, 6), magnetosomes can also be engineered *in vivo* by expression of foreign proteins via genetic fusion to native magnetosome anchors. For example, the small (12.5-kDa), highly abundant MamC protein was shown to provide tight and stable attachment of foreign proteins to the MM. This was first demonstrated by a MamC–green fluorescent protein (GFP) fusion, which displayed stable fluorescence *in vivo* and also after purification of magnetosomes (7). In different studies, a red fluorescent protein (RFP)–binding nanobody (RBP) and the endogenous RNA subunit C5 of the multisubunit chimeric bacterial RNase P enzyme were functionally expressed on magnetosomes by translational fusion with MamC (8, 9).

However, previous approaches were hampered by the unavailability of appropriate systems for controlled protein expression in *M. gryphiswaldense*. For example, so far only a few promoters have been identified as being functional for transcription in *M. gryphiswaldense*. The native P_{mamDC} which drives transcription of the

mamGFDC operon, yielded the highest constitutive expression of the reporter EGFP, while weaker expression was found with other promoters like P_{mamAB} (10, 11). Known inducible promoters yielded only weak (P_{lac} [10]) or no expression (e.g., P_{ure} [our unpublished data]). However, inducible expression systems are prerequisite for display of proteins that may interfere with magnetosome biomineralization or cellular processes. In the related strain *Magnetospirillum magneticum* AMB-1, the strong native *mSP13* and *mms16* promoters were employed for magnetosome display of fusion proteins (12, 13). A tetracycline (Tet)-inducible expression system was described based on a hybrid promoter consisting of the combined *mSP1* promoter and *tetO* sequences (14). However, the transcriptional strength of the hybrid promoter compared to the strong constitutive *mSP13* and *mms16* has not been reported. In addition, all expression studies so far were based on multicopy replicative plasmids, which have the disadvantage of segregational instability and nonuniform expression (10).

Here, we describe two versatile vectors for either inducible or

Received 16 January 2014 Accepted 10 February 2014

Published ahead of print 14 February 2014

Editor: S.-J. Liu

Address correspondence to Dirk Schüler, dirk.schueler@lmu.de.

* Present address: Anna Pollithy, Department of Gene Vectors, Helmholtz Center Munich, German Research Center for Environmental Health GmbH, Munich, Germany; Claus Lang, Department of Biology, Stanford University, Stanford, California, USA.

Supplemental material for this article may be found at <http://dx.doi.org/10.1128/AEM.00192-14>.

Copyright © 2014, American Society for Microbiology. All Rights Reserved.

doi:10.1128/AEM.00192-14

high-level constitutive chromosomal expression. We demonstrate their use for cytoplasmic and magnetosome expression of foreign proteins. Furthermore, we show that codon optimization and multicopy expression are powerful approaches to enhance heterologous expression of proteins in *M. gryphiswaldense*. We also provide an estimation of protein copies expressed per magnetosome particle.

MATERIALS AND METHODS

Bacterial strains, plasmids, and culture conditions. Plasmids and bacterial strains used in this study are listed in Tables S1 and S2 in the supplemental material. *M. gryphiswaldense* strains were grown microaerobically in modified flask standard medium (FSM) at 30°C (15) with moderate agitation (120 rpm). *Escherichia coli* strains were cultivated as previously described (16) for growth of *E. coli* BW29427 (K. Datsenko and B. L. Wanner, unpublished data) and WM3064 (W. Metcalf, unpublished data); 1 mM D,L- α , ϵ -diaminopimelic acid (DAP) was added to lysogeny broth (LB) medium. Strains were routinely cultured on plates solidified with 1.5% (wt/vol) agar. For strains carrying recombinant plasmids, media were supplemented with 25 $\mu\text{g ml}^{-1}$ kanamycin (Km) and 50 $\mu\text{g ml}^{-1}$ ampicillin (Amp) for *E. coli* strains and 5 $\mu\text{g ml}^{-1}$ Km for *M. gryphiswaldense* strains. For induction experiments, media were supplemented with various concentrations of anhydrotetracycline (Atet).

Molecular and genetic techniques. Oligonucleotides (see Table S3 in the supplemental material) were purchased from Sigma-Aldrich (Steinheim, Germany). Chromosomal DNA of *M. gryphiswaldense* was isolated using a genomic DNA isolation kit (Zymo Research, USA). Plasmids were constructed by standard recombinant techniques as described in detail below. All constructs were sequenced on an ABI 3730 capillary sequencer (Applied Biosystems, Darmstadt, Germany), utilizing BigDye Terminator v3.1. Sequence data were analyzed with Vector NTI Advance 11.5 software (Invitrogen, Darmstadt, Germany). *Magnetospirillum*-optimized EGFP (Mag-EGFP) was optimized by proprietary algorithms for increased mRNA stability and avoidance of sequence repetitions and secondary structures and was purchased from GeneArt (Invitrogen, Darmstadt, Germany).

Construction of insertional expression plasmids. For the construction of pSB6, first Mag-*egfp* was amplified from p11AAGJZC using the primers oEGFP BamHI Rev and oEGFP HindIII Fw. The resulting PCR fragment was subcloned into pJET1.2/blunt and after restriction with BamHI and HindIII inserted into pAP150 and pAP160 to replace *egfp* with Mag-*egfp*. Afterwards, the $P_{mamDC45}$ promoter, the spacing-optimized ribosomal binding site (oRBS) and Mag-*egfp* were amplified from modified pAP150 (pSB1) using pBam_pAP150 Fw and pBam_DC w/o Term Rev, adding EcoRI and SanDI restriction sites for insertion into pBAM1, generating pSB6. For the generation of pSB7, the whole expression cassette from modified pAP160, containing the optimized Mag-*egfp* version plus P_{tet} and TetR, was amplified using the primers pBam_pAP160 Fw and pBam_Tet w/o Term Rev and inserted into pBAM1. For the generation of the expression plasmids containing *gusA* as a transcriptional reporter, *gusA* was amplified from pLYJ97 using the primers GusA BamHI Fw and GusA NdeI Rev and cloned into pSB7, replacing Mag-*egfp* with *gusA*, thereby generating pSB8. Transposition of the expression cassettes resulted in single-copy genomic insertion into phenotypical neutral sites as verified by arbitrary PCR (17) and sequencing.

Construction of MamC fusion proteins. *mamC* and Mag-*egfp* were amplified and fused via overlap PCR (18) using the primers described in Table S3 in the supplemental material, resulting in C-terminal fusions of Mag-*egfp* to *mamC*; afterwards, the fusion gene was inserted into the NdeI and BamHI restriction sites of pSB6 and pSB7, resulting in pJH1 and pJH2. Additionally a tandem fusion of *mamC* with Mag-*egfp* and *egfp* was generated, following the same strategy, yielding plasmid pJH3. *M. gryphiswaldense* strains were conjugated with pJH1, pJH2, and pJH3 and were grown in 3 liters of FSM medium to stationary phase at 30°C and 120 rpm.

Cells were harvested by centrifugation at 4°C and 6,500 rpm and used for magnetosome isolation.

Analytical methods. Magnetic reaction of cells was detected by light microscopy applying a bar magnet. Optical density (OD) and magnetic response (C_{mag}) of exponentially growing cells were measured photometrically at 565 nm as previously reported (19). Iron concentrations of the isolated magnetosomes were determined by a modified ferrozine assay (7); 10 μl of magnetosome suspension was used for determination of iron concentration.

GFP expression in *M. gryphiswaldense* was assayed by fluorometry, as described previously (10).

GusA activity assay. Cells were grown to exponential phase, collected via centrifugation, resuspended in phosphate-buffered saline (PBS), and disrupted using a sonifier. Cell debris was spun down, and the supernatant was used to determine protein concentration using the bicinchoninic acid (BCA) kit from Thermo Scientific. β -Glucuronidase (GusA) activity in the supernatant was also measured, and the assay was carried out at 37°C as described by Wilson et al. (20). Units were nanomoles of product formed per minute per milligram of protein. Duplicate assays were performed, and reported values were averaged from at least three independent cultures.

Biochemical methods. Magnetosome isolation from *M. gryphiswaldense* strains was performed as described previously (7). Polyacrylamide gels were prepared according to the method of Laemmli (21). Magnetosome membranes were dissolved by incubation in 1% SDS at 65°C for 25 min. Protein concentrations were determined using the BCA protein kit (Thermo Scientific), and 100 ng to 1 μg of magnetosome membrane protein was loaded onto 10% (wt/vol) SDS gels and analyzed via quantitative immunoblotting to quantify the expression level of the MamC-GFP fusion protein.

Proteins were electroblotted onto polyvinylidene difluoride (PVDF) membranes (Roth, Germany). Membranes were blocked overnight at 4°C. Primary rabbit anti-GFP IgG antibody (1:500 dilution [Santa Cruz, USA]) was added to the blocking solution and incubated 1 h at room temperature. Membranes were washed 4 times with blocking solution (2.5% [wt/vol] milk powder in Tris-buffered saline [TBS] [50 mM Tris-HCl, pH 7.6; 150 mM NaCl]) for 10 min and incubated with a secondary horseradish peroxidase-labeled goat anti-rabbit IgG antibody (1:2,000 dilution [Promega, USA]) for 1 h. Membranes were washed 4 times with blocking solution for 10 min and finally 5 min in TBS, and immunoreactive proteins were visualized by using an Ace Glow substrate (Pierce, Erlangen) and detected with the LumiImager (Pierce, Erlangen).

RESULTS

Engineering of a cassette for high constitutive gene expression.

We used a stepwise approach (summarized in Fig. S1 in the supplemental material) to optimize the previously identified strong P_{mamDC} , which is located within a 325-bp region upstream of the *mamGFDC* operon. We first attempted to identify the smallest yet transcriptionally active fragment (see Fig. S1A in the supplemental material). Several fragments that were gradually truncated from the 5' end of the 325-bp upstream region of the *mamG* gene were cloned upstream of the *egfp* reporter, yielding the vectors pAP150 and pAP161-pAP164. Whereas a 270-bp fragment displayed the same fluorescence intensity as the untruncated 325-bp version, further truncation to 170, 102, and 45 bp increased the fluorescence 1.5-, 2.2-, and 3-fold, respectively (Fig. 1A). Truncation of the putative promoter region of the *mamGFDC* operon down to 45 bp (still comprising the -35 and -10 regions) increased expression of the reporter gene significantly, possibly because regulatory elements were excluded from the promoter region (22). Therefore, the 45-bp truncated version of P_{mamDC} (designated $P_{mamDC45}$) was chosen for all subsequent experiments.

As optimal spacing between the Shine-Dalgarno (SD) se-

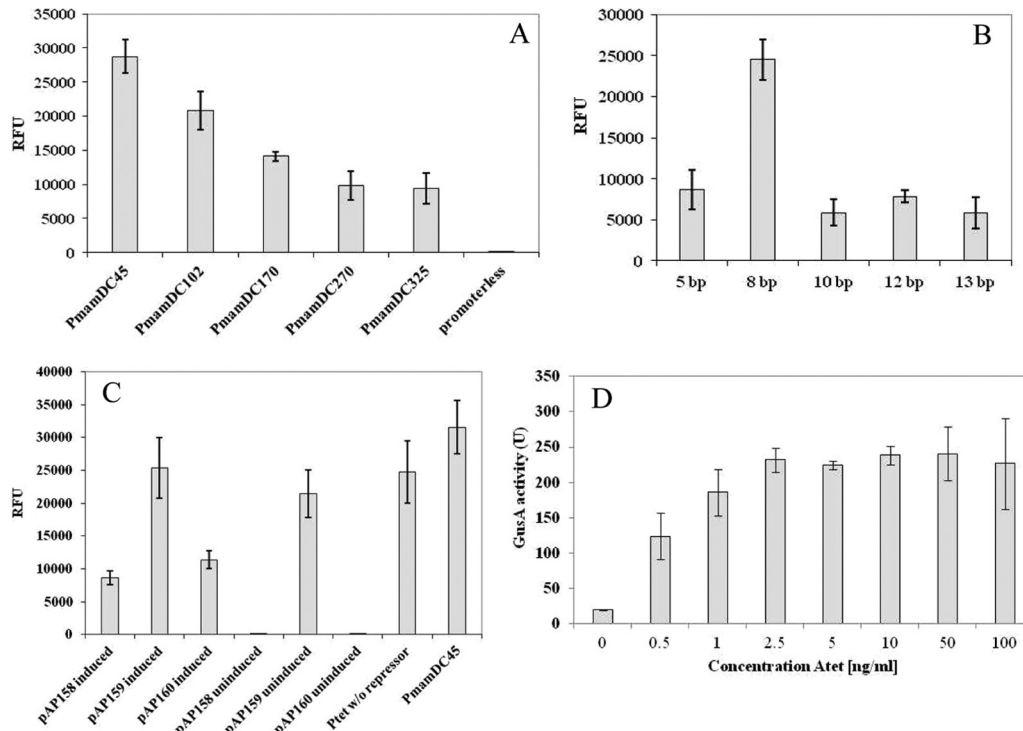


FIG 1 (A to C) Cellular EGFP fluorescence from various expression vectors in *M. gryphiswaldense* measured by fluorometry. Fluorescence was normalized to cell density and reported as relative fluorescence units (RFU). Error bars represent standard deviations, calculated from three independent experiments. (A) Effects of gradual truncation of the P_{mamDC} promoter region from 325 bp down to 45 bp. A strain carrying a promoterless vector displays only weak background fluorescence, also observed for untransformed cells. (B) Effects of variation of the spacing from the start codon from 13 to 5 bp in the RBS. (C) Influence of TetR expression from different promoters on the expression of the reporter EGFP from P_{tet} . (D) GusA activity of cell extract from *M. gryphiswaldense* expressing chromosomal GusA from P_{tet} promoter. GusA activity units are defined as nanomoles of product per minute per milligram of protein.

quence and the start codon has been shown to be crucial for bacterial gene expression (23, 24), we optimized the ribosomal binding site (RBS) for increased expression. To this end, we combined $P_{mamDC45}$ with the original RBS of *mamG*, spaced by variable lengths from the SD sequence to the start codon of *egfp* (see Fig. S1B in the supplemental material). Whereas random single-base-pair substitutions within this region did not increase EGFP fluorescence (data not shown), an 8-bp spacing in combination with $P_{mamDC45}$ caused 2.8-fold-higher fluorescence than the native RBS (13 bp), while spacings of 5, 10, or 12 bp did not increase fluorescence (Fig. 1B). Thus, a spacing-optimized RBS (AGGAGATCAG **CATATG**; RBS in italics and spacing in bold, followed by the start codon), referred to as oRBS, was used in all subsequent optimization steps.

Optimization of Tet-inducible expression. In the next step, we wanted to generate an inducible expression system, which should exhibit tight repression in the absence of inducer while allowing high and tunable expression after induction. A hybrid promoter similar to that described by Yoshino et al. (14), consisting of the $P_{mamDC45}$ promoter and two *tetO* sequences, yielded no expression in *M. gryphiswaldense*. Likewise, we failed to construct various hybrid promoters by combining operators from the Tet and the lactose systems with native *M. gryphiswaldense* promoters, including $P_{mamDC45}$ and the nitrate-responsive P_{nirS} (25). Also, we found none of the tested inducible expression systems reported for other alphaproteobacteria (26–29) to be sufficiently functional in *M. gryphiswaldense*. In a different approach, we failed to recon-

struct a riboswitch that reportedly was functional in the closely related species *M. magneticum* (30) but exhibited high fluorescence in the absence of the inducer theophylline in *M. gryphiswaldense* (data not shown). The widely used P_{lac} promoter yielded inducible yet very weak expression in *M. gryphiswaldense* (our unpublished data).

Therefore, we focused on optimization of the Tn10-derived Tet-inducible system (31), which in this study was found to be the only inducible expression system to be functional in *M. gryphiswaldense*. Cloning P_{tet} upstream of *egfp* (pAP160) yielded significant fluorescence in the presence of 70 ng ml⁻¹ Atet while remaining tightly repressed (i.e., no fluorescence) in the absence of the inducer (Fig. 1C). Previous studies utilizing the *tet* system have shown that constitutive expression of TetR is more favorable for the tight repression of strong promoters than the original auto-regulated expression approach derived from the Tn10 Tet resistance determinant (32); we tested pAP158, pAP159, and pAP160 for expression of the TetR repressor. However, only TetR expressed from the neomycin promoter P_{neo} resulted in tight repression (Fig. 1C). The construct carrying P_{neo} -TetR (pAP160) showed significant expression after induction (about 46% of the fluorescence observed for expression of *egfp* from P_{tet} without repressor). For further optimization, we combined P_{tet} containing two *tetO* sequences with the oRBS and cloned it upstream *egfp* as a reporter (see Fig. S1D in the supplemental material). Although P_{tet} reached only 30% of the fluorescence from constitutive $P_{mamDC45}$, this expression level is sufficiently high for practical purposes,

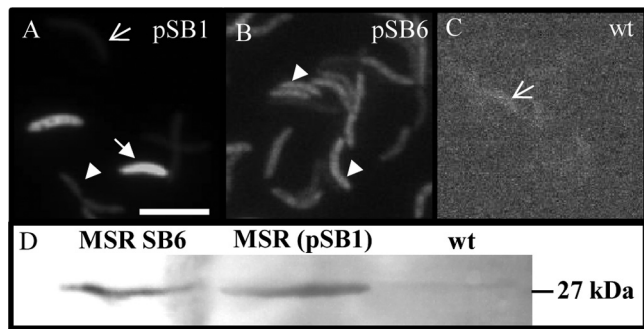


FIG 2 Fluorescence micrographs of *M. gryphiswaldense* expressing Mag-*egfp* under the control of $P_{mamDC45}$ from pSB1 (A) or a chromosomal insertion via pSB6 (B) compared to nonfluorescent *M. gryphiswaldense* wt (C). Arrows indicate nonfluorescent cells, filled arrows indicate strongly fluorescent cells, and arrowheads indicate moderately fluorescent cells. Bar, 2 μm . (D) Western blot of whole *M. gryphiswaldense* cells expressing Mag-*egfp* from the chromosome (pSB6) or plasmid (pSB1). Wt cells were included as a negative control. Mag-EGFP was detected using rabbit anti-GFP IgG as the primary antibody and goat anti-rabbit IgG alkaline phosphatase antibodies as the secondary antibody.

while still maintaining tight repression in the absence of inducer. Therefore, P_{neo} -TetR was chosen for further engineering of an inducible expression cassette.

Chromosomal insertion of an expression cassette with a codon-optimized *egfp* reporter gene results in brighter and uniform fluorescence. Expression of foreign genes in *M. gryphiswaldense* (average G+C content = 62.2%) might be limited by different codon usage. We therefore explored the effect of codon optimization, by synthesis of an *egfp* variant based on the average codon usage of *M. gryphiswaldense* (see Fig. S1C in the supplemental material), designated Mag-*egfp* (for *Magnetospirillum*-optimized EGFP) (see Fig. S2 in the supplemental material). If expressed from constitutive $P_{mamDC45}$ with oRBS, even minor adjustments increased fluorescence of the resulting Mag-EGFP by about 30% compared to EGFP (see Fig. S3A in the supplemental material). Western blots of *M. gryphiswaldense* cells expressing either Mag-EGFP (pSB1) or EGFP (pAP150) showed a more intense EGFP band for cells expressing Mag-EGFP than for cells expressing EGFP (see Fig. S3B in the supplemental material). Altogether, the combined optimizations amounted to an 8-fold-increased fluorescence and were cloned together into a single cassette, DC_Mag-EGFP, harbored on pSB1.

Cells expressing Mag-*egfp* from a medium-copy-number plasmid (pSB1) showed a highly heterogenous phenotype: while 50% of cells were not fluorescent at all, about 20% showed only weak and about 30% strong fluorescence (Fig. 2A). Therefore, we attempted single-copy chromosomal integration of the expression cassette Tet_Mag-EGFP_TetR by Tn5-mediated transposition from the pBAM1 (17)-derived insertion plasmids pSB6 ($P_{mamDC45}$) and pSB7 (P_{tet}) (for insertion sites, see Table S4 in the supplemental material). Fluorescence microscopy of populations with insertions of pSB6 and pSB7 showed a uniform phenotype, with about 98% of the cells showing identical levels of intermediate fluorescence (Fig. 2B), while the untransformed wild-type (wt) negative control showed only background fluorescence (Fig. 2C). In Western blots with whole cells of identical cell numbers (Fig. 2D), Mag-EGFP bands of approximately the same intensity were obtained, indicating that overall expres-

sion yields were comparable for populations expressing Mag-EGFP either from the plasmid (pSB1) or chromosomally, although single cells displayed the greatest amplitudes and variation of fluorescence in the population expressing Mag-EGFP from pSB1. We failed to detect intermediate fluorescence levels by varying the inducer concentration between 50 ng ml^{-1} (= saturated fluorescence) and 2.5 ng ml^{-1} (= no fluorescence) but instead observed an all-or-none response. Although different induction kinetics were observed with different amounts of Atet (e.g., after induction for 6 h with 70 ng ml^{-1} Atet, the fluorescence was approximately half of that of the constitutive promoter $P_{mamDC45}$), increasing induction time to 18 h resulted in nearly same expression levels of Mag-EGFP as constitutive conditions (data not shown).

Because of the known limitations of using GFP as the reporter (33), for estimation of induction kinetics we instead used the enzyme β -glucuronidase (GusA), which we recently demonstrated to be an efficient transcriptional reporter in *M. gryphiswaldense* (25). After replacement of Mag-*egfp* by *gusA*, we measured GusA activity in cells harboring a chromosomal copy of both the expression cassette and *gusA* (pSB8) in medium with and without Atet. As with Mag-EGFP, essentially no activity was detectable in the absence of inducer (Fig. 1D). While for Atet concentrations >2.5 ng ml^{-1} induction was maximal and could be not further enhanced by concentrations up to 100 ng ml^{-1} , between 0.5 and 1 ng ml^{-1} a nearly linear response was observed (Fig. 1D). In summary, this demonstrated that transcriptional activity of P_{tet} is tunable within a narrow range of inducer concentrations. As observed with Mag-EGFP, maximum induction of P_{tet} yielded about one-third of the constitutively expressed GusA activity (data not shown).

Next, we attempted inducible expression of fusion proteins displayed on magnetosomes (7). Therefore, Mag-*egfp* was replaced by *mamC*-Mag-*egfp*, which was fused via a 10-glycine linker and cloned into pSB7. The resulting construct, pJH2, was chromosomally inserted into *M. gryphiswaldense* strain ΔC (harboring a single gene deletion of *mamC* [34]) cells to eliminate the background of nonfused MamC. Uninduced cells showed no fluorescence at all, while after addition of 70 ng ml^{-1} Atet, a linear fluorescence pattern characteristic of chain localization at midcell was observed after 6 to 18 h by fluorescence microscopy (see Fig. S4B and C in the supplemental material). Magnetosomes purified from this strain exhibited strong and even fluorescence under the microscope (see Fig. S5 in the supplemental material). This also demonstrates that the expression of magnetosome proteins and foreign proteins fused to them as well as their subsequent targeting to MM can be induced.

Optimized magnetosome expression of fusion proteins. Because maximum expression levels obtained with both inducible and constitutive promoters proved to be limiting for even higher magnetosome expression, we attempted to further increase magnetosome expression of foreign genes by increasing their dosage. To this end, we fused the C terminus of our MamC anchor via 10 glycine residues to a sequence variant of *egfp*, connecting them to each other by an alpha helix linker. This was a precaution to reduce homologous recombination between the two copies, as *egfp* and Mag-*egfp* share only 89% nucleotide identity. The Mag-EGFP-EGFP construct was then cloned into pJH1, yielding pJH3, which carried the optimized constitutive expression cassette DC_MamC-Mag-EGFP-EGFP and was chromosomally inserted into

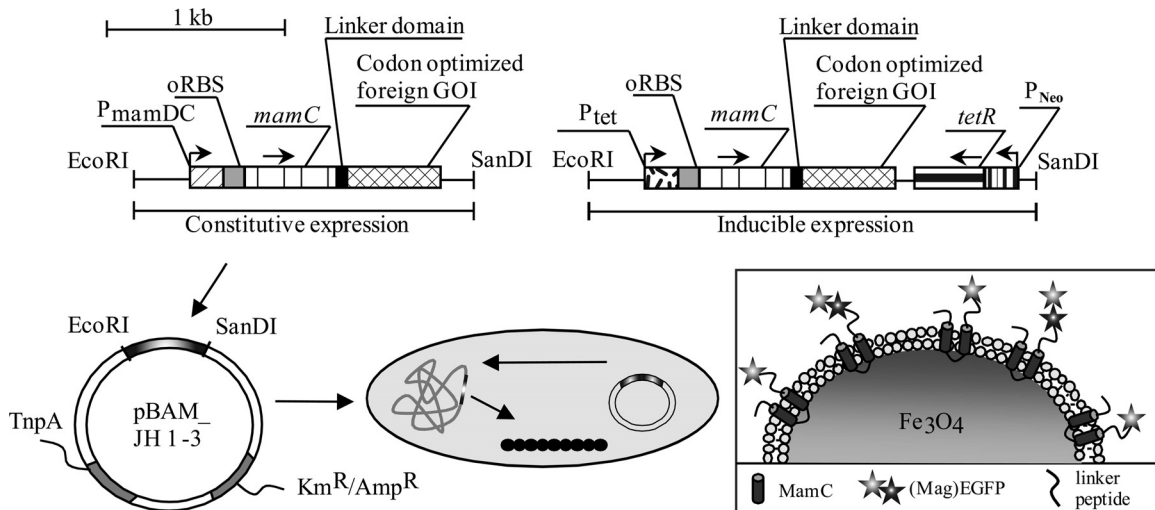


FIG 3 Schematics of optimized expression vectors (DC_Mag-EGFP and Tet_Mag-EGFP_TetR or Mag-EGFP-EGFP fusion) and chromosomal insertion. Expression vectors contained either the strong optimized $P_{mamDC45}$ or the inducible P_{tet} promoter, the optimized oRBS, and the magnetosome anchor *mamC*, which can be fused via a linker domain to any codon-optimized heterologous gene of interest (GOI). Insertion into the chromosome is via pBAM1-derived insertional plasmids and chromosome expression of fusion proteins.

M. gryphiswaldense ΔC (Fig. 3). Cells harboring Mag-EGFP-EGFP displayed much stronger fluorescence signals at midcell than cells with only a single Mag-EGFP fusion (see Fig. S4D in the supplemental material). Expression of the Mag-EGFP-EGFP fusion affected neither the biomineralization of magnetosomes nor the thickness and appearance of the MM (Fig. 4A and B). To estimate the amount of MamC-Mag-EGFP and MamC-Mag-EGFP-EGFP, we performed quantitative Western blots on extracted MM. As expected, immunostaining of Mag-EGFP-EGFP (pJH3) yielded a significantly stronger 74-kDa band than that of single Mag-EGFP (Mag-EGFP-EGFP was diluted 10 \times for quantitative Western blot analysis) (Fig. 4C). Using a GFP standard (Fig. 4D), we estimated that magnetosomes isolated from strain JH1 (displaying MamC-Mag-EGFP expressed from $P_{mamDC45}$)

contained approximately 33 ng Mag-EGFP per μg magnetite (as measured by iron content). If expressed from P_{tet} (strain JH2), 9 ng Mag-EGFP was detected per μg magnetite. Magnetosomes expressing a MamC-Mag-EGFP-EGFP fusion from $P_{mamDC45}$ (strain JH3) displayed a much stronger band than the other samples, corresponding to 83 ng (Mag-)EGFP per μg magnetite (Fig. 4C; for details, see Fig. S7A and B in the supplemental material).

DISCUSSION

We optimized and constructed versatile cassettes that allow either inducible or high-level constitutive expression and magnetosome display of foreign proteins in *M. gryphiswaldense*.

Increased constitutive expression was accomplished by the combined effect of various optimization steps, which altogether yielded an 8-fold-higher expression of the cytoplasmic Mag-EGFP reporter than previously available systems. The truncation also yielded a compact, easy-to-clone gene cassette, whose extension of 58 bp is within the typical range of other prokaryotic promoters (40 to 65 bp) (35).

None of the several tested inducible expression systems from other alphaproteobacteria were found to be functional in *M. gryphiswaldense*, because of lack of either expression or repression. We also failed to construct a functional tetracycline-responsive hybrid promoter by combining the optimized $P_{mamDC45}$ with operators (*tetO*) and the repressor (TetR) from the well-characterized *tet* system (31), which is functional in a vast variety of bacteria (36, 37). Although a similar system was reported for the related *M. magneticum* (14), in *M. gryphiswaldense* different variants of hybrid promoters lacked functionality, possibly due to the absence of further regulatory elements in the genetic neighborhood of $P_{mamDC45}$ (38).

However, we found that in *M. gryphiswaldense* the original $Tn10 P_{tet}$ promoter is tightly repressed but can be induced to reasonably high expression levels in the presence of saturating Atet concentrations as low as 2.5 ng ml $^{-1}$. This is 40-, 80-, 160-, and even 200-fold lower than in *Helicobacter pylori* (36), *E. coli* (39), *Bacillus subtilis* (37), and *M. magneticum* (14), respectively, while

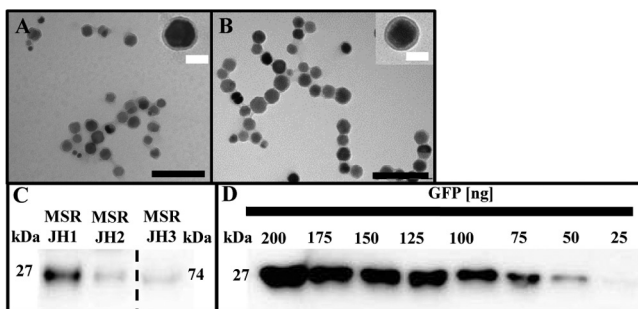


FIG 4 (A and B) Transmission electron micrographs of purified magnetosomes from *M. gryphiswaldense* ΔC JH3 (A) and wt (B), showing no effect on MM or magnetite crystals. Black scale bar, 200 nm; white scale bar, 40 nm. (C) Quantitative Western blot of (Mag-)EGFP in the MM, isolated from *M. gryphiswaldense* strains expressing different chromosomal *mamC*-Mag-*egfp* fusions from $P_{mamDC45}$ (JH1) and P_{tet} (JH2) and *mamC*-Mag-*egfp*-*egfp* fusions (JH3) from $P_{mamDC45}$. (Mag-)EGFP was detected by rabbit anti-GFP IgG as the primary antibody and goat anti-rabbit IgG horseradish peroxidase antibodies as secondary antibodies. The sample containing the Mag-EGFP-EGFP fusion was diluted 10 \times for quantitative Western blot analysis. Band sizes are as follows: GFP, 27 kDa; 2 \times GFP, 74 kDa. (D) Recombinant GFP was used as a standard.

the regulatory range (up to 12-fold with the reporter GusA) is comparable to *tet*-responsive systems in other bacteria (*S. aureus*, 50- to 100-fold; *S. pneumoniae*, 5-fold [40, 41]). We also found that a chromosomal insertion of Tet_MamC–Mag-EGFP_TetR from vector pJH2 provides tight TetR-mediated silencing of MamC–Mag-EGFP, while induction in magnetosome-containing wt cells caused Mag-EGFP to be reasonably expressed on magnetosomes after only 6 h. This implies that insertion of newly synthesized MamC–Mag-EGFP fusion proteins into the MM of pre-existing magnetosome particles is possible. In addition to magnetosome display, the TetR-controlled expression system could also be used for the generation of conditional knockouts and gene depletion studies and thus extends the genetic toolbox available in *M. gryphiswaldense*. Despite these improvements, maximum expression of fully induced P_{tet} reaches only 30% of constitutive $P_{mamDC45}$ -driven expression. However, this level is sufficient and appropriate for many practical purposes.

Inhomogeneous expression (that is, uneven expression levels varying between individuals) of the reporter gene from plasmids in isogenic cultures is frequently observed in bacteria (42, 43). We achieved a much more homogenous Mag-EGFP expression by chromosomal insertion of single copies than did previous attempts with multicopy expression (7, 8). Tn5-mediated transposition allows straightforward, single-site integration into the host chromosome, despite the possible disadvantage of random insertion. One caveat of using Tn5-mediated transposition is that the expression cassette integrates randomly into genomic loci of unknown function, possibly causing unwanted mutations. However, all insertants lacked obvious phenotypes with respect to growth and magnetosome formation (compare Fig. S6A and B in the supplemental material), indicating the absence of effects on host metabolism. On the other hand, reporter expression in the absence or presence of inducer were similar in all insertants, suggesting that no interference such as read-through from external promoters occurred.

In addition to increased transcription, using GFP as a model we explored two strategies to enhance translation of foreign proteins. First, we demonstrated that even minor adjustments of the codon usage closer to that of *M. gryphiswaldense* (62.2% G+C) increased the fluorescence of the resulting synthetic Mag-EGFP (*Magnetospirillum*-optimized EGFP) by 30%, which thus represents a reporter with increased sensitivity for future tagging and localization studies. Codon optimization seems promising also for boosting expression of other foreign proteins, as demonstrated in other bacteria (44).

Second, we showed that magnetosome expression of foreign proteins can also be enhanced by increasing their copy number. In similar approaches, Choi and coworkers integrated double copies of the *cym* repressor into *Methylobacterium extorquens*, thereby achieving tight repression of an inducible promoter (45). In the same organism, expression of five chromosomal copies of *gfp* resulted in 20-fold-higher expression than single-copy expression (46). Multicopy insertion of recombinant pathways can increase gene expression by 60% in contrast to plasmid expression of the same pathway in *E. coli* (47). In our study, duplication of (Mag-) *egfp* fused in tandem to *mamC* resulted in strong fluorescence and 2.5-fold increased expression of the (Mag-)EGFP reporter on magnetosomes. Mag-EGFP–EGFP fusions displayed proteolytic stability, as no cleavage products could be detected via Western

blotting. These engineered magnetosomes represent magnetic nanoparticles with greatly enhanced fluorescence, which could be of immediate relevance for a number of applications, such as, for instance, as bimodal contrast agents for both magnetic resonance imaging (MRI) and near-infrared fluorescence optical (NIRF) imaging (48). In addition, magnetosome-expressed single and tandem EGFP fusions with enhanced fluorescence intensity and uniformity can be used as fluorescent tags to follow intracellular protein localization or to study the intricate cell biology of this and other magnetic bacteria. MamC–Mag-EGFP expression driven by $P_{mamDC45}$ resulted in 33 ng Mag-EGFP per μg magnetite, which was 3.6-fold higher than that from P_{tet} (9 ng μg^{-1} magnetite). The amount of (Mag-)EGFP obtained with Mag-EGFP–EGFP fusion per μg magnetite was 83 ng and thus 2.5-fold higher than single copy MamC–Mag-EGFP expressed constitutively. Based on these data, we attempted to estimate the copy number of GFP proteins expressed on single magnetosome particles. Assuming a diameter of 37.5 nm for a single magnetite crystal as determined by transmission electron microscopy, a density of 5.24 g/cm³ for magnetite, and for simplicity an approximately spherical shape, this would result in a volume of 2.76×10^{-17} cm³ and mass of 1.45×10^{-16} g for an average single magnetosome crystal (see Fig. S7C in the supplemental material). For MamC–Mag-EGFP expressed from $P_{mamDC45}$, we thus can estimate about 100 Mag-EGFP copies per magnetosome, while only about 30 copies were present if the same construct was expressed from P_{tet} . 250 (Mag-)EGFP copies per particle were calculated for the Mag-EGFP–EGFP fusion. This more-than-double amount of (Mag-)EGFP might be due to increased stability of the Mag-EGFP–EGFP fusion or, alternatively, just to the variability of magnetosome sizes, which to some extent depend on the growth stage of the cells. Assuming a lower size of only 35 nm and an upper size of 48 nm (as found within the typical range of variation [49]), the same calculations would yield GFP copy numbers of 80 to 210 in strain JH1 and 200 to 520 (Mag-EGFP–EGFP fusion) in strain JH3. Assuming MamC-to-Mag-EGFP ratios of 1:1 for the single protein and 1:2 for the Mag-EGFP–EGFP fusion, the number of MamC copies per magnetosome particle is most likely within the range of 80 to 260. Assuming a surface area of 4,417 nm² for a 37.5-nm magnetosome particle and a diameter of approximately 3.45 nm for the 12.5-kDa MamC protein (7), the theoretical number of MamC copies that would cover the entire particle surface would be 1,280. However, as previous estimations revealed MamC to be only a part (relative abundance, 16.3% [50]) of the MM, which contains about 20 different proteins (50), the estimated 80 to 250 copies occupying about 6 to 20% of the surface seem to be a realistic range. Thus, the number of MamC molecules that can serve as fusion anchors is unlikely to be further increased without disturbing MM function. Instead, increasing the number of protein units fused to a single MamC anchor, as shown by our Mag-EGFP–EGFP fusion, is a more appropriate route to increase yields of heterologous proteins expressed per particle.

ACKNOWLEDGMENTS

We thank J. Armitage, S. K. Farrand, P. S. Poole, and M. Thanbichler for providing several expression plasmids, V. de Lorenzo for providing the pBAM1 vector, and K. T. Silva for help with arbitrary PCR.

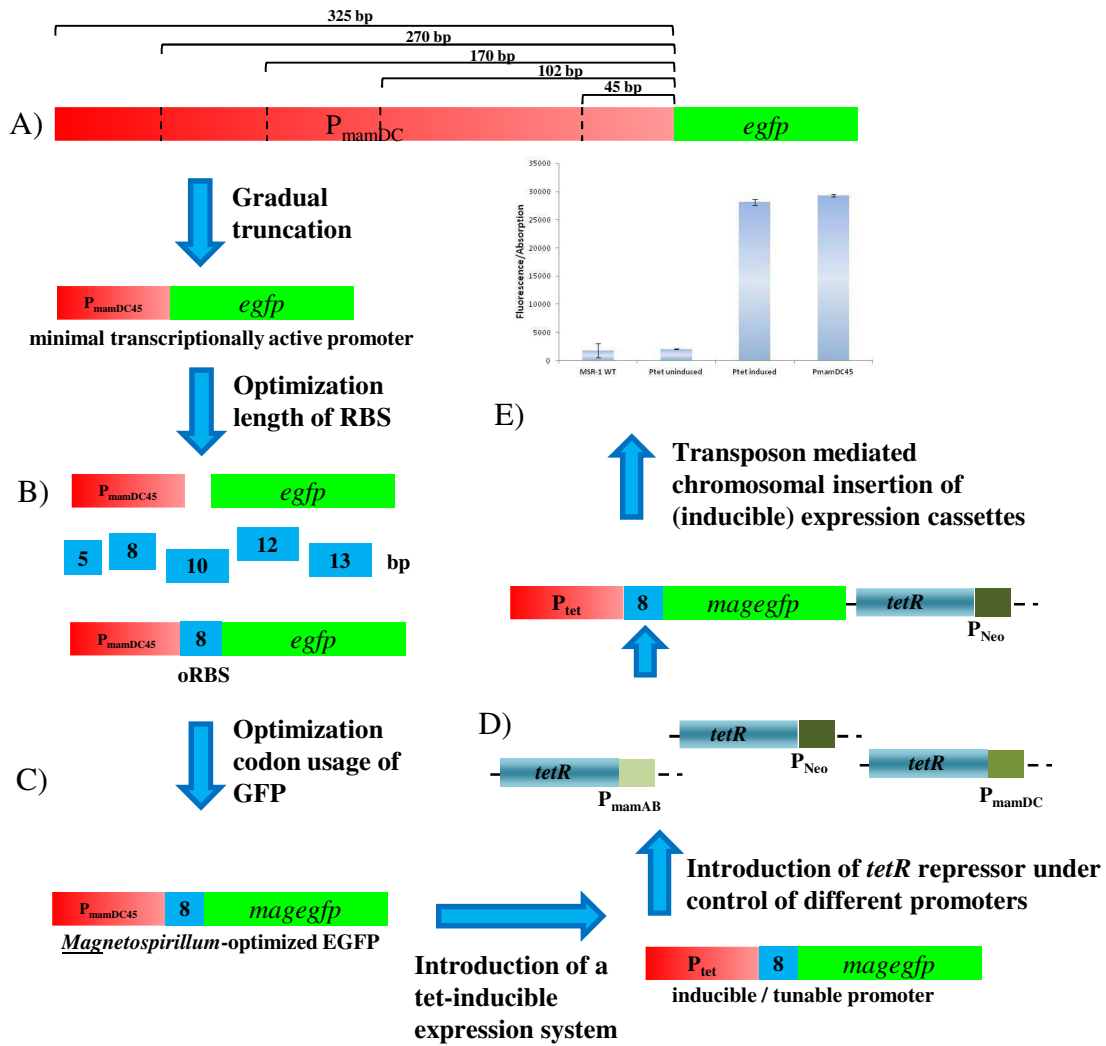
This project was funded by DFG grants Schu 12-1 and 15-1.

REFERENCES

- Jogler C, Schüler D. 2009. Genomics, genetics, and cell biology of magnetosome formation. *Annu. Rev. Microbiol.* 63:501–521. <http://dx.doi.org/10.1146/annurev.micro.62.081307.162908>.
- Komeili A. 2012. Molecular mechanisms of compartmentalization and biomineralization in magnetotactic bacteria. *FEMS Microbiol. Rev.* 36:232–255. <http://dx.doi.org/10.1111/j.1574-6976.2011.00315.x>.
- Lang C, Schüler D, Faivre D. 2007. Synthesis of magnetite nanoparticles for bio- and nanotechnology: genetic engineering and biomimetics of bacterial magnetosomes. *Macromol. Biosci.* 7:144–151. <http://dx.doi.org/10.1002/mabi.200600235>.
- Faivre D, Schüler D. 2008. Magnetotactic bacteria and magnetosomes. *Chem. Rev.* 108:4875–4898. <http://dx.doi.org/10.1021/cr078258w>.
- Ceyhan B, Alhorn P, Lang C, Schüler D, Niemeyer CM. 2006. Semi-synthetic biogenic magnetosome nanoparticles for the detection of proteins and nucleic acids. *Small* 2:1251–1255. <http://dx.doi.org/10.1002/smll.200600282>.
- Wacker R, Ceyhan B, Alhorn P, Schüler D, Lang C, Niemeyer CM. 2007. Magneto Immuno-MR: a novel immunoassay based on biogenic magnetosome nanoparticles. *Biochem. Biophys. Res. Commun.* 357:391–396. <http://dx.doi.org/10.1016/j.bbrc.2007.03.156>.
- Lang C, Schüler D. 2008. Expression of green fluorescent protein fused to magnetosome proteins in microaerophilic magnetotactic bacteria. *Appl. Environ. Microbiol.* 74:4944–4953. <http://dx.doi.org/10.1128/AEM.00231-08>.
- Ohuchi S, Schüler D. 2009. In vivo display of a multisubunit enzyme complex on biogenic magnetic nanoparticles. *Appl. Environ. Microbiol.* 75:7734–7738. <http://dx.doi.org/10.1128/AEM.01640-09>.
- Pollithy A, Romer T, Lang C, Müller FD, Helma J, Leonhardt H, Rothbauer U, Schüler D. 2011. Magnetosome expression of functional camelid antibody fragments (nanobodies) in *Magnetospirillum gryphiswaldense*. *Appl. Environ. Microbiol.* 77:6165–6171. <http://dx.doi.org/10.1128/AEM.05282-11>.
- Lang C, Pollithy A, Schüler D. 2009. Identification of promoters for efficient gene expression in *Magnetospirillum gryphiswaldense*. *Appl. Environ. Microbiol.* 75:4206–4210. <http://dx.doi.org/10.1128/AEM.02906-08>.
- Schütte S, Würdemann C, Peplies J, Heyen U, Wawer C, Glöckner FO, Schüler D. 2006. Transcriptional organization and regulation of magnetosome operons in *Magnetospirillum gryphiswaldense*. *Appl. Environ. Microbiol.* 72:5757–5765. <http://dx.doi.org/10.1128/AEM.00201-06>.
- Yoshino T, Kato F, Takeyama H, Nakai M, Yakabe Y, Matsunaga T. 2005. Development of a novel method for screening of estrogenic compounds using nano-sized bacterial magnetic particles displaying estrogen receptor. *Anal. Chim. Acta* 532:105–111. <http://dx.doi.org/10.1016/j.aca.2004.10.074>.
- Yoshino T, Takahashi M, Takeyama H, Okamura Y, Kato F, Matsunaga T. 2004. Assembly of G protein-coupled receptors onto nanosized bacterial magnetic particles using Mms16 as an anchor molecule. *Appl. Environ. Microbiol.* 70:2880–2885. <http://dx.doi.org/10.1128/AEM.70.5.2880-2885.2004>.
- Yoshino T, Shimojo A, Maeda Y, Matsunaga T. 2010. Inducible expression of transmembrane proteins on bacterial magnetic particles in *Magnetospirillum magneticum* AMB-1. *Appl. Environ. Microbiol.* 76:1152–1157. <http://dx.doi.org/10.1128/AEM.01755-09>.
- Heyen U, Schüler D. 2003. Growth and magnetosome formation by microaerophilic *Magnetospirillum* strains in an oxygen-controlled fermentor. *Appl. Microbiol. Biotechnol.* 61:536–544. <http://dx.doi.org/10.1007/s00253-002-1219-x>.
- Sambrook J, Russell D. 2001. *Molecular cloning: a laboratory manual*, 3rd ed, p 1–44. Cold Spring Harbor Laboratory Press, New York, NY.
- Martinez-Garcia E, Calles B, Arevalo-Rodriguez M, de Lorenzo V. 2011. pBAM1: an all-synthetic genetic tool for analysis and construction of complex bacterial phenotypes. *BMC Microbiol.* 11:38. <http://dx.doi.org/10.1186/1471-2180-11-38>.
- Bryksin AV, Matsumura I. 2010. Overlap extension PCR cloning: a simple and reliable way to create recombinant plasmids. *Biotechniques* 48:463–465. <http://dx.doi.org/10.2144/000113418>.
- Schüler D, Rainer U, Bäuerlein E. 1995. A simple light-scattering method to assay magnetism in *Magnetospirillum gryphiswaldense*. *FEMS Microbiol. Lett.* 132:139–145. <http://dx.doi.org/10.1111/j.1574-6968.1995.tb07823.x>.
- Wilson KJ, Hughes SG, Jefferson RA. 1992. The *Escherichia coli* gus operon: induction and expression of the gus operon in *E. coli* and the occurrence and use of GUS in other bacteria, p 7–22. *In* Gallagher SR (ed), *Using the GUS gene as reporter of gene expression*. Academic Press Inc., San Diego, CA.
- Laemmli UK. 1970. Cleavage of structural proteins during the assembly of the head of bacteriophage T4. *Nature* 227:680–685. <http://dx.doi.org/10.1038/227680a0>.
- Haugen SP, Ross W, Gourse RL. 2008. Advances in bacterial promoter recognition and its control by factors that do not bind DNA. *Nat. Rev. Microbiol.* 6:507–519. <http://dx.doi.org/10.1038/nrmicro1912>.
- Chen HY, Bjercknes M, Kumar R, Jay E. 1994. Determination of the optimal aligned spacing between the Shine-Dalgarno sequence and the translation initiation codon of *Escherichia coli* messenger RNAs. *Nucleic Acids Res.* 22:4953–4957. <http://dx.doi.org/10.1093/nar/22.23.4953>.
- Ma J, Campbell A, Karlin S. 2002. Correlations between Shine-Dalgarno sequences and gene features such as predicted expression levels and operon structures. *J. Bacteriol.* 184:5733–5745. <http://dx.doi.org/10.1128/JB.184.20.5733-5745.2002>.
- Li YJ, Katzmann E, Borg S, Schüler D. 2012. The periplasmic nitrate reductase Nap is required for anaerobic growth and involved in redox control of magnetite biomineralization in *Magnetospirillum gryphiswaldense*. *J. Bacteriol.* 194:4847–4856. <http://dx.doi.org/10.1128/JB.00903-12>.
- Ind AC, Porter SL, Brown MT, Byles ED, de Beyer JA, Godfrey SA, Armitage JP. 2009. Inducible-expression plasmid for *Rhodobacter sphaeroides* and *Paracoccus denitrificans*. *Appl. Environ. Microbiol.* 75:6613–6615. <http://dx.doi.org/10.1128/AEM.01587-09>.
- Khan SR, Gaines J, Roop RM, Farrand SK. 2008. Broad-host-range expression vectors with tightly regulated promoters and their use to examine the influence of TraR and TraM expression on Ti plasmid quorum sensing. *Appl. Environ. Microbiol.* 74:5053–5062. <http://dx.doi.org/10.1128/AEM.01098-08>.
- Tett AJ, Rudder SJ, Bourdes A, Karunakaran R, Poole PS. 2012. Regulatable vectors for environmental gene expression in *Alphaproteobacteria*. *Appl. Environ. Microbiol.* 78:7137–7140. <http://dx.doi.org/10.1128/AEM.01188-12>.
- Thanbichler M, Iniesta AA, Shapiro L. 2007. A comprehensive set of plasmids for vanillate- and xylose-inducible gene expression in *Caulobacter crescentus*. *Nucleic Acids Res.* 35:e137. <http://dx.doi.org/10.1093/nar/gkm818>.
- Topp S, Reynoso CMK, Seeliger JC, Goldlust IS, Desai SK, Murat D, Shen A, Puri AW, Komeili A, Bertozzi CR, Scott JR, Gallivan JP. 2010. Synthetic riboswitches that induce gene expression in diverse bacterial species. *Appl. Environ. Microbiol.* 76:7881–7884. <http://dx.doi.org/10.1128/AEM.01537-10>.
- Hillen W, Berens C. 1994. Mechanisms underlying expression of Tn10 encoded tetracycline resistance. *Annu. Rev. Microbiol.* 48:345–369. <http://dx.doi.org/10.1146/annurev.mi.48.100194.002021>.
- Kamionka A, Bertram R, Hillen W. 2005. Tetracycline-dependent conditional gene knockout in *Bacillus subtilis*. *Appl. Environ. Microbiol.* 71:728–733. <http://dx.doi.org/10.1128/AEM.71.2.728-733.2005>.
- Cubitt AB, Heim R, Adams SR, Boyd AE, Gross LA, Tsien RY. 1995. Understanding, improving and using green fluorescent proteins. *Trends Biochem. Sci.* 20:448–455. [http://dx.doi.org/10.1016/S0968-0004\(00\)89099-4](http://dx.doi.org/10.1016/S0968-0004(00)89099-4).
- Scheffel A, Gärdes A, Grünberg K, Wanner G, Schüler D. 2008. The major magnetosome proteins MamGFDC are not essential for magnetite biomineralization in *Magnetospirillum gryphiswaldense* but regulate the size of magnetosome crystals. *J. Bacteriol.* 190:377–386. <http://dx.doi.org/10.1128/JB.01371-07>.
- Hawley DK, McClure WR. 1983. Compilation and analysis of *Escherichia coli* promoter DNA sequences. *Nucleic Acids Res.* 11:2237–2255. <http://dx.doi.org/10.1093/nar/11.8.2237>.
- Debowski AW, Verbrugghe P, Sehnl M, Marshall BJ, Benghezal M. 2013. Development of a tetracycline-inducible gene expression system for the study of *Helicobacter pylori* pathogenesis. *Appl. Environ. Microbiol.* 79:7351–7359. <http://dx.doi.org/10.1128/AEM.02701-13>.
- Geissendörfer M, Hillen W. 1990. Regulated expression of heterologous genes in *Bacillus subtilis* using the Tn10 encoded Tet regulatory elements. *Appl. Microbiol. Biotechnol.* 33:657–663. <http://dx.doi.org/10.1007/BF00604933>.
- Guss AM, Rother M, Zhang JK, Kulkarni G, Metcalf WW. 2008. New methods for tightly regulated gene expression and highly efficient chromosomal integration of cloned genes for *Methanosarcina* species. *Archaea* 2:193–203. <http://dx.doi.org/10.1155/2008/534081>.

39. Skerra A. 1994. Use of the tetracycline promoter for the tightly regulated production of a murine antibody fragment in *Escherichia coli*. *Gene* 151: 131–135. [http://dx.doi.org/10.1016/0378-1119\(94\)90643-2](http://dx.doi.org/10.1016/0378-1119(94)90643-2).
40. Ji YD, Marra A, Rosenberg M, Woodnutt G. 1999. Regulated antisense RNA eliminates alpha-toxin virulence in *Staphylococcus aureus* infection. *J. Bacteriol.* 181:6585–6590.
41. Stieger M, Wohlgensinger B, Kamber M, Lutz R, Keck W. 1999. Integrational plasmids for the tetracycline-regulated expression of genes in *Streptococcus pneumoniae*. *Gene* 226:243–251. [http://dx.doi.org/10.1016/S0378-1119\(98\)00561-7](http://dx.doi.org/10.1016/S0378-1119(98)00561-7).
42. Davidson CJ, Surette MG. 2008. Individuality in bacteria. *Annu. Rev. Genet.* 42:253–268. <http://dx.doi.org/10.1146/annurev.genet.42.110807.091601>.
43. Siegele DA, Hu JC. 1997. Gene expression from plasmids containing the *araBAD* promoter at subsaturating inducer concentrations represents mixed populations. *Proc. Natl. Acad. Sci. U. S. A.* 94:8168–8172. <http://dx.doi.org/10.1073/pnas.94.15.8168>.
44. Grosjean H, Fiers W. 1982. Preferential codon usage in prokaryotic genes: the optimal codon-anticodon interaction energy and the selective codon usage in efficiently expressed genes. *Gene* 18:199–209. [http://dx.doi.org/10.1016/0378-1119\(82\)90157-3](http://dx.doi.org/10.1016/0378-1119(82)90157-3).
45. Choi YJ, Morel L, Bourque D, Mullick A, Massie B, Miguez CB. 2006. Bestowing inducibility on the cloned methanol dehydrogenase promoter (P_{mxaf}) of *Methylobacterium extorquens* by a applying regulatory elements of *Pseudomonas putida* F1. *Appl. Environ. Microbiol.* 72:7723–7729. <http://dx.doi.org/10.1128/AEM.02002-06>.
46. Choi YJ, Bourque D, Morel L, Groleau D, Miguez CB. 2006. Multicopy integration and expression of heterologous genes in *Methylobacterium extorquens* ATCC 55366. *Appl. Environ. Microbiol.* 72:753–759. <http://dx.doi.org/10.1128/AEM.72.1.753-759.2006>.
47. Tyo KEJ, Ajikumar PK, Stephanopoulos G. 2009. Stabilized gene duplication enables long-term selection-free heterologous pathway expression. *Nat. Biotechnol.* 27:760–765. <http://dx.doi.org/10.1038/nbt.1555>.
48. Lisy MR, Hartung A, Lang C, Schüler D, Richter W, Reichenbach JR, Kaiser WA, Hilger I. 2007. Fluorescent bacterial magnetic nanoparticles as bimodal contrast agents. *Invest. Radiol.* 42:235–241. <http://dx.doi.org/10.1097/01.rli.0000255832.44443.e7>.
49. Lohße A, Ullrich S, Katzmann E, Borg S, Wanner G, Richter M, Voigt B, Schweder T, Schüler D. 2011. Functional analysis of the magnetosome island in *Magnetospirillum gryphiswaldense*: the *mamAB* operon is sufficient for magnetite biomineralization. *PLoS One* 6:e25561. <http://dx.doi.org/10.1371/journal.pone.0025561>.
50. Grünberg K, Müller EC, Otto A, Reszka R, Linder D, Kube M, Reinhardt R, Schüler D. 2004. Biochemical and proteomic analysis of the magnetosome membrane in *Magnetospirillum gryphiswaldense*. *Appl. Environ. Microbiol.* 70:1040–1050. <http://dx.doi.org/10.1128/AEM.70.2.1040-1050.2004>.

Optimization of gene expression cassette for *M. gryphiswaldense*

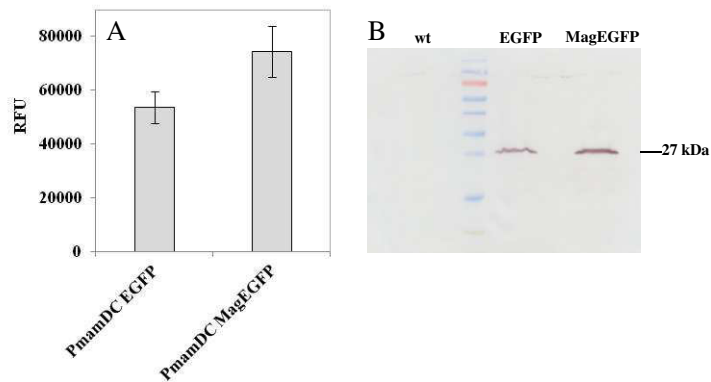


Suppl. Fig. S1: Optimization strategy of (inducible) expression cassette.

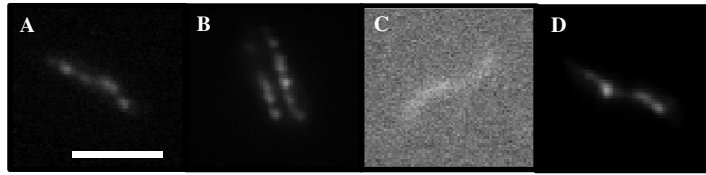
CLUSTAL 2.1 multiple sequence alignment

```
non-opt      ATGGTGAGCAAGGGCGAGGAGCTGTTACCGGGGTGGTGCCATCCTGGTCGAGCTGGAC 60
opt          ATGGTGTGCAAGGGCGAGGAACTGTTACCGGCGTCTGTCGCCATCCTGGTCGAGCTGGAC 60
*****
non-opt      GCGACGTAAACGGCCACAAGTTCAGCGTGTCCGGCGAGGGCGAGGGCGATGCCACCTAC 120
opt          GCGACGTCAACGGCCATAAGTTCAGCGTGTCCGGCGAGGGCGAAGGGCGAGCCACCTAI 120
*****
non-opt      GGCRAAGCTGACCCTGAAGTTCATCTGCACCACCGGCAAGCTGCCCGTGCCTGSCCCACC 180
opt          GGCRAAGCTGACCCTGAAGTTCATCTGCACCACCGGCAAGCTGCCCGTGCCTGSCCCACC 180
*****
non-opt      CTCGTGACCACCCTGACCTACGGCGTGCAGTGTTCAGCGGCTACCCCGACCACATGAAG 240
opt          CTCGTGACCACCCTGACCTACGGCGTGCAGTGTTCAGCGGCTACCCCGACCACATGAAG 240
*****
non-opt      CAGCAGACTTCTTCAAGTCCGCCATGCCGAGGCTACGTCCAGGAGCGCACCAITTC 300
opt          CAGCAGACTTCTTCAAGTCCGCCATGCCGAGGCTACGTCCAGGAGCGCACCAITTC 300
*****
non-opt      TTCRAAGGACGACGGCACTACAAAGACCGCGCCGAGGTGAAGTTCGAGGGCGACACCCTG 360
opt          TTCRAAGGACGACGGCACTACAAAGACCGCGCCGAGGTGAAGTTCGAGGGCGACACCCTG 360
*****
non-opt      GTGAACCGCAICGAGCTGAAGGGCAICGACTTCAAGGAGGACGGCAACATCCTGGGGCAC 420
opt          GTCAACCGCAICGAGCTGAAGGGCAICGACTTCAAGGAGGATGGCAACATCCTGGGGCAC 420
*****
non-opt      AAGCTGGAGTACAACCTACAACAGCCACAACGCTATATATCAITGGCCGACAAAGCAGAAGAAC 480
opt          AAGCTGGAAATATAACTATAACTCGCACACGCTATATATCAITGGCCGACAAAGCAGAAGAAC 480
*****
non-opt      GGCATCAAGGTGAACCTTCAAGATCCGCCACAACATCGAGGACGGCGAGCTGCAGCTCGCC 540
opt          GGCATCAAGGTCAACTTCAAGATCCGCCATAACATCGAGGACGGCTCGGTCCAGCTGGCC 540
*****
non-opt      GACCACTACCAGCAGAACACCCCAICGGCGACGGCCCGGTGCTGCTGCCGACAAACCAAC 600
opt          GACCAITATCAGCAGAACACCCGATCGGCGACGGCCCGGTCTGCTGCCGACAAACCAI 600
*****
non-opt      TACCTGAGCACCAGTCCGCCCTGAGCAAGACCCCAACGAGAGCGCGATCACATGGTC 660
opt          TATCTGTCCACCAGTCCGCCCTGTGCAAGACCCCAACGAGAGCGCGACCAATGGTC 660
*****
non-opt      CTGCTGGAGTTCGTGACCGCCGCCGGATCACTCTCGGCAITGGACGAGCTGTACAAGTAA 720
opt          CTGCTGGAGTTCGTGACCGCCGCCGGATCACTCTCGGCAITGGACGAGCTGTATAAGTGA 720
*****
```

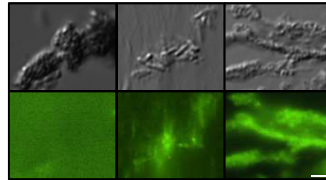
Suppl. Fig S2: Sequence alignment of non-optimized *egfp* and *Magnetospirillum*-optimized *magegfp* using CLUSTALW (version 2.1, <http://www.ebi.ac.uk/Tools/msa/clustalw2/>). Sequence similarity is 89 %, start and stop codon are overlined.



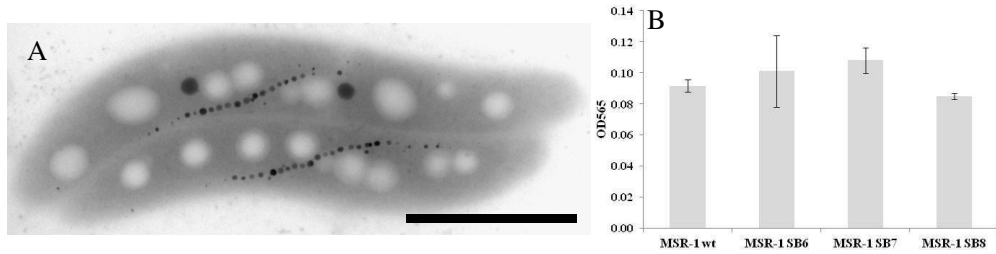
Suppl. Fig S3: (A) Fluorescence of *Magnetospirillum*-optimized (MagEGFP) versus non-optimized GFP (EGFP) expressed from the P_{mamDC45} promoter. Fluorescence was normalized to the cell density and described as relative fluorescence units (RFU). Error bars represent standard deviations, calculated from three independent experiments. (B) Western blot of whole *M. gryphiswaldense* cells expressing EGFP or MagEGFP from the control of the P_{mamDC45}. (Mag)EGFP was detected using rabbit α GFP IgG as primary, and goat anti-rabbit IgG alkaline phosphatase antibodies as secondary antibody. PageRuler™ Prestained Protein Ladder from fermentas was used as a standard.



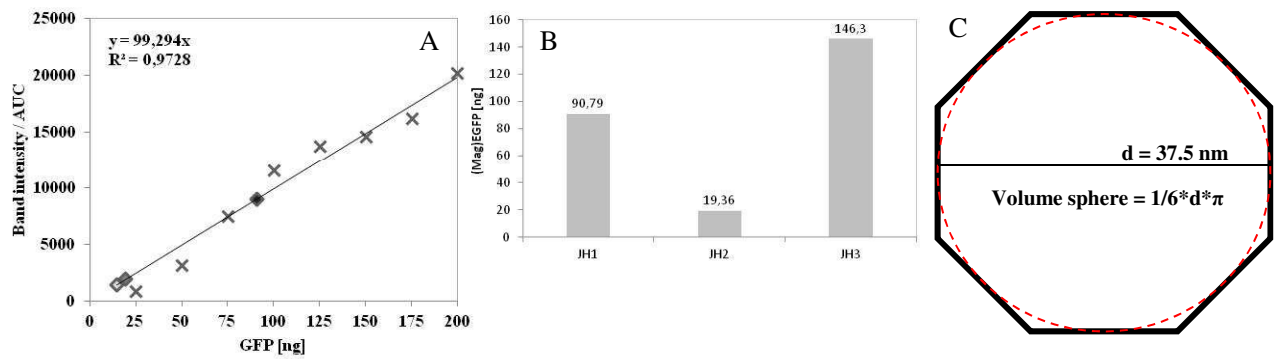
Suppl. Fig. S4: Fluorescence micrographs of *M. gryphiswaldense* ΔC strains carrying chromosomal insertions of (A) $P_{\text{mamDC45}}\text{-mamC-magegfp}$ (JH1) (B) $P_{\text{tet}}\text{-mamC-magegfp}$ (JH2) induced with 70 ng ml^{-1} Atet, (C) uninduced and (D) $P_{\text{mamDC45}}\text{-mamC-egfp-magegfp}$ (JH3) expression cassettes. White bar corresponds to 2 μm .



Suppl. Fig. S5: Fluorescence and DIC micrographs of isolated magnetosomes from *M. gryphiswaldense* MSR-1 ΔC (A) JH2 (induced) (B) JH1 and (C) JH3. White bar corresponds to 2 μm .



Suppl. Fig. S6: A) Transmission electron micrographs of *M. gryphiswaldense* SB6, expressing MagEGFP chromosomally from P_{mamDC45}. The black scale bar represents 200 nm. B) Optical density (OD₅₆₅) after overnight growth of strains SB6, SB7 and SB8 in comparison to wt. Error bars represent standard deviations calculated from triplicate cultures, experiment was repeated three times, data is from one representative experiment.



Suppl. Fig. S7: (A) Quantitative Western blot of GFP standard curve (marked by "x") and MM samples from strains JH1 (black square), JH2 (grey square) and JH3 (light grey square, 10x diluted). (B) Corresponding GFP protein concentrations of strains JH1, JH2 and JH3. (C) Schematic drawing of approximation of magnetosome size.

Suppl. Tab. S1: Plasmids used in this study

Plasmid name	Description	Source or reference
pJET1.2/blunt	Cloning vector; Amp ^R	Fermentas
pBBR-MCS2	Mobilizable broad-host-range vector; Km ^R	Kovach, M. E., <i>et al.</i> , 1995
pBAM1	Km ^R , Amp ^R , oriR6K, <i>tnpA</i>	Martinez-Garcia, E., <i>et al.</i> , 2011
p11AAGJZC	Amp ^R , ColE1 ori, oRBS, <i>magegfp</i>	GeneArt® (Invitrogen), life technologies, Darmstadt
pAP150	pBBR-MCS2, with P _{mamDC45} , <i>egfp</i> , terminator-fragment; Km ^R	A. Pollithy (unpublished)
pAP158	pBBR-MCS2, with P _{tet} , <i>egfp</i> , terminator-fragment, P _{mamAB} -TetR; Km ^R	A. Pollithy (unpublished)
pAP159	pBBR-MCS2, with P _{tet} , <i>egfp</i> , terminator-fragment, P _{mamDC} -TetR; Km ^R	A. Pollithy (unpublished)
pAP160	pBBR-MCS2, with P _{tet} , <i>egfp</i> , terminator-fragment, P _{Neo} -TetR; Km ^R	A. Pollithy (unpublished)
pAP161	pBBR-MCS2, with P _{mamDC325} , <i>egfp</i> , terminator-fragment; Km ^R	A. Pollithy (unpublished)
pAP162	pBBR-MCS2, with P _{mamDC102} , <i>egfp</i> , terminator-fragment; Km ^R	A. Pollithy (unpublished)
pAP163	pBBR-MCS2, with P _{mamDC170} , <i>egfp</i> , terminator-fragment; Km ^R	A. Pollithy (unpublished)
pAP164	pBBR-MCS2, with P _{mamDC270} , <i>egfp</i> , terminator-fragment; Km ^R	A. Pollithy (unpublished)
pLYJ97	pBBR-MCS2 with <i>gusA</i>	Li, Y., <i>et al.</i> , 2012
pSB1	pBBR-MCS2, with P _{mamDC45} , <i>magegfp</i> , terminator-fragment; Km ^R	this study
pSB6	pBAM1 with P _{mamDC45} , <i>magegfp</i> , Km ^R , Amp ^R	this study
pSB7	pBAM1 with P _{tet} , <i>magegfp</i> , P _{Neo} -TetR, Km ^R , Amp ^R	this study
pSB8	pBAM1 with P _{tet} , <i>gusA</i> , P _{Neo} -TetR, Km ^R , Amp ^R	this study
pJH1	pBAM1 with P _{mamDC45} , <i>mamC-magegfp</i> , Km ^R , Amp ^R	this study
pJH2	pBAM1 with P _{tet} , <i>mamC-magegfp</i> , P _{Neo} -TetR, Km ^R , Amp ^R	this study
pJH3	pBAM1 with P _{mamDC45} , <i>mamC-magegfp-egfp</i> , Km ^R , Amp ^R	this study

Suppl. Tab. S2: Strains used in this study

Strain	Description	Source or reference
<i>Escherichia coli</i>		
DH5 α	F ⁻ <i>supE44</i> Δ <i>lacU169</i> (Φ 80 <i>lacZDM15</i>) <i>hsdR17</i> <i>recA1</i> <i>endA1</i>	
WM3064	<i>gyrA96</i> <i>thi-1</i> <i>relA1</i> <i>thrB1004</i> <i>pro</i> <i>thi</i> <i>rpsL</i> <i>hsdS</i> <i>lacZ</i> Δ <i>M15</i> <i>RP4-1360</i> Δ (<i>araBAD</i>)567 Δ <i>dapA1341::[erm pir]</i>	W. Metcalf, unpublished
BW29427	DAP auxotroph derivative of <i>E. coli</i> strain B2155	K. Datsenko and B. L. Wanner, unpublished
<i>Magnetospirillum</i>		
<i>gryphiswaldense</i>		
<i>M. gryphiswaldense</i> MSR-1 R3/S1	Rif ^R , Sm ^R spontaneous mutant, lab strain	D. Schultheiss, <i>et al.</i> , 2003
<i>M. gryphiswaldense</i> Δ C	Δ <i>mamC</i>	A. Scheffel, <i>et al.</i> , 2007
<i>M. gryphiswaldense</i> (pAP150)	Km ^R , conjugated with pAP150	A. Pollithy, unpublished
<i>M. gryphiswaldense</i> (pAP160)	Km ^R , conjugated with pAP160	A. Pollithy, unpublished
<i>M. gryphiswaldense</i> (pSB1)	Km ^R , conjugated with pSB1	this study
<i>M. gryphiswaldense</i> MSR-1 SB6	Km ^R , transposon mutant with inserted <i>magegfp</i> from P _{mamDC45}	this study
<i>M. gryphiswaldense</i> MSR-1 SB7	Km ^R , transposon mutant with inserted <i>magegfp</i> from P _{tet}	this study
<i>M. gryphiswaldense</i> MSR-1 SB8	Km ^R , transposon mutant with inserted <i>gusA</i> from P _{tet}	this study
<i>M. gryphiswaldense</i> MSR-1 JH1	Km ^R , transposon mutant with inserted <i>mamC</i> - <i>magegfp</i> from P _{mamDC45}	this study
<i>M. gryphiswaldense</i> MSR-1 JH2	Km ^R , transposon mutant with inserted <i>mamC</i> - <i>magegfp</i> from P _{tet}	this study
<i>M. gryphiswaldense</i> MSR-1 JH3	Km ^R , transposon mutant with inserted <i>mamC</i> - <i>magegfp-egfp</i> from P _{mamDC45}	this study

Suppl. Tab. S3: Primers used in this study. Restriction sites indicated in bold

Primer name	Sequence	Restriction site
oEGFP BamHI Rev	cgaac ggatcct cacttatacagctcg	BamHI
oEGFP HindIII Fw	cggetc aaagctt aggagatcagcatatg	HindIII
pBam_pAP160 Fw	atc gggacccc ttccggctggctggttt	SanDI
pBam_ Tet w/o Term Rev	atc gaattc ggcggattgtcctactca	EcoRI
pBam_pAP150 Fw	atc gggacccc ggatcctcacttatacagct	SanDI
pBam_DC w/o Term Rev	gc gaattc ctcagactttttcgctttac	EcoRI
GusA BamHI Fw	gt ggatcccc gggtcattgtttgcc	BamHI
GusA NdeI Rev	tt catatg ttacgtcctgtagaaa	NdeI
optGFP San/Bam Fw	g agggacccc ggatcctcacttatacagctcgcc	BamHI/SanDI
optGFP linker Rev	ggaggcggaggcgggtggcggaggtggcgg aatcgat atg gtgtcgaagggcga	ClaI
mamC ov linker Fw	cgccaccgectccgctc ccatggg ccaatttcttccctca	NcoI
mamC NdeI Rev	t acatag actttcaacttgccgc	NdeI
optGFP2x Fw	agt ggatcct cacttatacagctcgtcca	BamHI
optGFP2x Rev	ctgtgcct gcagg ggcagatgggtgcgaagggcg	PstI
eGFP overl Fw	atctcgc ctgcagg cacagcttgtagagctcgtccatgc	PstI
mamC_RBS Rev	c gaagctt aggagatcagcatatgagctttcaact	HindIII

Suppl. Tab. S4: Insertion sites of expression cassettes in *M. gryphiswaldense* strains

Strain	Gene	Putative function
MSR-1 SB6 K7	MGR_1519	hypothetical protein
MSR-1 SB6 K8	Inter region between MGR_1092 and MGR_2997	MGR_1092 - D-alanine-D-alanine ligase MGR_2997 - acyl carrier protein
MSR-1 SB7 K1	MGR_1581	sugar kinase, ribokinase family
MSR-1 SB7 K2	MGR_1519	hypothetical protein
MSR-1 SB8	MGR_1702	transposase IS3/IS911
MSR-1 JH1	MGR_3776	insertion element ISR1 from not characterized 10 kDa protein A3
MSR-1 JH2	MGR_3148	TorC, trimethylaminoxide (TMAO)-reductase I, cytochrom C subunit
MSR-1 JH3	MGR_612	hypothetical protein

References Supplements:

1. **Kovach ME, Elzer PH, Hill DS, Robertson GT, Farris MA, Roop RM, Peterson KM.** 1995. 4 New Derivatives of the Broad-Host-Range Cloning Vector pBBR1MCS, Carrying Different Antibiotic-Resistance Cassettes. *Gene* **166**:175-176.
2. **Martinez-Garcia E, Calles B, Arevalo-Rodriguez M, de Lorenzo V.** 2011. pBAM1: an all-synthetic genetic tool for analysis and construction of complex bacterial phenotypes. *Bmc Microbiol* **11**.
3. **Li YJ, Katzmann E, Borg S, Schüler D.** 2012. The Periplasmic Nitrate Reductase Nap Is Required for Anaerobic Growth and Involved in Redox Control of Magnetite Biomineralization in *Magnetospirillum gryphiswaldense*. *J Bacteriol* **194**:4847-4856.
4. **Schultheiss D, Schüler D.** 2003. Development of a genetic system for *Magnetospirillum gryphiswaldense*. *Arch Microbiol* **179**:89-94.
5. **Scheffel A, Gärdes A, Grünberg K, Wanner G, Schüler D.** 2008. The major magnetosome proteins MamGFDC are not essential for magnetite biomineralization in *Magnetospirillum gryphiswaldense* but regulate the size of magnetosome crystals. *J Bacteriol* **190**:377-386.

2. Publications and manuscripts

Publication 2:

Bioengineered bioluminescent magnetotactic bacteria as a powerful tool for chip-based whole-cell biosensors

Aldo Roda^{ab}, Luca Cevenini^b, Sarah Borg^c, Elisa Michelini^{ab}, Maria Maddalena Calabretta^b
and Dirk Schüler^c

Lab on Chip 2013, 13, 4881-4889

Laboratory of Analytical and Bioanalytical Chemistry, Department of Chemistry “G. Ciamician”, Alma Mater Studiorum-University of Bologna, Italy^a

INBB, Istituto Nazionale di Biostrutture e Biosistemi, INBB, Roma, Italy^b

Ludwig Maximilian University Munich, Department of Biology I, Martinsried, Germany^c

Bioengineered bioluminescent magnetotactic bacteria as a powerful tool for chip-based whole-cell biosensors†

Cite this: *Lab Chip*, 2013, 13, 4881

Aldo Roda,^{a,b} Luca Cevenini,^b Sarah Borg,^c Elisa Michelini,^{a,b} Maria Maddalena Calabretta^b and Dirk Schüler^c

This paper describes the generation of genetically engineered bioluminescent magnetotactic bacteria (BL-MTB) and their integration into a microfluidic analytical device to create a portable toxicity detection system. *Magnetospirillum gryphiswaldense* strain MSR-1 was bioengineered to constitutively express a red-emitting click beetle luciferase whose bioluminescent signal is directly proportional to bacterial viability. The magnetic properties of these bacteria have been exploited as “natural actuators” to transfer the cells in the chip from the reaction to the detection area, optimizing the chip’s analytical performance. A robust and cost-effective biosensor for the evaluation of sample toxicity, named MAGNETOX, based on lens-free contact imaging detection, has been developed. A microfluidic chip has been fabricated using multilayered black and transparent polydimethyl siloxane (PDMS) in which BL-MTB are incubated for 30 min with the sample, then moved by microfluidics, trapped, and concentrated in detection chambers by an array of neodymium–iron–boron magnets. The chip is placed in contact with a cooled CCD *via* a fiber optic taper to perform quantitative bioluminescence imaging after addition of luciferin substrate. A model toxic compound (dimethyl sulfoxide, DMSO) and a bile acid (taurochenodeoxycholic acid, TCDCA) were used to investigate the analytical performance of the MAGNETOX. Incubation with DMSO and TCDCA drastically reduces the bioluminescent signal in a dose-related manner. The generation of bacteria that are both magnetic and bioluminescent combines the advantages of easy 2D cell handling with ultra sensitive detection, offering undoubted potential to develop cell-based biosensors integrated into microfluidic chips.

Received 24th July 2013,
Accepted 30th September 2013

DOI: 10.1039/c3lc50868d

www.rsc.org/loc

Introduction

The increasing demand for robust and cost-effective portable analytical devices for on-site environmental toxicity screening has prompted the development of miniaturized whole-cell biosensors which are able to provide information about potential *in vivo* toxicity, thus predicting risks for human and animal health.¹ Advances in molecular biology techniques offer the opportunity to enable cells to express specific recognition elements such as receptors or regulatory proteins which trigger intracellular signaling events as a result of a specific interaction with target analyte(s). Reporter gene technology is based on a cascade of signaling events which

ultimately result in the expression of a reporter protein, such as green fluorescent protein (GFP) or luciferase, whose expression can be measured by fluorescence or bioluminescence (BL).² Thanks to the high signal/noise ratio and no need for an external light source or special sample geometry, measurement of BL represents one of the most powerful detection strategies for miniaturized devices.³ Besides, the availability of several luciferases with different BL emission properties allows development of cell-based BL assays in multiplex formats or use of an internal control to correct the analytical signal according to cell viability.⁴ Whole-cell biosensors are suitable for implementation in miniaturized and/or microfluidic devices, with the advantages of low sample and reagent consumption, portability, and short analysis time. Several examples of detection of different classes of analytes, ranging from heavy metals to endocrine disruptors have been reported.^{5,6} Nonetheless, the majority of previously reported devices lack adequate analytical performance for real-life applications, and have thus failed to reach the market.^{7,8} To increase the robustness of such devices, several cell immobilization strategies have been investigated, aiming to keep the

^a Laboratory of Analytical and Bioanalytical Chemistry, Department of Chemistry “G. Ciamician”, Alma Mater Studiorum-University of Bologna, Via Selmi 2, 40126 Bologna, Italy. E-mail: aldo.roda@unibo.it; Tel: +39 051343398

^b INBB, Istituto Nazionale di Biostrutture e Biosistemi, INBB, Roma, Italy

^c Ludwig-Maximilians-Universität München, Department Biologie I, Mikrobiologie, Planegg-Martinsried, Germany

† Electronic supplementary information (ESI) available. See DOI: 10.1039/c3lc50868d

cells alive and responsive to the target analyte. However, analyte and/or reagent (e.g., oxygen, BL substrates...) diffusion through the immobilization matrix may result in prolonged analysis time and reproducibility issues.

A promising strategy to improve the sensitivity of BL-based devices is to move the cells between different areas of the chip which are appointed to carry out specific functions such as: incubation of the sample, reagent(s) addition, washing and detection. To this end the exploitation of magnetotactic bacteria (MTB) magnetism as a “natural actuator” could represent a valuable approach.

MTB have the innate ability to produce magnetosomes (or bacterial magnetic nanoparticles, BacMPs), *i.e.* nanoparticles of magnetite (Fe_3O_4) or greigite (Fe_3S_4) enveloped in a 3–4 nm thick lipid membrane, which are aligned in a well-ordered chain to achieve the maximum magnetic moment. Owing to the presence of magnetosomes, MTB orient and migrate along geomagnetic field lines. In past years, extensive research has been focused on the elucidation of the mechanisms regulating magnetosome biosynthesis and on the optimization of culture techniques for the production and purification of BacMPs.^{9,10}

Two major strategies can be envisaged to exploit MTB for bioanalytical applications: (i) the use of genetically engineered MTB as living biosensors, and (ii) the use of BacMPs as an alternative to chemically synthesized magnetic nanoparticles (MNPs). So far, the latter has been explored more extensively. Thanks to their size, ranging from 30 to 120 nm,¹¹ and their biocompatibility, due to the presence of a surrounding lipid bilayer membrane, BacMPs are highly advantageous for developing several kinds of biosensors, and more generally for binding assays^{12,13} and drug delivery systems.¹⁴

Although significant advances in genomic studies of MTB have been reported,¹⁵ the genetic engineering of MTB necessary to obtain magnetic bioluminescent whole-cell biosensors (BL-MTB) has not been accomplished. In addition, a miniaturized device integrating BL-MTB and a light detector has not been reported in the scientific literature.

As a first proof of concept of this new approach, *M. gryphiswaldense* MSR-1 strain was genetically engineered to constitutively express a red-emitting luciferase. A microfluidic chip prototype has been fabricated using multilayered polydimethylsiloxane (PDMS) constituted of three diamond-shaped incubation chambers connected with detection areas. After incubation with the sample, bacteria can be magnetically trapped and concentrated in the detection areas which are placed in contact with a charge-coupled device (CCD) sensor *via* a fiber optic taper to maintain adequate spatial resolution. Quantitative BL imaging is performed over a period of a few minutes, upon substrate addition (D-luciferin). This prototype was used as a rapid and sensitive biosensor for the evaluation of sample toxicity.

Results and discussion

In this study we genetically engineered magnetotactic bacteria to obtain BL magnetic biosensors. Some so-called

“magnetically labeled biosensors” have been previously obtained by chemical functionalization of cells (mammalian cell lines, yeast and bacteria) with synthetic MNPs.^{16,17} Indeed this approach has some technical limitations requiring functionalization steps that may create standardization problems; the cells divide during the incubation time and the number of MNPs on each cell's surface decreases, thus negatively affecting the reproducibility of an assay relying on the movement or trapping of biosensing cells within a microfluidic chip *via* magnetic fields. Our strategy exploits the intrinsic capability of magnetotactic bacteria, such as *Magnetospirillum gryphiswaldense*, to produce a chain of magnetic nanoparticles (magnetosomes) within the cell which confer the ability to orient and migrate along magnetic field lines. The number and shape of the genetically encoded magnetic particles is strictly regulated by the bacterial genome.

When grown in microaerobic conditions the majority of the cells are magnetic and retain magnetic properties through cell divisions. For the purpose of microfluidic chip integration we choose magnetotactic bacteria in order to have a homogenous population of magnetic cells.

The biosensors were integrated into a newly designed magnetic microfluidic chip, named MAGNETOX, which facilitates rapid, sensitive and direct toxicity screening without the need for sample pre-treatment steps.

The use of a magnetic array to separate the biosensing cells from the sample allows simultaneous removal of interferents and concentration of the BL-MTB in front of the CCD device, improving BL detection in terms of light output and sensitivity.

Preparation and characterization of bioluminescent magnetotactic bacteria

M. gryphiswaldense has been selected as the host strain because it is well characterized and its genetic toolbox is well developed.¹⁸

The *M. gryphiswaldense* strain MSR-1 was genetically engineered to express the red-emitting click beetle luciferase (CBR, $\lambda_{\text{max}} = 615$ nm) under the control of the constitutive P_{mamDC45} minimal promoter which ensures high expression levels of heterologous proteins (unpublished data). To this end, CBR luciferase, a mutant of a yellow-green luciferase from *Pyrophorus plagiophthalmus*, was selected as the reporter protein because of its thermostability, pH-insensitivity and glow type emission.¹⁹

When expressed in bacterial cells, CBR has a much longer half-life than the wild-type *P. pyralis* luciferase (5 h *vs.* 0.26 h).²⁰ Since CBR requires endogenous bacterial ATP for the chemical reaction, any change in light output truly reflects alterations in the viability and metabolic state of the cell. A shuttle vector containing the cDNA encoding for CBR under the regulation of a constitutive promoter was used to transform an *E. coli* donor strain and was transferred to MSR-1 strain by conjugation.

The BL emission of the BL-MTB cells was investigated in terms of kinetics and spectral emission properties to obtain

information useful for the subsequent implementation of the cells in the microfluidic chip. For this reason we measured the BL signals emitted by intact living cells in 96-well microplates after addition of the BL substrate *D*-luciferin at pH 5.0. The BL-MTB emission kinetics showed that after injection of the BL substrate the signal reached a peak within a few seconds followed by rapid decay and stabilization at a signal corresponding to about 50% of the maximum BL emission (see Fig. 1(a)). Therefore a suitable temporal window from 5 to 15 min was identified for the BL measurements. This glow-type emission is particularly interesting for imaging applications since it allows integration of the BL signal over several minutes, thus increasing sensitivity. The BL emission spectrum showed a λ_{max} at 615 nm with a half bandwidth of 53 nm (see Fig. 1(b)), consistent with CBR expression in other bacterial systems such as *E. coli* strains (data not shown).

As known from other proteins previously expressed in MSR, cytoplasmic expression of the luciferase enzyme is not likely to influence magnetosome formation. This was confirmed by transmission electron microscope (TEM) characterization which revealed that the magnetosome number and morphology in BL-MTB was indistinguishable from those of MSR-1 wild-type strain (see Fig. 1(d)).

Investigation of the time dependent luciferase expression and cell magnetism led to 3 day-old cultures being selected for inclusion in the MAGNETOX biosensor. Fig. 1(c) shows both the BL signal and the cell magnetism (C_{mag}) of BL-MTB cultured in a medium containing Fe(III) citrate. Luciferase BL reached a maximum intensity at 72 h after inoculation, when micro-aerobic conditions prevailed and cell magnetism was $1.40 \pm 5\%$ (corresponding to 90% of the maximum C_{mag} obtained after 6 days incubation). Magnetic properties were also macroscopically confirmed by moving the BL-MTB with a permanent magnet (see movie M1†).

Design and fabrication of the MAGNETOX microfluidic chip

Exploiting multilayer PDMS casting, a microfluidic chip comprising incubation and detection chambers, in which BL-MTB can be loaded and trapped into specific positions for analysis, has been fabricated. The chip comprises three, 60 μl volume, diamond-shaped incubation chambers, each of them connected to two detection areas to which the BL-MTB can be navigated *via* a microfluidic system, then trapped and accumulated using permanent magnets (see Fig. 2). Subsequently the BL substrate can be delivered to the 6 detection chambers allowing simultaneous imaging. Lens-free BL

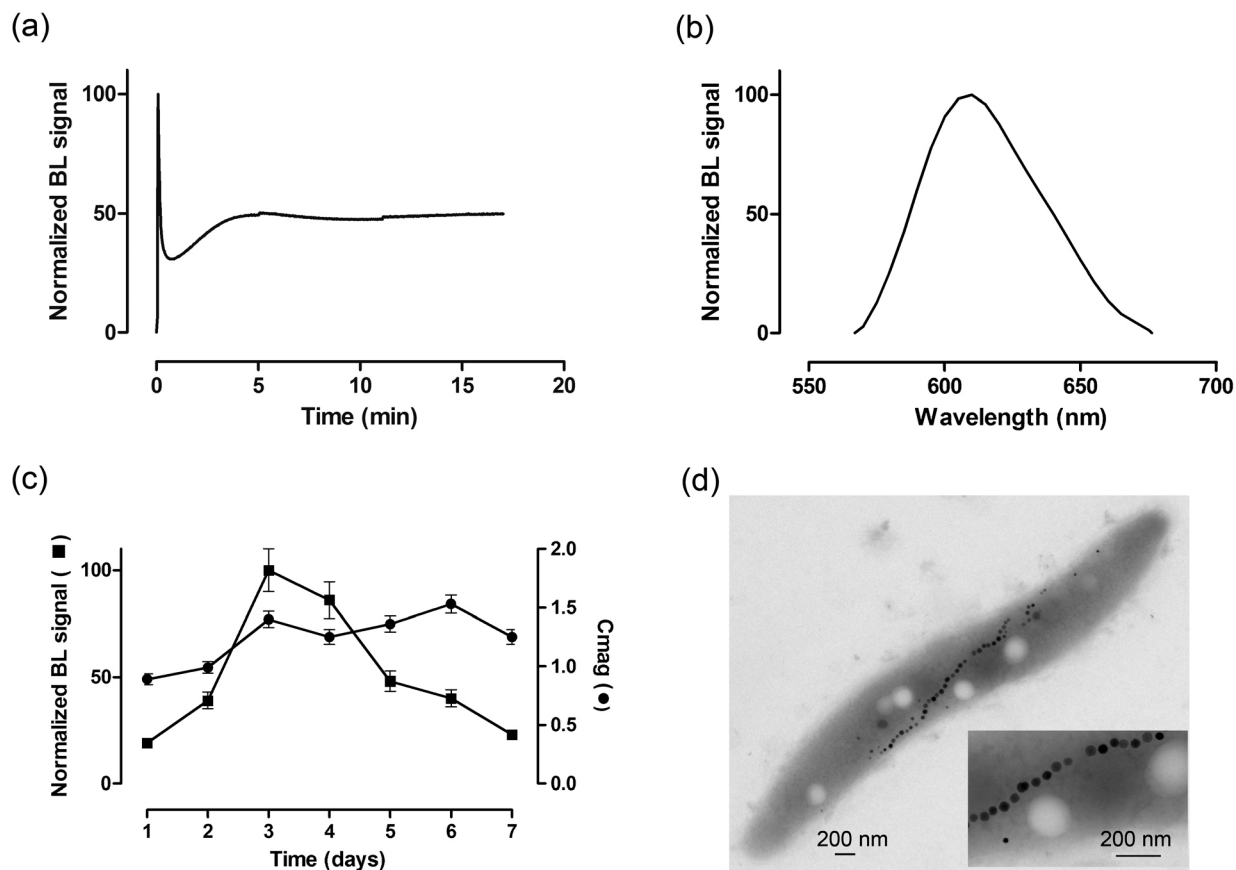


Fig. 1 Characterization of the bioluminescent magnetotactic bacteria BL-MTB. (a) Normalized BL emission kinetics. (b) Normalized emission spectrum ($\lambda_{\text{max}} = 615$ nm). (c) Time dependent expression of the CBR luciferase and cell magnetism (C_{mag}) of the growing BL-MTB cultures. (d) TEM micrographs of MSR-1 expressing CBR luciferase taken with a Morgagni 268 at 80 kV. Inset shows a magnified image of the magnetosome chain.

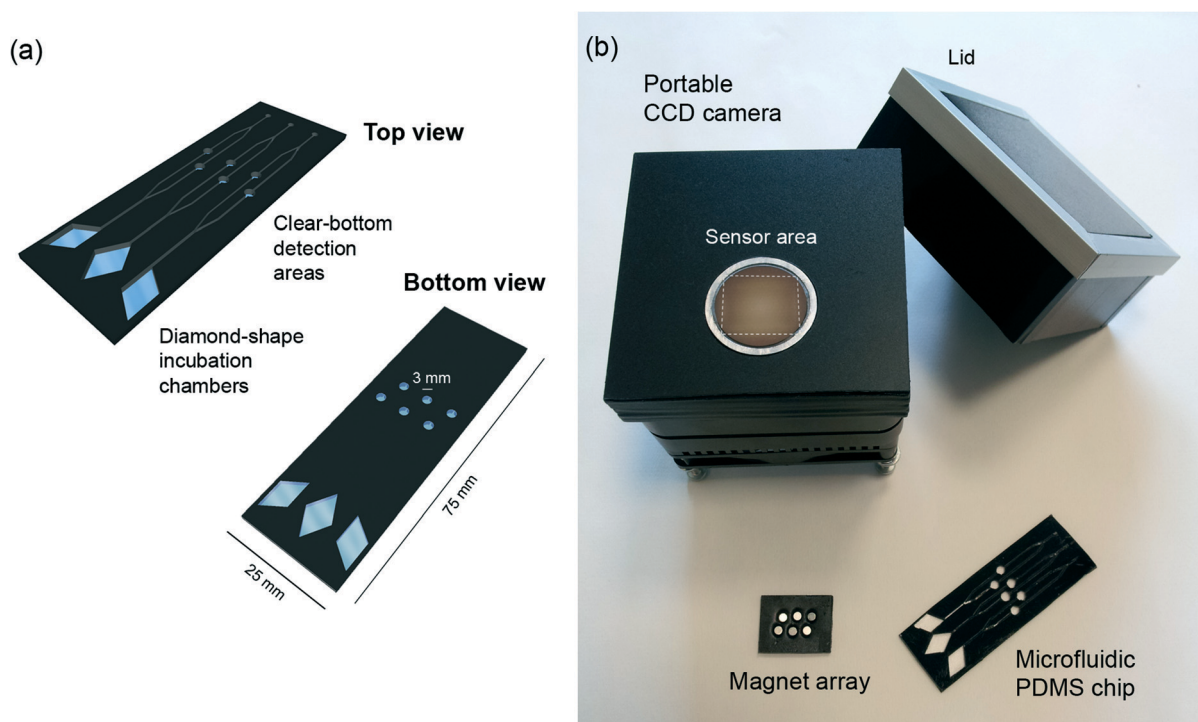


Fig. 2 The MAGNETOX biosensor. (a) Schematic representation of the microfluidic chip comprising three diamond-shaped incubation chambers and clear-bottom detection areas. (b) Main components of the MAGNETOX biosensor: the microfluidic chip, the magnet array, the portable CCD camera with a fiber optic taper for lens-free BL imaging, and a lid for shielding against ambient light.

imaging was performed using a CCD camera interfaced with a fiber optic taper to maintain adequate sample resolution.²¹ This prototype configuration was designed to concentrate the cells in a reduced volume, thus improving light collection from the detection chambers. This strategy will be pursued to further miniaturize the MAGNETOX chip and increase the number of detection areas.

Another feature of the MAGNETOX is that, after analysis, the cells are washed out of the chip so that it can be re-used. Since incubation of cells with the analyte lasts only 30 min no sterility is required and the chip can simply be washed with 70% ethanol before reuse. This makes the device suitable for applications in low-resource settings.

As we previously reported, CCD contact lens-less imaging does not require any optical system, thus simplifying the fabrication of compact and miniaturized analytical devices.²² In addition lens-less imaging achieves a higher level of detection by taking advantage of the light collection efficiency of the system.

The Sony ICX285 monochrome CCD sensor has been selected since it has a quantum efficiency higher than 50% in the range of 420–680 nm which covers the whole emission of the CBR reporter. A fiber optic mosaic taper which transmits the emitted light directly to the CCD sensor was used to increase the sensing surface by 2.3 times compared to the actual size of the CCD sensor (*i.e.*, from $9.0 \times 6.7 \text{ mm}^2$ to $20.7 \times 15.4 \text{ mm}^2$), whilst still maintaining good resolution. A double Peltier cooling system reduced the thermal noise of the CCD, thus improving the signal/noise ratio and a lid provided shielding against ambient light.

The most significant improvements made to the device are: i) the implementation of a straightforward strategy to cast black and transparent PDMS; ii) the integration of a magnet array into the chip; iii) the design and fabrication of a microfluidics platform optimized for magnetic biosensors.

Although the use of black PDMS (a suspension of charcoal in PDMS) to fabricate microfluidic devices has been already reported elsewhere,²³ to the best of our knowledge the present work represents the first proof of concept for a black PDMS microfluidic chip that includes detection chambers with transparent bottoms for BL imaging detection. In addition this approach may have a more general application for optical detection.

We first investigated the ability of neodymium–iron–boron (NdFeB) magnets to rapidly and efficiently trap BL-MTB within the chip. Fig. 3(a) shows BL images of the MAGNETOX chip obtained after *D*-luciferin addition. At first, the signal is homogeneously distributed in the incubation chambers. As expected, after magnetic trapping, the BL signal is mostly concentrated in the detection chambers (approximately 85% of total light emission) (see Fig. 3(b)). Weak signals still appear along the microfluidic channels, indicating that the magnetic trapping could be further optimized to improve reproducibility. The prototype was purposely designed to disregard the signal emitted by BL-MTB in the microfluidic channels or in the incubation chambers. In fact the background signal of the non-trapped cells does not interfere with the CCD detection since the channels are made from black PDMS.

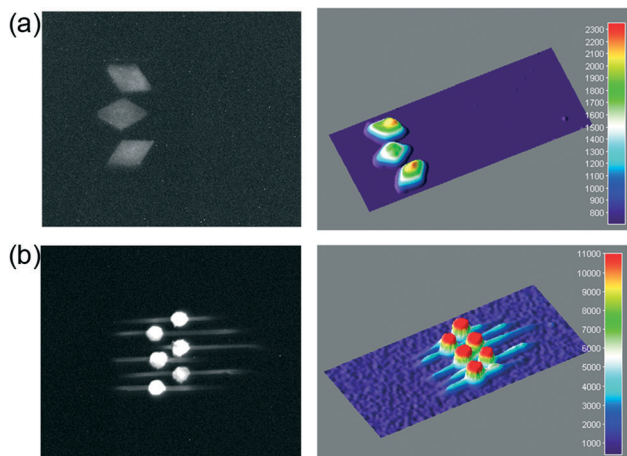


Fig. 3 BL images of BL-MTB inside the incubation chambers (a) and after cell movement and magnetic trapping in the detection chambers (b). The MAGNETOX chip was imaged from the top using a Night Owl LB 981 luminograph (EG&G Berthold, Bad Wildbad, Germany) with 5 min integration. A 3D surface plot visualization was obtained using ImageJ software.

In addition, thanks to the reflective surface of the magnets, BL emitted towards the opposite side of the sensor can also be detected, thus increasing the sensitivity of the analysis. The use of a reflecting surface increases the light signal by approximately 30% compared to that obtained with black tape covered magnets (data not shown).

Evaluation of sample toxicity with the MAGNETOX platform

The feasibility of the MAGNETOX platform as a general toxicity biosensor was assessed using standard solutions of DMSO, as model toxic compound and TCDCA, a detergent bile acid that causes structural and dynamic effects in membranes. The toxic effect of DMSO is mainly due to its activity in the cell membrane,²⁴ which affects cell metabolism and viability. The alteration of cell energy systems dramatically alters intracellular ATP levels, which can be monitored with an ATP-dependent luciferase. Therefore only metabolically active cells are able to provide the bioluminescent signal, which reflects their viability.

Concentration-response curves for DMSO were obtained and compared to those obtained for BL-MTB in a miniaturized 6-well cartridge (see Fig. S1(a)†). This microwell cartridge, containing 6 wells of 60 μL volume each, was purposely designed for integration in the same portable device. This allowed the actual advantage of concentrating BL-MTB *via* microfluidics and adding the BL substrate after a washing step to be assessed in comparison to a conventional microwell format using the same CCD detector. The BL recombinant cells were incubated for 30 min at room temperature with different concentrations of toxic compounds inside the MAGNETOX chip or inside the microwells. For the MAGNETOX assay, after incubation the cells were moved towards the detection chamber, and trapped by the magnetic array. Upon addition of the D-luciferin substrate, images were acquired with the CCD detector and analyzed to

quantify BL emission (see Fig. 4(a)). Fig. 4(b) shows that the BL signal is strongly affected by DMSO with an LC_{50} of 7.5% v/v DMSO obtained in both configurations. The two curves showed a similar sensitivity with slight differences at low DMSO concentrations (*e.g.*, in the MAGNETOX a 2.5% v/v DMSO produces a signal of $75 \pm 12\%$ whereas $85 \pm 5\%$ is recorded in the microwell configuration) while at DMSO concentrations higher than 40% v/v complete cell death is observed in both the configurations.

We then used the bile acid TCDCA (0.001–10 mM). An increasing toxic effect was observed (see Fig. 5) while approaching the TCDCA critical micelle concentration (CMC 3 mM).²⁵ Micelles can modify the membrane constituents, thus resulting in a change in physicochemical properties causing adverse effects on cell viability.^{26,27}

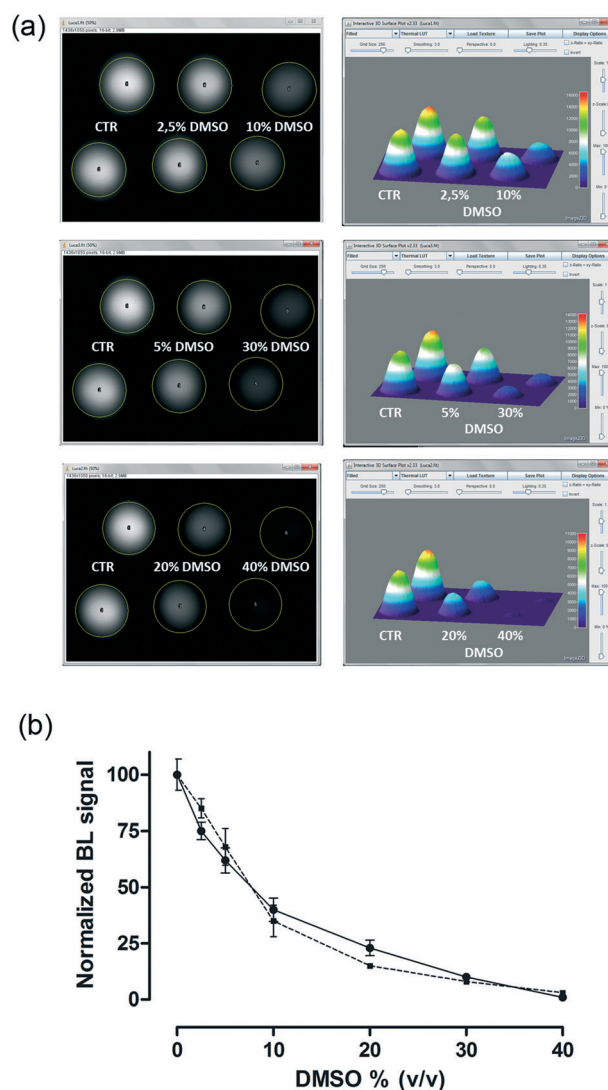


Fig. 4 (a) BL images obtained with the MAGNETOX and 3D surface plot visualization using ImageJ software. Circular ROI were selected and the BL signals were quantified. (b) Normalized toxicity curves for DMSO (30 min incubation) obtained with the BL-MTB in the microwell cartridge (dashed line) and with the MAGNETOX chip (solid line).

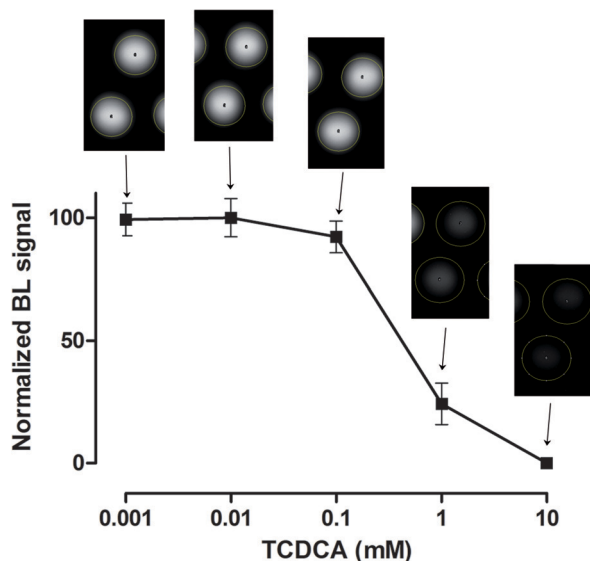


Fig. 5 Toxicity curve for TCDCA (0.001–10 mM) obtained with the MAGNETOX chip. BL images corresponding to each duplicate are shown in the inset. The BL-MTB cells are incubated for 30 min at room temperature with increasing concentrations of TCDCA inside the MAGNETOX chip. After incubation the cells are moved towards the detection chamber, and trapped by applying the magnetic array. Upon addition of the *D*-luciferin substrate, images are acquired with the CCD sensor and analyzed to quantify BL emission.

The response measured by the MAGNETOX assay was quite reproducible with an intra-assay variability of 15% calculated by considering the 6 detection chambers as replicates and an inter-assay variability of 18% with four replicates. We also compared the results with the closest widely recognized assay, the Microtox[®] system, which measures the light output of luminescent bacteria (*Vibrio fischeri*) after they have been exposed to a sample. Using 1 h incubation with standard solutions containing different concentrations of DMSO we observed an LC₅₀ of 8.3% v/v DMSO with the first toxic effects appearing at 2.5% v/v DMSO (BL signal 81 ± 9%) and complete cell death at DMSO concentrations higher than 40% v/v, (see Fig. S2[†]), these results are consistent with the MAGNETOX assay.

These preliminary results show that it is possible to exploit magnetic concentration to increase light output and reduce assay volume. Despite this, the reproducibility of the MAGNETOX assay could be improved by optimizing the microfluidic chip design and fabrication. These results support the use of BL-MTB as a powerful tool suitable for microfluidic (bio)sensors.

In addition, the generation of BL-MTB with a codon-optimized version of the luciferase integrated into the bacterial chromosome would surely result in a more robust biosensor. The use of a codon optimized luciferase coding sequence could reduce the time required for its expression. Indeed MAGNETOX assays performed using overnight and 36 h-old cultures resulted in lower analytical performance (*e.g.*, no significant bioluminescent signal at concentrations higher than 20% DMSO v/v and an increased coefficient of variation (CV% = 20%)).

To circumvent this limitation, lyophilized BL-MTB will be obtained providing a ready-to-use suspension of organisms for use in the chip. The implementation of BL-MTB in field-deployable devices could be exploited for direct analysis of environmental or clinical samples containing matrix components, which may interfere with the BL detection but could be easily removed from detection areas. As an alternative, a microelectromagnetic pad actuator could be used to precisely control the movement and positioning of BL-MTB within the microfluidic chip and further miniaturize the system.

Experimental

Chemicals and reagents

All chemicals used for cell culture media preparation and toxic compounds were purchased from Sigma (St. Louis, Missouri, USA). The enzymes required for cloning were from Fermentas (Vilnius, Lithuania). The kits for plasmid extraction and purification were from Qiagen (Hilden, Germany). Sylgard 184 (Dow Corning, USA) was used to create the PDMS chip. *D*-Luciferin solution, 1 mM at pH 5.0, was prepared by dissolving 28.3 mg *D*-luciferin sodium salt (Synchem, Kassel, Germany) in 35 mL of 0.1 M citric acid and 65 mL of 0.1 M trisodium citrate solution. Taurochenodeoxycholic acid sodium salt (TCDCA) dilutions were prepared in FSM medium.

Organism and growth conditions

The *M. gryphiswaldense* strain (MSR-1 R3/S1; Rif^r Smr spontaneous mutant)²⁸ was cultured at 28 °C in 10 mL hungate tubes (GPE Scientific UK) in microaerobic conditions (1% O₂ in the headspace). The oxygen concentration in the gas phase was reduced to less than 1% O₂ by repeated flushing with N₂. An MSR-1 medium with 50 μM Fe(III) citrate was used as described by Heyen and Schüler.²⁹

Obtainment of bioluminescent magnetotactic bacteria (BL-MTB) and characterization of emission properties

M. gryphiswaldense strain was genetically engineered to constitutively express the red-emitting click beetle luciferase (CBR, λ_{max} = 615 nm). Briefly, the cDNA encoding for CBR was PCR amplified from the vector pCBRbasic (Promega, WI, USA) using the primers CBR Fw AGTGGATCCTTACTAACC GCCGCCTT and CBR Rev CAGCATATGGTAAAGCGTGAGAAAAAT, adding BamHI and NdeI restriction sites, shown in bold. These restriction enzymes were then used to digest and insert the luciferases into the pAP150 vector under the control of the P_{mamDC45} constitutive promoter. The resulting vector pAP150-CBR was used to transform the *E. coli* donor strain (BW29427 [thrB1004 pro thi rpsL hsdS lacZ-M15 RP4-1360-(araBAD)567-dapA1341::(erm-pir-)]) (K. Datsenko and B. L. Wanner, unpublished) *via* heat shock³⁰ and transferred to the MSR strain by conjugation.²⁸ The obtained strain (MSR-CBR) was routinely grown microaerobically at 28 °C in a selective MSR medium containing 5 μg mL⁻¹ kanamycin. MSR-CBR

emission kinetics and bioluminescence emission spectra were obtained in a 96-well plate using 100 μL overnight liquid cultures; the BL signal was acquired for 10 minutes (300 ms integration time) with a Varioskan Flash spectral scanning multimode reader (Thermo Scientific, Waltham, MA, USA) after automatic injection of 100 μL D-luciferin 1 mM, pH 5.0. Bandwidths (nm) of the emission spectra were measured at 50 and 20% of the intensity at the maximum wavelength. Data were analyzed with GraphPad Prism v5.02 (Software, Inc., San Diego, CA, USA). All light measurements were performed in triplicate.

TEM micrographs of MSR-1 expressing CBR luciferase were taken at 18k \times and 71k \times with a Morgagni 268 at 80 kV.

Evaluation of luciferase time dependence and magnetic orientation

The magnetic orientation (C_{mag}) of the MSR-CBR cells was evaluated spectrophotometrically using the optical density at 565 nm as previously described.³¹ Briefly, at given time intervals, cell suspensions of 1.0 mL were withdrawn from the culture for C_{mag} measurement. Cell density was set to an OD of 0.1 and an external magnetic field was applied to align the cells at different angles towards the light beam of the spectrometer. This results in maximum and minimum light extinction and the ratio of these correlates with the average number of magnetosomes per cell. This method is used to semi-quantitatively assess the magnetism of a culture (non-magnetic cells have a C_{mag} value of 0).

Design and fabrication of the MAGNETOX microfluidic chip

The microfluidic chip fabrication process is based on multiple layer casting of black and transparent PDMS on a home-made master mold.

Transparent PDMS was prepared using a monomer curing agent in a weight ratio of 5:1, 25 mg mL⁻¹ of activated charcoal powder was added to obtain black PDMS. The solutions were then centrifuged at 4000 rpm for 10 min to remove bubbles and stored at -20 °C until use.

Black PDMS was first poured in to fill up to the edge of the relief structures on the mask, which creates the diamond-shaped chambers (7.0 \times 14.0 mm diagonals, height 1.5 mm), the microfluidics channels (1 mm width) and detection areas (3 mm diameter, height 1.5 mm). To avoid mixing with transparent PDMS, black PDMS was allowed to harden for 1 h at 60 °C; then a thin layer of transparent PDMS was poured on top of the black PDMS layer, to create the transparent bottom of the wells, and allowed to harden for 2 h at 60 °C. During the curing process the black and transparent PDMS layers fuse together.

A separate layer of transparent PDMS was cast in a different mold, comprising inlets and outlets, to create the top of the chip and allowed to harden as previously described. The two partially-cured PDMS layers were then removed from their masks, superimposed and hardened overnight at 70 °C to obtain the final chip (see Fig. 2(a)).

An array of neodymium-iron-boron circular disc magnets (NdFeB; NeoDeltaMagnet NE32, 3 mm diameter, $L = 2$ mm, remanence 1170–1250 mT, IBS Magnet, Berlin, Germany) was placed over the detection chambers of the PDMS chip.

The MAGNETOX device consists of the microfluidic device connected to a CCD camera modified for lens-free CL imaging detection. The CCD imaging detector was built from a MZ-2PRO CCD camera (MagZero, Pordenone, Italy) equipped with a Sony ICX285 monochrome CCD image sensor (1360 \times 1024 pixels, pixel size 6.45 \times 6.45 μm^2) and a 16 bit analog-to-digital (A/D) converter. To reduce thermal noise, the CCD sensor was thermoelectrically cooled by a double Peltier cell. A round fiber optic taper (25/11 mm size, Edmund Optics, Barrington, NJ) was placed in contact with the CCD sensor as previously described by our group.²² The MAGNETOX is computer controlled *via* a USB 2.0 interface using software (EZ Cap, v3.13) that facilitates data acquisition and parameter settings.

Design of a microwell cartridge

A custom made PDMS 6-well cartridge was produced using black and transparent PDMS as previously described. The mask for PDMS casting has been designed in order to obtain an array of 2 \times 3 wells of 4 mm diameter and 4.5 mm deep each.

First, black PDMS was poured in to fill up to the edge of the mask followed by addition of a thin (<200 μm) layer of transparent PDMS to create the bottom of the wells (see Fig. S1(b)†). After overnight incubation at 70 °C the cartridge was carefully separated from the mask.

Toxicity evaluation using the MAGNETOX platform

Different concentrations of dimethyl sulfoxide (DMSO) (in the range 2–50% v/v) and TCDCa (in the range 0.001–10 mM) were used as model toxic compounds to evaluate the feasibility of using BL magnetotactic bacteria as a toxicity biosensor. All serial dilutions of compounds were performed using FSM medium as a diluent.

Different experimental conditions were optimized to improve the biosensor performance (*e.g.*, incubation temperature and time, volumes and ratio of cell suspension to sample). Under optimized conditions, an analysis with the MAGNETOX chip includes the following steps: i) 40 μL of 3 day-old liquid culture is driven into the chip by an air-displacement pipette; ii) cells are incubated for 30 min at room temperature with 20 μL of sample (medium is used as blank); iv) cells are moved and concentrated in the detection chambers by adding the array of permanent magnets; v) BL imaging measurements after addition of 1 mM D-luciferin pH 5.0. Images are acquired for 5 min and analyzed with ImageJ software v.1.46 (National Institutes of Health, Bethesda, MD). Images are recorded in the FITS (Flexible Image Transport System) format. Regions of interest (ROIs) corresponding to detection chambers are selected and light emissions quantified as raw integrated densities.

For toxicity experiments, normalized BL signals (the BL emission of the untreated control was set as 100%) were plotted against toxic compound concentration. The lethal concentration (LC₅₀) of each compound was calculated as the concentration producing a 50% reduction in light.

All experiments were performed in duplicate and repeated at least three times.

The toxic effects of DMSO and TCDCA solutions (in the range 2–50% v/v and 0.001–10 mM, respectively) were also assessed using a Microtox[®] assay with *Vibrio fischeri*.³² Different exposure times were tested (10, 30 and 60 min at 25 °C) in 96 microplate format using 90 μL of cell suspension and 10 μL of analyte or control (medium). The results were analyzed as described for the MAGNETOX assay.

Conclusions

Here, for the first time, the use of bioengineered bioluminescent magnetotactic bacteria in combination with microfabrication technologies is reported for biosensing applications. The novel concept of a black and transparent PDMS microfluidic chip has been developed which could find broad use in the optofluidic field. The chip has been integrated with a portable CCD sensor for lens-less imaging detection of light signals emitted by the BL magnetotactic bacteria used as biosensing “living actuators”. Unlike other whole-cell biosensors, BL-MTB can be easily moved and concentrated in specific detection chambers, where the sample matrix is removed and bacteria are washed, thus increasing the analytical signal and performance of the system. The interaction of BL-MTB with the analyte is facilitated in the detection chamber since this interaction takes place in a dispersed suspension, resulting in a shorter incubation time. In this regard, the MAGNETOX assay facilitates rapid (30 min) measurement of sample toxicity with the non negligible advantage of chip re-usability.

This is the first attempt to integrate bioengineered magnetotactic bacteria into an analytical device and several optimizations regarding both the cell and the chip design will be addressed. An array of electromagnets or a microelectromagnetic pad actuator will be included to better control the BL-MTB within the chip by tuning the magnetic trapping or continuously directing their swimming to the detection area.

Although many improvements are required before applying BL magnetic biosensors to real-life needs, we are confident that they represent the forerunner of a new concept in whole-cell biosensing.

Acknowledgements

This work was partially supported grants PRIN 2009MB4AYL and FIRB 2008 RBFR08SZTR from the Ministry for Education, Universities, and Research (MIUR, Italy).

References

- 1 S. K. Checa, M. D. Zurbruggen and F. C. Soncini, *Curr. Opin. Biotechnol.*, 2012, **23**, 766–772.
- 2 A. Roda, P. Pasini, M. Mirasoli, E. Michelini and M. Guardigli, *Trends Biotechnol.*, 2004, **22**, 295–303.
- 3 E. Michelini, L. Cevenini, L. Mezzanotte and A. Roda, *Methods Mol. Biol.*, 2009, **574**, 1–13.
- 4 A. Roda, B. Roda, L. Cevenini, E. Michelini, L. Mezzanotte, P. Reschiglian, K. Hakikila and M. Virta, *Anal. Bioanal. Chem.*, 2011, **401**, 201–211.
- 5 S. Melamed, T. Elad and S. Belkin, *Curr. Opin. Biotechnol.*, 2012, **23**, 2–8.
- 6 A. Rohert, S. K. Deo, L. Millner, L. G. Puckett, M. J. Madou and S. Daunert, *Anal. Biochem.*, 2005, **342**, 11–9.
- 7 E. Michelini, L. Cevenini, M. M. Calabretta, S. Spinozzi, C. Camborata and A. Roda, *Anal. Bioanal. Chem.*, 2013, **405**, 6155–6163.
- 8 I. Barbulovic-Nad, H. Yang, P. S. Park and A. R. Wheeler, *Lab Chip*, 2008, **8**, 519–26.
- 9 D. Faivre and D. Schüler, *Chem. Rev.*, 2008, **108**, 4875–4898.
- 10 D. Schüler and R. B. Frankel, *Appl. Microbiol. Biotechnol.*, 1999, **52**, 464–73.
- 11 D. A. Bazylinski and R. B. Frankel, *Nat. Rev. Microbiol.*, 2004, **2**, 217–230.
- 12 Y. Amemiya, T. Tanaka, B. Yoza and T. Matsunaga, *J. Biotechnol.*, 2005, **120**, 308–314.
- 13 T. Yoshino, C. Kaji, M. Nakai, F. Saito, H. Takeyama and T. Matsunaga, *Anal. Chim. Acta*, 2008, **626**, 71–77.
- 14 T. Tang, L. Zhang, R. Gao, Y. Dai, F. Meng and Y. Li, *Appl. Microbiol. Biotechnol.*, 2012, **94**, 495–503.
- 15 C. T. Lefèvre, D. Trubitsyn, F. Abreu, S. Kolinko, C. Jogler, L. G. de Almeida, A. T. de Vasconcelos, M. Kube, R. Reinhardt, U. Lins, D. Pignol, D. Schüler, D. A. Bazylinski and N. Ginet, *Environ. Microbiol.*, 2013, **15**, 2712–2735.
- 16 D. Zhang, R. F. Fakhrullin, M. Özmen, H. Wang, J. Wang, V. N. Paunov, G. Li and W. E. Huang, *Microb. Biotechnol.*, 2011, **4**, 89–97.
- 17 M. R. Dzumukova, A. I. Zamaleeva, D. G. Ishmukhametova, Y. N. Osin, A. P. Kiyasov, D. K. Nurgaliev, O. N. Ilinskaya and R. F. Fakhrullin, *Langmuir*, 2011, **27**, 14386–14393.
- 18 K. H. Schleifer, D. Schüler, S. Spring, M. Weizenegger, R. Amann, W. Ludwig and M. Köhler, *Syst. Appl. Microbiol.*, 1991, **14**, 379–385.
- 19 U. Stolz, S. Velez, K. V. Wood, M. Wood and J. L. Feder, *Proc. Natl. Acad. Sci. U. S. A.*, 2003, **100**, 14955–14959.
- 20 M. I. Koksharov and N. N. Ugarova, *PEDS*, 2011, **24**, 835–844.
- 21 A. Roda, M. Mirasoli, L. S. Dolci, A. Buragina, F. Bonvicini, P. Simoni and M. Guardigli, *Anal. Chem.*, 2011, **83**, 3178–3185.
- 22 A. Roda, L. Cevenini, E. Michelini and B. R. Branchini, *Biosens. Bioelectron.*, 2011, **26**, 3647–3653.
- 23 L. S. Roach, H. Song and R. F. Ismagilov, *Anal. Chem.*, 2005, **77**, 785–796.
- 24 S. A. Markarian, A. A. Poladyan, G. R. Kirakosyan, A. A. Trchounian and K. A. Bagramyan, *Lett. Appl. Microbiol.*, 2002, **34**, 417–421.
- 25 A. Roda and A. F. Hofman, *J. Lipid Res.*, 1984, **25**, 1477–1489.
- 26 Z. Y. Zheng and C. Bernstein, *Nutr. Cancer*, 1992, **18**, 157–164.

- 27 P. Chieco, E. Romagnoli, G. Aicardi, A. Suozzi, G. C. Forti and A. Roda, *Histochem. J.*, 1997, **29**, 875–883.
- 28 D. Schultheiss and D. Schüler, *Arch. Microbiol.*, 2003, **179**, 89–94.
- 29 U. Heyen and D. Schüler, *Appl. Microbiol. Biotechnol.*, 2003, **61**, 536–544.
- 30 *Molecular Cloning: A Laboratory Manual*, ed. J. Sambrook, E. F. Fritsch and T. Maniatis, Cold Spring Harbor Laboratory Press, Cold Spring Harbor, NY, 1989, vol. 1.
- 31 D. Schüler, R. Uhl and E. Baeuerlein, *FEMS Microbiol. Lett.*, 1995, **132**, 139–145.
- 32 K. L. E. Kaiser and J. M. Ribo, *Toxic. Assess.*, 1988, **3**, 195–237.

Manuscript 1:

An intracellular nanotrap re-directs proteins and organelles in live bacteria

Sarah Borg^a, Felix Popp^a, Julia Hofmann^{a*}, Ulrich Rothbauer^b, Heinrich Leonhardt^a and Dirk Schüler^{ac#}

mBio

submitted

Sarah Borg and Felix Popp contributed equally to this work

Ludwig Maximilian University Munich, Dept. Biology I, LMU Biozentrum, Martinsried,
Germany^a

University of Tübingen, NMI, Markwiesenstraße 55, 72770 Reutlingen, Germany

University of Bayreuth, Dept. Microbiology, Universitätsstraße 30, 95447 Bayreuth,
Germany^c

*Present address: Sequiserve GmbH, Germany.

Abstract

Owing to their small size and enhanced stability, nanobodies derived from camelids have previously been used for the construction of intracellular “nanotraps“, which enable redirection and manipulation of GFP-tagged targets within living plant and animal cells. Although prokaryotic cells also contain highly organized subcellular structures, there are no tools available equivalent to the well-established methods used in eukaryotes. By taking advantage of intracellular compartmentalization in the magnetic bacterium *Magnetospirillum gryphiswaldense*, we demonstrate that proteins and even entire organelles can be re-targeted within prokaryotic cells by versatile nanotrap technology. Expression of multivalent GFP-binding nanobodies on magnetosomes ectopically recruited the chemotaxis protein CheW₁-GFP from polar chemoreceptor clusters to midcell, resulting in gradual knockdown of aerotaxis. Conversely, the entire magnetosome chains could be redirected from midcell and tethered to one of the cell poles. Similar approaches could potentially be used for building synthetic cellular structures and targeted protein knock-downs in other bacteria.

Importance

Intrabodies are commonly used in eukaryotic systems for intracellular analysis and manipulation of proteins with distinct subcellular compartments. In particular, so-called nanobodies have great potential for synthetic biology approaches because they can be easily expressed in heterologous hosts and actively interact with intracellular targets, for instance by the construction of intracellular “nanotraps” in living animal and plant cells. Although prokaryotic cells also exhibit a considerable degree of intracellular organization, there are only few tools available equivalent to well-established methods used in eukaryotes. Here we demonstrate ectopic re-targeting and depletion of polar membrane proteins and entire organelles to distinct compartments in a magnetotactic bacterium, resulting in a gradual knockdown of magneto-aerotaxis. This intracellular “nanotrap” approach has the potential to be applied in other bacteria for building synthetic cellular structures, manipulating protein function and creating gradual targeted knock-downs. Our findings provide proof-of-principle for the universal use of fluorescently tagged proteins as targets for nanotraps to fulfill these tasks.

Introduction

Intrabodies are recombinant fragments of full-length antibodies that are commonly expressed in heterologous hosts and which specifically recognize their antigen within cells. In various eukaryotic systems, they have been demonstrated to be powerful tools that enable the intracellular analysis and manipulation of protein functions [1-5]. Among the various types of intrabodies, so-called nanobodies have proven to be particularly useful due to their small size, enhanced stability and the relative ease of screening, cloning and expression procedures [6-9]. Nanobodies are routinely derived from camelid heavy-chain antibodies, which lack the light chains present in conventional IgG antibodies and recognize their target by interaction with single VHH domains [10]. After extracting the genetic repertoire of B cells from an immunized camelid, antigen-binding VHHs can be selected and expressed as highly robust single-domain antibodies. Because of their special topology, nanobodies preferentially bind to concave surfaces of antigens which are often inaccessible to conventional antibodies [11]. Examples for nanobody-based applications in living plant and animal cells comprise the inhibition of enzyme activity through specific binding to the active site [7, 12], modulation of spectral properties of fluorescent proteins [13] and the construction of nanobody-mediated synthetic regulatory circuits [14]. Furthermore, different strategies for nanobody-based protein knockdowns have been reported, either by targeting nanobody-bound proteins to degradation pathways [15], or by artificially retargeting interaction partners to specific intracellular localizations [16-18]. Artificial relocation of targeted proteins was either caused by trapping of nanobody-bound proteins in the cytoplasm due to interference with protein translocation to cellular compartments [18], or by specifically anchoring the nanobody to distinct structures and compartments of the eukaryotic cell such as distinct DNA regions or the centrioles of animal cells, resulting in ectopic recruitment of GFP (“green fluorescent protein”)-tagged targets [16, 17]. The application of anchored nanobodies against GFP (“green binding protein, GBP”) as nanotrap is a particularly versatile tool because of the widespread use of fluorescence tags.

It has been realized only rather recently that also prokaryotic cells also contain highly organized subcellular structures [19]. Bacteria possess, for example, structural homologs to eukaryotic cytoskeletal elements that define cell shape, structure and function [20, 21]. In addition, they form large supramolecular protein complexes, contain microcompartments and

2. Publications and manuscripts

even biosynthesize canonical membrane-enveloped organelles that show distinct subcellular localization patterns [21-23].

The ability to target proteins intracellularly and possibly even redirect macromolecular complexes to defined subcellular locations in bacteria would be an invaluable tool for synthetic cytoskeletal scaffolding and targeting [24, 25]. For instance, such techniques could be used for protein knockdowns through spatial separation of interaction partners. Other possible applications comprise specific targeting of proteins to bacterial subcellular compartments [26-28], the setup of synthetic intracellular spatial gradients [29], or even artificially compartmentalizing and distributing different cellular processes and organelles to distinct subcellular localizations. However, so far there are only few tools equivalent to the well-established methods used in eukaryotic cells that would efficiently fulfill these tasks in bacteria.

One of the most intricate examples of natural compartmentalization in prokaryotic cells are magnetosomes, which are nano-sized ferromagnetic crystals synthesized within intracellular membrane vesicles by magnetotactic bacteria such as *Magnetospirillum gryphiswaldense*. These organelles are attached to a cytoskeletal filament formed by the actin-like protein MamK and arranged in a chain that is positioned at mid-cell [30, 31]. The resulting magnetic dipole moment rotates the bacterial cell into alignment with the geomagnetic field, thereby probably enhancing the movement of the bacteria towards growth-favoring oxygen levels [32]. Recently, our lab demonstrated the display of nanobodies on magnetosomes that were functional in recognizing their antigen not only *in vitro* but also *in vivo*. Expression of MamC-Red binding protein (RBP) fusions resulted in the recruitment of cytoplasmic red fluorescent protein (RFP) to the magnetosomes [33], showing that intracellular localization of soluble heterologous proteins can be manipulated in bacteria. This motivated us to further investigate whether magnetosome anchors can also be used to trap proteins with distinct functions from other cellular compartments. For this purpose we chose the chemotaxis protein CheW which is part of the chemoreceptor clusters that are universally found in chemotactic bacteria and typically display a distinct polar localization [34]. We demonstrate that CheW₁ fused to EGFP can be depleted from the cell poles by expression of multivalent GBP nanobodies fused to the magnetosome protein MamC, resulting in ectopic recruitment of CheW₁ to the magnetosome chain of *M. gryphiswaldense*. Depletion of CheW₁ from polar clusters resulted in a gradual impairment of aerotaxis. Intriguingly, the interaction

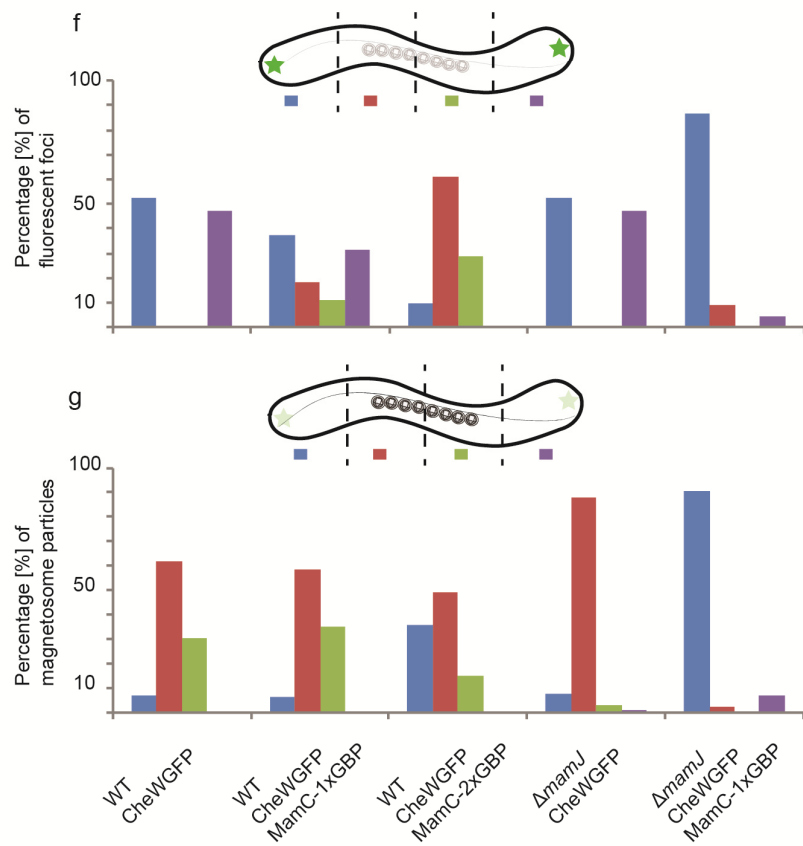
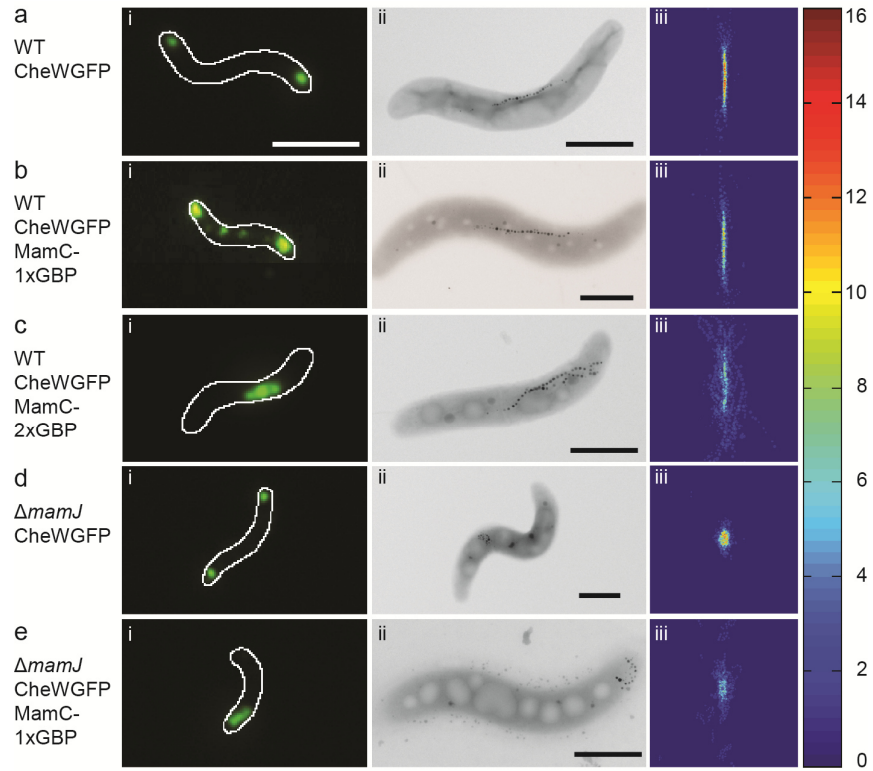
between the magnetosome anchor and polar CheW₁-EGFP also led to artificial re-positioning of the entire magnetosome chain from its midcell position towards one of the cell poles, indicating that entire organelles can be redirected by nanobodies and tethered to ectopic positions. Our study establishes the application of nanotrap technology for artificial targeting of proteins and even entire organelles to bacterial cells. Similar approaches could be used for building tailored subcellular structures in synthetic biology and for gradual protein knock-downs in other bacteria.

Results

Recruitment of CheW₁-EGFP to magnetosomes with a GBP nanotrap

We chose the chemotaxis protein CheW as a target for nanobody-directed intracellular binding and repositioning. In *M. gryphiswaldense* CheW₁ is encoded within chemotaxis operon *cheOp1* that was recently demonstrated to control magneto-aerotactic swimming polarity [35]. It is well established in various bacteria that CheW acts as linker protein and interacts both with the chemoreceptors and the histidine kinase CheA proteins, thereby enhancing the polar chemoreceptor clustering and function [36]. First, we replaced the native *cheW₁* gene by *cheW₁-egfp* via chromosomal insertion. Similar as observed in other bacteria [37-39], spot-like fluorescent signals originating from EGFP-tagged CheW₁ were exclusively found at both cell poles in the wild type background in fluorescence micrographs (Fig. 1a_i & f). This is consistent with previous results of cryo-electron microscopy of *M. gryphiswaldense* cells, where chemoreceptor complexes were identified near the poles [30]. Only in elongated cells close to completion of cell division, two new clusters were formed at midcell (Supplementary Fig. S1). When expressed in mutant backgrounds either forming magnetosome clusters instead of chains (Δ *mamJ*) [31] or entirely lacking any magnetite particles (Δ *mamM*) [40], the same CheW₁-EGFP fluorescence localization pattern as in the wild type background was observed (Fig. 1d_i & Supplementary Fig. S2b), indicating that polar chemoreceptor localization was independent of the presence and configuration of magnetosome chains as expected.

2. Publications and manuscripts



2. Publications and manuscripts

Figure 1: Analysis of subcellular CheW₁-EGFP and magnetosome localization. Fluorescence (i) and TEM micrographs (ii) of representative *M. gryphiswaldense* CheW₁-EGFP (a), CheW₁-EGFP MamC-1xGBP (b), CheW₁-EGFP MamC-2xGBP (c), $\Delta mamJ$ CheW₁-EGFP (d) and $\Delta mamJ$ CheW₁-EGFP MamC-1xGBP cells. Cells were analyzed by CHAP (iii) and scored for the distribution of fluorescence signal, represented by percentage of fluorescent foci detected within 4 equidistant compartments (f) and magnetosomes, represented by percentage of magnetosomes detected within 4 equidistant compartments (g). White scale bar 2 μm , black scale bar 1 μm . 20 cells were aligned by CHAP for each strain, heatmaps display number of magnetosomes. Single cells were segmented into four compartments and for each strain 20 cells were scored to obtain fluorescence and magnetosome distributions.

Next, we asked whether the localization of CheW₁-EGFP was affected by co-expression of a GFP-binding nanobody that had been identified by Rothbauer and colleagues before and termed **GFP-binding protein** (GBP) [41]. To trap CheW₁-EGFP, GBP was expressed either alone in the cytoplasm (MagGBP_{cyt}) or fused to the abundant magnetosome membrane protein MamC [42] which has routinely been used as magnetosome anchor for immobilization of various functional moieties such as EGFP, enzymes or a RFP-binding protein (RBP) [33, 42-45]. In addition to the native *gbp* gene, we used a synthetic allele that was specifically optimized for the expression in *M. gryphiswaldense* (“**magnetospirillum-optimized green-binding protein**”, *maggbp*). MamC was fused to either one single copy of GBP connected to mCherry (mCherry-GBP, also referred to as “chromobody”) [41], the resulting MamC-mCherry-GBP fusion was referred to as MamC-1xGBP hereafter, or to a tandem copy of *maggbp-gbp* (resulting MamC-MagGBP-GBP, referred to as MamC-2xGBP hereafter). All different *gbp* constructs were chromosomally inserted into parent strains co-expressing CheW₁-EGFP. Western blot analysis of cell extracts of all wild type strains carrying the generated fusions revealed reacting protein bands with expected sizes indicating that the mono- and bivalent GBP nanobodies were stably expressed on magnetosomes (Supplementary Fig. S3).

Cytoplasmic expression of unfused MagGBP_{cyt} alone had no effect on the localization of CheW₁-EGFP fluorescence in the wild type background (Supplementary Fig. S2d). However, upon co-expression of MamC-1xGBP and CheW₁-EGFP we detected weaker, secondary fluorescent foci at approximately midcell position in addition to the two polar CheW₁-EGFP signals (Fig. 1b_i). We scored the number of fluorescent foci in four equidistant

2. Publications and manuscripts

sectors along the length of a representative set of cells and calculated the relative abundance of fluorescence intensity in each of the sectors (see Methods for details). In contrast to the wild type background, which displayed only polar foci, about 30% of fluorescence intensity was detected within the cytoplasm upon co-expression of MamC-1xGBP (a representative cell is shown in Fig. 1b_i; Fig. 1f). Recruitment of CheW₁-EGFP was likely due to interaction with GBP expressed on magnetosomes, as green (CheW₁-EGFP) and red fluorescence (mCherry-tagged magnetosomes) signals coincided in all analyzed cells, indicating that direct GBP-EGFP interaction caused the observed redirection of CheW₁ (Supplementary Fig. S2e&f). In cells co-expressing two GBP copies in tandem (MamC-2xGBP) a single, large non-polar fluorescence signal was detected in the vast majority of cells. 90% of the CheW₁-EGFP fluorescence intensity was shifted towards midcell (Fig. 1c_i & Supplementary Fig. 4), while only 10% of the fluorescence signal remained at the cell pole (Fig. 1f). Instead of the spot-like, exclusively polar foci of the parent strain, a linear fluorescence signal was present near midcell in most MamC-2xGBP expressing cells, demonstrating efficient redirection of membrane complex-associated proteins (Fig. 1c_i & Supplementary Fig. S4).

Next, we investigated whether the absence of magnetic nanoparticles would affect the recruitment of CheW₁-EGFP through MamC-GBP fusions by analyzing non-magnetic cells. Due to loss of the magnetosomal iron transporter MamM $\Delta mamM$ cells lack any magnetite crystals, but still produce empty magnetosome membrane vesicles [40]. CheW₁-EGFP fluorescence was shifted towards midcell in the $\Delta mamM$ strain co-expressing MamC-2xGBP to the same extent as in the magnetite-containing strains (Supplementary Fig. S2c). To analyze whether the configuration of magnetosome chains had an effect on CheW₁-EGFP recruitment, we also expressed MamC-1xGBP in the $\Delta mamJ$ background, in which the physical interaction of magnetosome chains with the actin-like MamK filaments is abolished [31], resulting in agglomerated clusters rather than linear well-ordered chains of magnetosomes (Fig. 1d_{ii}&e_{ii}). In the vast majority of analyzed $\Delta mamJ$ MamC-1xGBP cells the major proportion of CheW₁-EGFP fluorescence (>85 % of all foci) was located at only one cell pole (Fig. 1f) and appeared to be slightly distorted longitudinally (Fig. 1e_i).

Effect of CheW₁-EGFP recruitment on magnetosome localization

We noticed that all strains which showed strong CheW₁-mislocalization were increasingly affected in their magnetic alignment as indicated by reduced C_{mag} values (e.g. MamC-2xGBP: 0.60 ± 0.07 , wild type: 1.24 ± 0.20). The C_{mag} provides an optical measure of

2. Publications and manuscripts

the relative alignment of cells in a cuvette by applying a strong magnetic field either parallel or perpendicular to the light beam of a photometer. TEM analysis revealed that wild type cells expressing CheW₁-EGFP alone displayed the same magnetosome localization pattern as their parent strain (Fig. 1a_{ii}). Both automated image analysis by Chain Analysis Program (CHAP) [46] and manual scoring of magnetosome position (see Methods for details; Fig. 1g) indicated that the linear chains of magnetosomes were consistently positioned at midcell and displayed the same configuration as typically observed for the *M. gryphiswaldense* parent strain [47, 48], with approximately 35 particles per cell that had an average crystal size of 35-47 nm [48]. Additional cytoplasmic expression of MagGBP_{cyt} in the same background did not affect magnetosome chain configuration (Supplementary Fig. S5b). Co-expression of MamC-1xGBP and CheW₁-EGFP did not affect the midcell position of magnetosome chains either, but chains were less compact, i.e. particles were more widely spaced as indicated by the fuzzier, slightly stretched appearance of magnetosome chains in CHAP analysis heat maps (Fig. 1b_{iii}). TEM analysis of Δ *mamJ* cells expressing CheW₁-EGFP alone revealed the same magnetosome localization pattern as their parent strain (Fig. 1d_{ii}). Consistent with the observed shift of the CheW₁-EGFP fluorescence towards one pole in the Δ *mamJ* MamC-1xGBP strain, 90% of magnetosome clusters detected in TEM micrographs were localized at a single cell pole only, while clusters were no longer observed at midcell or along the cell length as commonly found in the Δ *mamJ* parent strain [31, 49] (Fig. 1g). Moreover, the loose magnetosome assemblies observed at the poles were slightly elongated, compared to the compact rounded magnetosome clusters of the parent strain (Fig. 1d_{iii}&e_{iii}). This indicated that targeted recruitment and partial rearrangement of magnetosomes was facilitated in cells in which magnetosome particles were no longer bound to the MamK filament by their molecular connector MamJ [31]. As observed for mislocalization of CheW₁-EGFP fluorescence, in wild type cells co-expressing divalent tandem fusions of GBP (MamC-2xGBP) magnetosome chains were predominantly drawn to one of the cell poles (Fig. 1c_{ii} & Supplementary Fig. S6). Magnetosome chains were even less compact than in the presence of the monovalent nanobody, as reflected by the rather scattered pattern of poorly aligned magnetosome chains (Fig. 1c_{iii}). Consistent with the overall shift of the chain, the mean fraction of magnetosome particles located at one of the cells' poles increased from 7 to 36% (Fig. 1g).

2. Publications and manuscripts

Effect of CheW₁-EGFP recruitment on chemotaxis of M. gryphiswaldense

The observed mislocalization of chains also affected the magnetic alignment of swimming cells. While wild type cells expressing only CheW₁-EGFP predominantly swam aligned to the ambient magnetic field as the parent strain, a large fraction of cells co-expressing MamC-2xGBP displayed trajectories that were oriented at random angles to the ambient magnetic field (Fig. 2a). As indicated by video microscopy, motility and mean swimming speed were not affected in any of the analyzed strains. Compared to the control strains $\Delta cheW_1$ and $\Delta cheOp1$, in which aerotaxis was entirely abolished as indicated by the formation of small aerotactic halos in swim plate assays (Supplementary Fig. S7) [35], co-expression of cytoplasmic MagGBP_{cyt} and CheW₁-EGFP in the wild type background did not affect the size of swim halos that were virtually identical to those of the parent strain (Fig. 2b&c).

While $\Delta cheW_1$ did not show any response when shifted from anaerobic conditions to 2% oxygen in a microscopic gas perfusion chamber (Fig. 2d) and displayed a straight-swimming phenotype comparable to the $\Delta cheOp1$ deletion strain, wild type cells expressing CheW₁-EGFP showed a reaction very similar to that observed in the parent strain [35]. The reversal frequency instantaneously rose from less than 0.1 s⁻¹ to more than 0.2 s⁻¹ after microoxic up-shift. This was followed by a rapid drop in reversal frequency below pre-stimulus levels within 15 s (Fig. 2d). However, co-expression of MamC-1xGBP and CheW₁-EGFP led to slightly reduced halo sizes in swim plates and a lower number of reversals in response to the oxygen shift. The maximum reversal frequency remained below 0.15 s⁻¹ and peaked at approximately 60% of the wild type rate. Interestingly, co-expression of MamC-1xGBP also caused delayed adaptation after the shift as the reversal frequency remained above pre-stimulus levels within 20 s post-shift.

Co-expression of MamC-2xGBP and CheW₁-EGFP, which completely depleted CheW₁-EGFP from the cell poles as suggested by fluorescence microscopy (Fig. 1c_i), also had a dramatic effect on the cells' switching behavior under anoxic equilibrium conditions and the response elicited by oxygen exposure. The pre-stimulus reversal frequency was comparable to that of the $\Delta cheW_1$ strain and rose only minimally after oxygen up-shift to 2% O₂ remaining on a very low level (maximum frequency below 0.05 s⁻¹). In conclusion, an increase in copy number of GBP led to gradually stronger impairment of aerotaxis, eventually

2. Publications and manuscripts

reducing the number of reversals in a strain co-expressing CheW₁-EGFP and the divalent MamC-2xGBP fusion to the level of a $\Delta cheW_1$ null mutant.

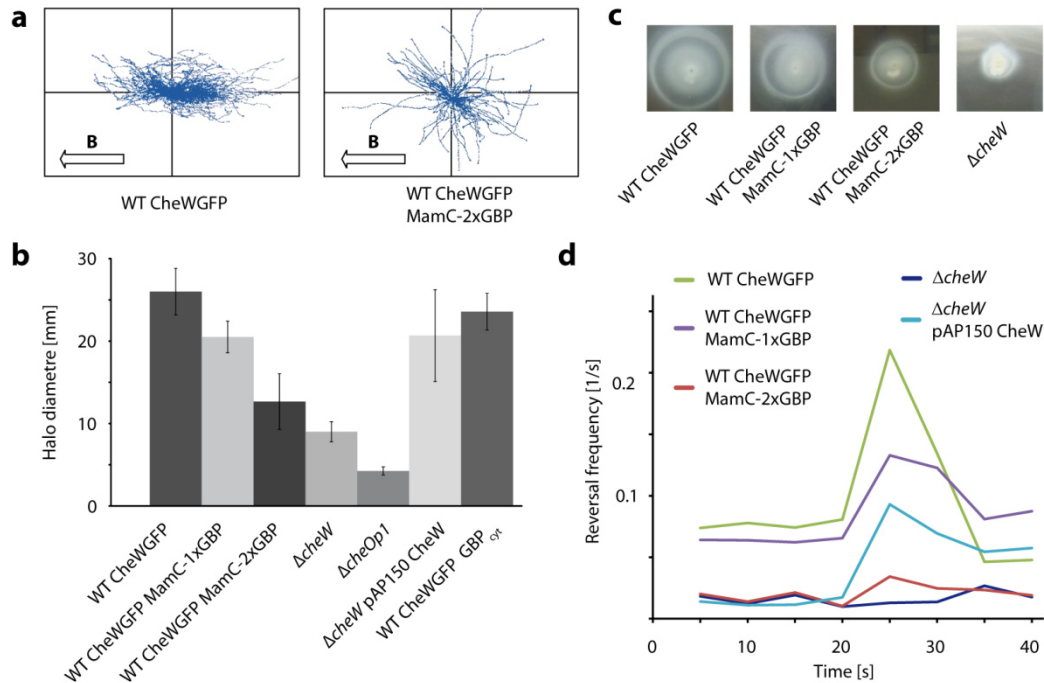


Figure: 2 Magneto-aerotactic swimming behavior of *M. gryphiswaldense* strains expressing CheW₁-EGFP and MamC-GBP fusions. (a) Magnetic alignment of swimming cells expressing CheW₁-EGFP alone or in combination with MamC-2xGBP. A plot of all tracks from a representative video record is shown for each strain. Cells swimming in the gas perfusion chamber were exposed to a homogenous vertical magnetic field of 0.26 mT (**B**). (b) Average halo diameter of strains expressing MamC-GBP fusions in swim plates (mean \pm s.d. of at least 3 independent replicates). Chemotaxis gene deletion mutants $\Delta cheW_1$ and $\Delta cheOp1$ were used as controls. *Trans*-complementation of the $\Delta cheW_1$ mutant strain by constitutive expression of CheW₁-EGFP from a plasmid restored chemotactic efficiency to 80% of the wild type cells expressing CheW₁-EGFP at physiological levels. (c) Halo formation of wild type CheW₁-EGFP, CheW₁-EGFP MamC-1xGBP, CheW₁-EGFP MamC-2xGBP and $\Delta cheW$ cells in 0.2 % motility agar 3 days after inoculation. (d) Aerotactic reversal response upon abrupt shift from 0% to 2% oxygen in a microscopic gas perfusion chamber. Video records were analyzed by automated tracking software to obtain swim tracks and reversal events of individual cells [35] and reversal rates were calculated for 5-s intervals by averaging single cell data from at least 3 independent recordings.

Discussion

We investigated the interaction between components of the universal bacterial chemotaxis signaling pathway and nanobodies expressed on the magnetosome organelles of *M. gryphiswaldense*, which enabled us to easily follow the structural and behavioral effects of artificial recruitment by TEM and FM imaging, and by video microscopy at the single cell level. We observed that by anchoring GBP to the magnetosome membrane the localization of CheW₁-GFP was shifted from the poles to midcell, i.e. to the typical position of the magnetosome chain. There are two possible explanations for the observed redirection of CheW₁ from the polar clusters to the magnetosomes: (i) Unbound CheW₁, in equilibrium with the receptor bound form, could be recruited from a cytoplasmic pool, whereas (ii) membrane-bound CheW₁ could be directly withdrawn from pre-existing polar clusters. CheW is a soluble protein that lacks transmembrane domains but *in vitro* forms ultrastable ternary complexes together with CheA and chemoreceptors [50]. However, in living cells signaling complexes are weakly dynamic and display slow turnover (of approximately 12 min) as indicated by FRAP experiments on CheA and CheW constructs [51]. Consistent with these observations it has been suggested that small amounts of CheA might be permanently present in an unbound state in the cytoplasm [52]. However, the relative copy numbers of all cluster components are tightly regulated, and since overexpression of CheW leads to impaired chemotactic signaling (due to competitive inhibition of CheA binding to the chemoreceptors) [50], the pool of free CheW in the cytoplasm must be rather small. Thus, it seems most probable that soluble CheW present in low concentration in the cytoplasm is sequestered by magnetosome-anchored GBP, and over time also those molecules initially bound to the chemoreceptors clusters might gradually be released and trapped at ectopic positions by strong interaction with the nanobody.

The localization of CheW₁-GFP was unaffected by co-expression of cytoplasmic (unfused) GBP in the wild type background, but shifted towards midcell upon MamC-2xGBP expression in the non-magnetic *ΔmamM* strain, which lacks any electron-dense magnetic crystals, but still forms empty vesicles of the magnetosome membrane [40]. This demonstrates that GBP fixed on magnetite-free membrane vesicles is sufficiently effective to specifically re-direct localized proteins. Furthermore, this suggests that recruitment and retargeting could be achieved in other bacteria lacking magnetosomes by using different spatial determinants as intracellular traps.

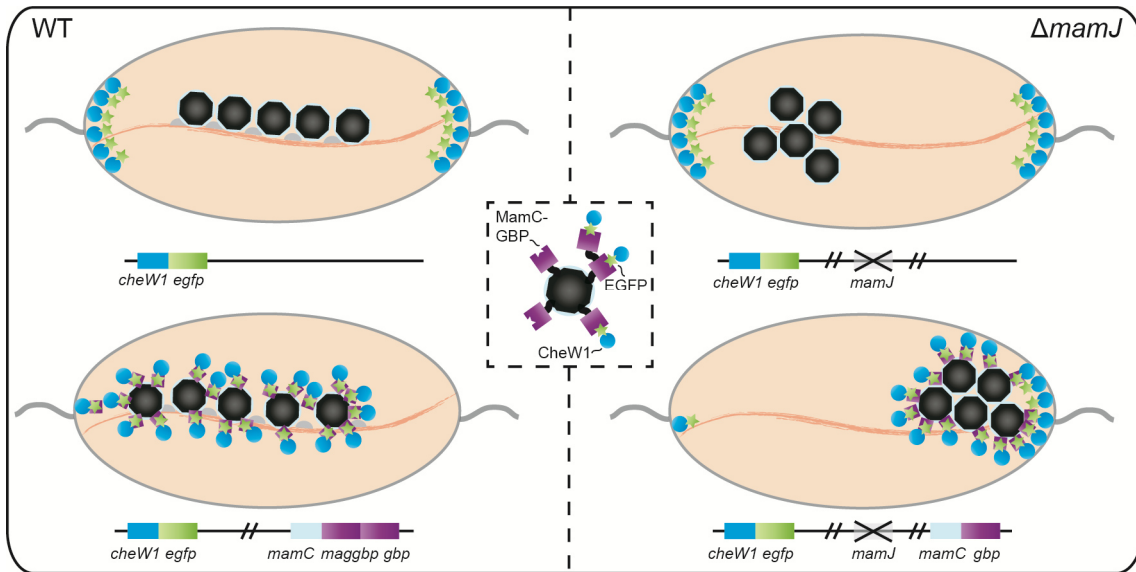


Figure 3: Model of MamC-GBP and CheW₁-EGFP interaction. CheW₁-EGFP localizes distinctly at the cell poles if expressed chromosomally in wild type and $\Delta mamJ$ background (upper panel right and left). If MamC-GBP is co-expressed in the wild type (lower left panel), CheW₁-EGFP is depleted completely from the poles. Expression of MamC-GBP in the $\Delta mamJ$ CheW₁-EGFP background leads to recruitment of whole magnetosomes to the cell poles (lower right panel). Expression of mono- and divalent nanobodies on a magnetosomes and interaction with CheW₁-EGFP is illustrated in the inset. Expressed proteins are illustrated in same colors as genes.

Although presence of magnetic particles was no absolute prerequisite for efficient recruitment, redistribution of CheW was strongly affected by magnetosome chain configuration. Magnetosome clusters were drawn to only one pole in the $\Delta mamJ$ background upon expression of MamC-1xGBP and acted as efficient nanotraps for CheW₁-GFP. In contrast to the undefined midcell fluorescence caused by partial depletion from polar clusters observed upon expression of MamC-1xGBP in the wild type background, virtually no CheW₁-GFP signal was detected at midcell or the opposite pole in the $\Delta mamJ$ mutant strain. This might either be due to increased avidity of nanobodies concentrated in the tightly clustered magnetosome assemblies, or might reflect a stochastic shift of CheW diffusion equilibrium due to the concentration of two sinks (i.e., the native chemoreceptor cluster and the artificial magnetosomal nanobody cluster) at a single pole (Fig. 3, right lower panel).

Interaction of MamC-GBP and CheW₁-GFP reciprocally affected configuration and positioning of the magnetosome chain. Binding of CheW₁-GFP to magnetosome particles

2. Publications and manuscripts

disturbed their proper alignment into regular, densely spaced chains. Increasing the expression of GBP (MamC-1xGBP and 2xGBP) also gradually increased the inter-particle spacing, possibly by additional protein bound to the magnetosome surface which might weaken the magnetostatic interactions between particles. Overexpression of MamC-2xGBP in the wild type background caused a nearly complete shift of the magnetosome chains towards the poles, with the majority of magnetosome chains originating at polar or sub-polar positions (Supplementary Fig. S6), which was probably caused by redirecting and tethering the chains to a fraction of membrane-bound CheW₁-GFP remaining at the cell pole (Fig. 3, left lower panel). Although the magnetosome chain of wild type cells generally occupies mid-cell position, it becomes mobilized during cell division when the chain is split in half and repositioned by MamK dynamics to mid-cell of daughter cells [49]. We found that magnetosome chain localization was most severely impaired in cells lacking the acidic MamJ protein, which is assumed to connect magnetosome particles to the cytoskeletal magnetosome filament formed by the actin-like MamK protein [31]. In the $\Delta mamJ$ background overexpression of the monovalent nanobody was already sufficient to rearrange (Fig. 1e_{iii}) and recruit (Fig. 1e_{ii}) the magnetosome cluster to one cell pole (Fig. 3, right lower panel). The increased intracellular mobility of $\Delta mamJ$ magnetosome clusters might be explained by lack of the presumed MamK-mediated interactions with divisome constituents [49]. In wild type cells these interactions need to be overcome by interaction with polar CheW, whereas in $\Delta mamJ$ cells magnetosome redirection is facilitated because MamK-magnetosome interactions are abolished.

The level of CheW₁-GFP recruitment clearly depended on gene dosage. While redirection of CheW₁-GFP was only partial in cells expressing MamC-1xGBP, overexpression of MamC-2xGBP caused a complete shift of CheW₁-GFP localization towards midcell. There is precedence for significantly increased avidity (500x) of a nanobody consisting of a fusion of two identical domains compared to the monovalent nanobody [53]. Similarly, in our experiments the binding of CheW₁-GFP to the monovalent GBP was apparently comparable to the in vivo turnover of the chemoreceptor-CheW complexes, since polar and midcell localized CheW₁-GFP could be detected. In contrast, the avidity of the bivalent nanobody was much stronger, more CheW₁-GFP was bound and the equilibrium was shifted towards the GBP-bound state.

2. Publications and manuscripts

In addition to demonstrating the efficient redirection of entire organelles to distinct locations, we observed that ectopic redirection of CheW₁-GFP also gradually modulated chemotactic efficiency of *M. gryphiswaldense* cells. While chemoreceptors readily form complexes in the absence of CheA and CheW, the latter is essential for stabilizing native CheA-receptor interactions and lattice formation [36, 52]. Partial depletion of CheW₁ gradually reduced chemotactic efficiency, while expression of the bivalent nanobody essentially phenocopied the deletion of *cheW₁* (Fig. 2c). As GBP expressed in the cytoplasm had no effect on aerotaxis, this was not due to inactivation of CheW₁-GFP, but caused by redirection and depletion from its native polar environment. Although bacteria do not display the same level of compartmentalization as eukaryotic cells, the functionality of many bacterial proteins similarly depends on their localization. Our results show that testing protein function by manipulating its subcellular localization which has been applied to eukaryotic systems [2, 18], can be extended to the much smaller bacterial cells and be used to efficiently modulate protein function by subcellular retargeting.

Compared to other approaches for silencing or manipulating the expression of selected genes at the DNA or RNA [54, 55] level, the biggest advantage of regulating gene expression at the protein level is that there is no change of mRNA transcript or native protein expression level [56]. Especially for bacterial genes encoded in operons, gradual knockdown of individual proteins might be difficult to achieve at the transcriptional level, if polar effects on transcription of downstream genes are to be avoided. Additionally, it would be desirable to develop inducible systems, e.g. to gradually control *in vivo* the stoichiometry of proteins in larger clusters. This might facilitate the study of complex regulatory pathways, such as cell division or cell differentiation processes in other bacteria.

Intrabodies are well established as powerful tools in eukaryotic cells for trapping soluble proteins at defined subcellular locations [16-18] or for inhibition of protein function [12]. Although recombinant nanobodies can be produced easily in bacteria such as *E. coli* [10], to date the use of intrabodies in bacterial cells has been restricted to only very few studies. Two early publications reported the intracellular expression of single-chain Fv antibody fragments (e.g. to block transcriptional activation) [57, 58], and more recently also nanobodies have been applied in bacteria to inhibit enzyme activity [59]. However, in these approaches intrabodies were not anchored to defined positions and inhibition of enzymes was achieved by neutralization, rather than redirection to completely different compartments of

2. Publications and manuscripts

the cell. Although for proof-of-principle we took advantage of the specific compartmentalization in *M. gryphiswaldense*, in which the magnetosomes provide a natural anchor for setting up an intracellular nanotrap, this approach could also be extended and adapted for application in other bacteria. By using universal tags like GFP for recruitment, many proteins can be targeted with the same nanobody applying the same strategy, obviating the need of camelid immunization and screening of whole libraries. Multiple other applications are possible because GFP fusion proteins can be combined with any cellular anchor point, such as subcellular compartments (e. g. poles, midcell), specific protein complexes, organelles, or other spatial determinants. For instance, potential applications of our approach in bacteria could be building synthetic cellular structures (e.g. artificial tethering of heterologously expressed bacterial microcompartments) or compartmentalization of biosynthetic pathways, which can dramatically increase production by restricting reactions spatially to subcellular compartments [60, 61].

Methods

Bacterial strains, plasmids, and culture conditions

Bacterial strains and plasmids used in this study are listed in Supplementary Table S1&S2. *M. gryphiswaldense* strains were grown microaerobically with 1% oxygen in modified flask standard medium (FSM) at 30°C [62] and moderate shaking (120 rpm). *E. coli* strains were cultivated as previously described [63], for growth of *E. coli* WM3064 (W. Metcalf, unpublished) or BW29427 (K. Datsenko and B. L. Wanner, unpublished data) 1 mM DL- α , ϵ -diaminopimelic acid (DAP) was added to lysogeny broth media (LB). Strains were routinely cultured on plates solidified with 1.5% (w/v) agar. For strains carrying recombinant plasmids, media were supplemented with 25 $\mu\text{g ml}^{-1}$ kanamycin and 50 $\mu\text{g ml}^{-1}$ ampicillin (Amp) for *E. coli* strains, and 5 $\mu\text{g ml}^{-1}$ kanamycin (Km) for *M. gryphiswaldense* strains, respectively.

For the preparation of swim plates only 0.2% agar was used, the concentration of carbon source (lactate) was lowered to 1.5 mM and peptone was omitted from FSM medium. 5 μl of overnight culture were pipetted into the swim agar and plates were incubated under microoxic conditions for 2 days (protocol modified from Schultheiss 2004) [64].

Molecular and genetic techniques

Oligonucleotides were purchased from Sigma-Aldrich (Steinheim, Germany) and sequences can be supplied on request. Plasmids were constructed by standard recombinant techniques as described in detail below. All constructs were sequenced on an ABI 3730 capillary sequencer (Applied Biosystems, Darmstadt, Germany), utilizing BigDye Terminator v3.1. Sequence data were analyzed with Software Vector NTI Advance[®] 11.5 (Invitrogen, Darmstadt, Germany). The GBP nanobody [41] was provided by ChromoTek GmbH (Planegg-Martinsried) and a synthetic GBP was specifically optimized for the expression in *M. gryphiswaldense* with respect to its codon usage and purchased from ATG:biosynthetics (Merzhausen, Germany).

Construction of plasmids for chromosomal gene insertion, deletion and fusion

For chromosomal exchange of *cheW₁* against *cheW₁-egfp*, the fluorescence marker was fused via overlap extension PCR [65] to *cheW₁* and to a 1000 bp downstream fragment of the gene. The fused product was inserted into pORFM and the native *cheW₁* copy was

2. Publications and manuscripts

exchanged chromosomally against *cheW₁-egfp* by homologous recombination facilitated by GalK counter selection [66]. Deletion of *cheW₁* was achieved following a similar strategy by fusion of approximately 1000 bp fragments upstream and downstream of *cheW₁* connected by 12 nonsense bp replacing the native *cheW₁*. For complementation of *cheW₁* deletion, *cheW₁* was amplified from the genome and inserted into pAP150 [45].

All *mamC-gbp* fusions were chromosomally introduced by transposition, therefore all gene fusions created by overlap PCR were inserted into transposable pSB6 and pSB7 plasmids [45].

Analytical methods

Magnetic reaction of cells was validated by light microscopy applying a bar magnet. Optical density (OD) and magnetic response (C_{mag}) of exponentially growing cells were measured photometrically at 565 nm as previously reported [67]. For C_{mag} measurement a magnetic field of approximately 70 mT was used.

Biochemical Methods

Polyacrylamide gels were prepared according to the method of Laemmli [68]. Strains were grown overnight and spun down via centrifugation, OD_{565} was set to 10 and 20 μl was loaded onto 12% (wt/vol) SDS gels and analyzed via immunoblotting. Proteins were electroblotted onto polyvinylidene difluoride (PVDF) membranes (Roth, Germany). Membranes were blocked for 1h at room temperature with blocking solution (2.5% (w/v) milk powder in Tris-buffered saline (TBS) (50 mM Tris-HCl; pH 7.6; 150 mM NaCl)) and incubated for another hour with primary rabbit anti-MamC IgG antibody (1:500 dilution [Santa Cruz, USA]). Membranes were washed 4 times with TBS for 5 min and incubated with a secondary alkaline phosphatase-labeled goat anti-rabbit IgG antibody (1:2000 dilution [Promega, USA]) for 45 min. Membranes were washed 4 times with TBS for 5 min and immunoreactive proteins were visualized with NBT/BCIP (Roche Kit).

Phase Contrast and Fluorescence Microscopy

Strains with genomic *CheW₁-EGFP* fusions and additional *MamC-GBP* fusions were grown in 1 ml FSM in 24-well plates for 16 h at 30°C and 1% O_2 without agitation. For microscopy cells were immobilized on agarose pads (PBS buffer supplemented with 1% agarose), and imaged with an Olympus BX81 microscope equipped with a 100

2. Publications and manuscripts

UPLSAPO100XO objective (numerical aperture of 1.40) and a Hamamatsu Orca AG camera. The Olympus xcellence pro software was used to capture and analyze images.

To analyze relative position of fluorescent foci we manually segmented each cell along its long axis into four equal sectors and scored the fluorescent foci within each sector. The strongest fluorescence signal(s) was scored as “++”, weaker signals were scored as “+”. Since the orientation of imaged cells was random and in many cases the distribution of fluorescent foci was not perfectly symmetric, we rotated the cells where necessary so that the sectors with the highest cumulated score were sector 1 and 2. We then calculated relative frequencies of fluorescent foci position based on the ratio of cumulated scoring points of all analyzed cells per sector divided by the total number of scoring points in all cells.

Transmission electron microscopy

Magnetosome chain localization was examined by transmission electron microscopy (TEM), for which cells were concentrated via centrifugation and adsorbed onto carbon-coated copper grids. Cells were imaged with a FEI Morgagni 268 (FEI, Eindhoven, Netherlands) electron microscope at an accelerating voltage of 80 kV. For analysis of magnetosome alignment and chain compactness, we used the CHAP script implemented in MATLAB and run the program for 20 cells for each strain [46]. For analysis of magnetosome position we manually segmented each cell along its long axis into four equal sectors and scored the number of magnetosomes within each sector. Since the orientation of imaged cells was random and in many cases the distributions of magnetosomes were not perfectly symmetric, we rotated the cells where necessary so that the sector with most magnetosomes scored was either sector 1 or 2. We then calculated relative frequencies of magnetosome position based on the ratio of cumulated magnetosomes of all analyzed cells per sector divided by the total number of magnetosomes in all cells.

Video microscopy and analysis of swimming parameters

Swimming behavior of cells was analyzed and recorded using dark-field microscopy on an upright Zeiss Axioplan microscope (Zeiss, Jena, Germany) at 100x magnification. All microscopic motility experiments were performed within a microscopic gas perfusion chamber (Ludin Chamber, Life Imaging Services) that was equilibrated with variable moisturized and precisely adjusted O₂-N₂ gas mixtures containing between 0 and 2% oxygen [35].

2. Publications and manuscripts

Homogeneous conditions were maintained by using strongly diluted cell suspensions (OD 0.005) and exposing cell suspensions to a constant gas flow of 50 ml min^{-1} , protected against turbulence by placing a gas-permeable agar sheet on top.

Videos were recorded with a UK1158–M camera (EHD, Damme, Germany) at a frame rate of 15 fps and a standard resolution of 1360 x 1024 pixels using VirtualDub software. Dark-field video records were analyzed by a custom-made automated tracking software (“WimTaxis – Bacteria Tracking”, Wimasis GmbH, München, Germany) specifically adapted to determine basic swimming characteristics. The software automatically detected swimming reversals and provided the x-y coordinates of every tracked cell for each frame.

The minimum track length was set to be 50 frames. Within the usual tracking times (depending on the time bacteria stayed in the viewing field, usually below 10 s) reversals generally were too infrequent to simply average reversal rates of single cells. Therefore, the reversal frequency analysis for each experiment was performed at the population level, and all detected reversals were divided by the total respective tracking time (sum of the temporal length of all tracks) to obtain the population average.

To analyze the cells’ reaction to oxygen shifts, the gas stream was manually switched between oxic and anoxic. For this purpose we equipped our setup with a three-way valve and a flow meter to adjust the flow of N_2 gas to 50 ml min^{-1} [35].

Cells were first equilibrated for 3 min under anoxic conditions before the video recording was started. After 20 s the gas flow was shifted to 2% O_2 and cells were recorded for additional 20 s. To determine the average reversal frequency over time, the number of detected reversals within 5-s intervals was added up from three independent video recordings and normalized to the total corresponding tracking time.

References

1. Carlson, J.R. and I.L. Weissman, *Molecular tools for inactivating a yeast enzyme in vivo*. Mol. Cell. Biol., 1988. **8**(6): p. 2647-2650.
2. Kaiser, P.D., et al., *Recent progress in generating intracellular functional antibody fragments to target and trace cellular components in living cells*. BBA-Proteins Proteom, 2014.
3. Marasco, W.A., W.A. Haseltine, and S.Y. Chen, *Design, intracellular expression, and activity of a human anti-human-immunodeficiency-virus type-1 Gp120 single-chain antibody*. Proc. Natl. Acad. Sci. USA, 1993. **90**(16): p. 7889-7893.
4. Tavladoraki, P., et al., *Transgenic plants expressing a functional single-chain Fv antibody are specifically protected from virus attack*. Nature, 1993. **366**(6454): p. 469-472.
5. Wesolowski, J., et al., *Single domain antibodies: promising experimental and therapeutic tools in infection and immunity*. Med. Microbiol. Immun., 2009. **198**(3): p. 157-174.
6. Bodelón, G., C. Palomino, and L.Á. Fernández, *Immunoglobulin domains in Escherichia coli and other enterobacteria: from pathogenesis to applications in antibody technologies*. FEMS Microbiol. Rev., 2013. **37**(2): p. 204-250.
7. Lauwereys, M., et al., *Potent enzyme inhibitors derived from dromedary heavy-chain antibodies*. EMBO J, 1998. **17**(13): p. 3512-3520.
8. Pellis, M., et al., *A bacterial-two-hybrid selection system for one-step isolation of intracellularly functional Nanobodies*. Arch. Biochem. Biophys., 2012. **526**(2): p. 114-123.
9. De Meyer, T., S. Muyldermans, and A. Depicker, *Nanobody-based products as research and diagnostic tools*. Trends Biotechnol., 2014. **32**(5): p. 263-270.
10. Muyldermans, S., *Nanobodies: Natural single-domain antibodies*. Annu. Rev. Biochem., 2013. **82**(1): p. 775-797.
11. De Genst, E., et al., *Molecular basis for the preferential cleft recognition by dromedary heavy-chain antibodies*. Proc. Natl. Acad. Sci. USA, 2006. **103**(12): p. 4586-4591.
12. Jobling, S.A., et al., *Immunomodulation of enzyme function in plants by single-domain antibody fragments*. Nat. Biotechnol., 2003. **21**(1): p. 77-80.

2. Publications and manuscripts

13. Kirchhofer, A., et al., *Modulation of protein properties in living cells using nanobodies*. Nat. Struct. Mol. Biol., 2010. **17**(1): p. 133-138.
14. Tang, J.C.Y., et al., *A nanobody-based system using fluorescent proteins as scaffolds for cell-specific gene manipulation*. Cell, 2013. **154**(4): p. 928-939.
15. Caussin, E., O. Kanca, and M. Affolter, *Fluorescent fusion protein knockout mediated by anti-GFP nanobody*. Nat. Struct. Mol. Biol., 2012. **19**(1): p. 117-121.
16. Herce, H.D., et al., *Visualization and targeted disruption of protein interactions in living cells*. Na. Commun., 2013. **4**.
17. Rothbauer, U., et al., *A versatile nanotrapp for biochemical and functional studies with fluorescent fusion proteins*. Mol. Cell Proteomics, 2008. **7**(2): p. 282-289.
18. Schornack, S., et al., *Protein mislocalization in plant cells using a GFP-binding chromobody*. Plant Journal, 2009. **60**(4): p. 744-754.
19. Gitai, Z., *The new bacterial cell biology: Moving parts and subcellular architecture*. Cell, 2005. **120**(5): p. 577-586.
20. Margolin, W., *Sculpting the bacterial cell*. Current Biology, 2009. **19**(17): p. R812-R822.
21. Shapiro, L., H.H. McAdams, and R. Losick, *Why and how bacteria localize proteins*. Science, 2009. **326**(5957): p. 1225-1228.
22. Cornejo, E., N. Abreu, and A. Komeili, *Compartmentalization and organelle formation in bacteria*. Curr. Opin. Cell Biol., 2014. **26**: p. 132-138.
23. Murat, D., M. Byrne, and A. Komeili, *Cell biology of prokaryotic organelles*. Cold Spring Harbor Perspectives in Biology, 2010. **2**(10).
24. Chen, A.H. and P.A. Silver, *Designing biological compartmentalization*. Trends Cell Biol., 2012. **22**(12): p. 662-670.
25. Bashor, C.J., et al., *Rewiring cells: synthetic biology as a tool to interrogate the organizational principles of living systems*. Annu. Rev. Biophys., Vol 39, 2010. **39**: p. 515-537.
26. Choudhary, S., et al., *Engineered protein nano-compartments for targeted enzyme localization*. PLoS One, 2012. **7**(3).
27. Frank, S., et al., *Bacterial microcompartments moving into a synthetic biological world*. J. Biotechnol., 2013. **163**(2): p. 273-279.
28. Kerfeld, C.A., S. Heinhorst, and G.C. Cannon, *Bacterial microcompartments*. Annu. Rev. Microbiol., 2010. **64**: p. 391-408.

2. Publications and manuscripts

29. Chau, A.H., et al., *Designing synthetic regulatory networks capable of self-organizing cell polarization*. Cell, 2012. **151**(2): p. 320-332.
30. Katzmann, E., et al., *Loss of the actin-like protein MamK has pleiotropic effects on magnetosome formation and chain assembly in Magnetospirillum gryphiswaldense*. Mol. Microbiol., 2010. **77**(1): p. 208-224.
31. Scheffel, A., et al., *An acidic protein aligns magnetosomes along a filamentous structure in magnetotactic bacteria (vol 440, pg 110, 2006)*. Nature, 2006. **441**(7090): p. 248-248.
32. Faivre, D. and D. Schüler, *Magnetotactic bacteria and magnetosomes*. Chem. Rev., 2008. **108**(11): p. 4875-4898.
33. Pollithy, A., et al., *Magnetosome expression of functional camelid antibody fragments (nanobodies) in Magnetospirillum gryphiswaldense*. Appl. Environ. Microbiol., 2011. **77**(17): p. 6165-6171.
34. Briegel, A., et al., *Universal architecture of bacterial chemoreceptor arrays*. Proc. Natl. Acad. Sci. USA, 2009. **106**(40): p. 17181-17186.
35. Popp, F., J.P. Armitage, and D. Schüler, *Polarity of bacterial magnetotaxis is controlled by aerotaxis through a common sensory pathway*. Nat. Commun., 2014. **5**(5398).
36. Kentner, D., et al., *Determinants of chemoreceptor cluster formation in Escherichia coli*. Mol. Microbiol., 2006. **61**(2): p. 407-417.
37. Maddock, J.R. and L. Shapiro, *Polar location of the chemoreceptor complex in the Escherichia coli cell*. Science, 1993. **259**(5102): p. 1717-1723.
38. Wadhams, G.H., et al., *Targeting of two signal transduction pathways to different regions of the bacterial cell*. Mol. Microbiol., 2003. **50**(3): p. 763-770.
39. Ringgaard, S., et al., *A family of ParA-like ATPases promotes cell pole maturation by facilitating polar localization of chemotaxis proteins*. Genes & Development, 2011. **25**(14): p. 1544-1555.
40. Uebe, R., et al., *The cation diffusion facilitator proteins MamB and MamM of Magnetospirillum gryphiswaldense have distinct and complex functions, and are involved in magnetite biomineralization and magnetosome membrane assembly*. Mol. Microbiol., 2011. **82**(4): p. 818-835.
41. Rothbauer, U., et al., *Targeting and tracing antigens in live cells with fluorescent nanobodies*. Nat. Methods, 2006. **3**(11): p. 887-889.

2. Publications and manuscripts

42. Lang, C. and D. Schüler, *Expression of green fluorescent protein fused to magnetosome proteins in microaerophilic magnetotactic bacteria*. Appl. Environ. Microbiol., 2008. **74**(15): p. 4944-4953.
43. Grünberg, K., et al., *Biochemical and proteomic analysis of the magnetosome membrane in Magnetospirillum gryphiswaldense*. Appl. Environ. Microbiol., 2004. **70**(2): p. 1040-1050.
44. Ohuchi, S. and D. Schüler, *In vivo display of a multisubunit enzyme complex on biogenic magnetic nanoparticles*. Appl. Environ. Microbiol., 2009. **75**(24): p. 7734-7738.
45. Borg, S., et al., *New vectors for chromosomal integration enable high-level constitutive or inducible magnetosome expression of fusion proteins in Magnetospirillum gryphiswaldense*. Appl. Environ. Microbiol., 2014. **80**(8): p. 2609-2616.
46. Katzmann, E., et al., *Analysis of magnetosome chains in magnetotactic bacteria by magnetic measurements and automated image analysis of electron micrographs*. Appl. Environ. Microbiol., 2013. **79**(24): p. 7755-7762.
47. Jogler, C. and D. Schüler, *Genomics, genetics, and cell biology of magnetosome formation*. Annu. Rev. Microbiol., 2009. **63**: p. 501-521.
48. Lohße, A., et al., *Functional analysis of the magnetosome island in Magnetospirillum gryphiswaldense: The mamAB operon is sufficient for magnetite biomineralization*. PLoS ONE, 2011. **6**(10): p. e25561.
49. Katzmann, E., et al., *Magnetosome chains are recruited to cellular division sites and split by asymmetric septation*. Mol. Microbiol., 2011. **82**(6): p. 1316-1329.
50. Erbse, A.H. and J.J. Falke, *The core signaling proteins of bacterial chemotaxis assemble to form an ultrastable complex*. Biochemistry, 2009. **48**(29): p. 6975-6987.
51. Schulmeister, S., et al., *Protein exchange dynamics at chemoreceptor clusters in Escherichia coli*. Proc. Natl. Acad. Sci. USA, 2008. **105**(17): p. 6403-6408.
52. Briegel, A., et al., *New insights into bacterial chemoreceptor array structure and assembly from electron cryotomography*. Biochemistry, 2014. **53**(10): p. 1575-1585.
53. Coppieters, K., et al., *Formatted anti-tumor necrosis factor α VHH proteins derived from camelids show superior potency and targeting to inflamed joints in a murine model of collagen-induced arthritis*. Arthritis & Rheumatism, 2006. **54**(6): p. 1856-1866.

2. Publications and manuscripts

54. Man, S.A., et al., *Artificial trans-encoded small non-coding RNAs specifically silence the selected gene expression in bacteria*. Nucleic Acids Res., 2011. **39**(8).
55. Na, D., et al., *Metabolic engineering of Escherichia coli using synthetic small regulatory RNAs*. Nat. Biotechnol., 2013. **31**(2): p. 170-174.
56. Melchionna, T. and A. Cattaneo, *A protein silencing switch by ligand-induced proteasome-targeting intrabodies*. J. Mol. Biol., 2007. **374**(3): p. 641-654.
57. Garcillan-Barcia, M.P., et al., *Conjugative transfer can be inhibited by blocking relaxase activity within recipient cells with intrabodies*. Mol. Microbiol., 2007. **63**(2): p. 404-416.
58. Jurado, P., L.A. Fernandez, and V. De Lorenzo, *In vivo drafting of single-chain antibodies for regulatory duty on the sigma(54)-promoter Pu of the TOL plasmid*. Mol. Microbiol., 2006. **60**(5): p. 1218-1227.
59. Zafra, O., et al., *Monitoring biodegradative enzymes with nanobodies raised in Camelus dromedarius with mixtures of catabolic proteins*. Environ. Microbiol., 2011. **13**(4): p. 960-974.
60. Avalos, J.L., G.R. Fink, and G. Stephanopoulos, *Compartmentalization of metabolic pathways in yeast mitochondria improves the production of branched-chain alcohols*. Nat. Biotechnol., 2013. **31**(4): p. 335-341.
61. DeLoache, W.C. and J.E. Dueber, *Compartmentalizing metabolic pathways in organelles*. Nat. Biotechnol., 2013. **31**(4): p. 320-321.
62. Heyen, U. and D. Schüler, *Growth and magnetosome formation by microaerophilic Magnetospirillum strains in an oxygen-controlled fermentor*. Appl. Environ. Microbiol., 2003. **61**(5-6): p. 536-544.
63. Sambrook, J. and D. Russell, *Molecular cloning: a laboratory manual*. 2001, New York: Cold Spring Harbor Laboratory Press. 1-44.
64. Schultheiss, D., M. Kube, and D. Schüler, *Inactivation of the flagellin gene flaA in Magnetospirillum gryphiswaldense results in nonmagnetotactic mutants lacking flagellar filaments*. Appl. Environ. Microbiol., 2004. **70**(6): p. 3624-3631.
65. Heckman, K.L. and L.R. Pease, *Gene splicing and mutagenesis by PCR-driven overlap extension*. Nat. Protocols, 2007. **2**(4): p. 924-932.
66. Raschdorf, O., et al., *A tailored galK counterselection system for efficient markerless gene deletion and chromosomal tagging in Magnetospirillum gryphiswaldense*. Appl. Environ. Microbiol., 2014.

2. Publications and manuscripts

67. Schüler, D., U. Rainer, and E. Bäuerlein, *A Simple Light-Scattering Method to Assay Magnetism in Magnetospirillum Gryphiswaldense*. FEMS Microbiol. Lett., 1995. **132**(1-2): p. 139-145.
68. Laemmli, U.K., *Cleavage of structural proteins during assembly of head of bacteriophage-T4*. Nature, 1970. **227**(5259): p. 680-685.

2. Publications and manuscripts

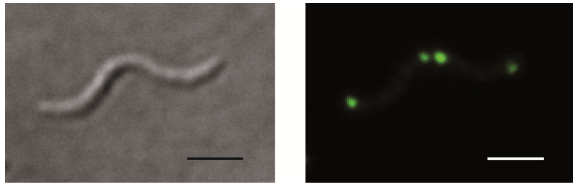
Acknowledgment:

We thank the ChromoTek GmbH for providing the GBP nanobody. We also thank M. Eibauer and A. Heins for help with CHAP implementation. This work was funded by DFG grants Schu1080/9-1, 15-1 and 16-1 to D. S.

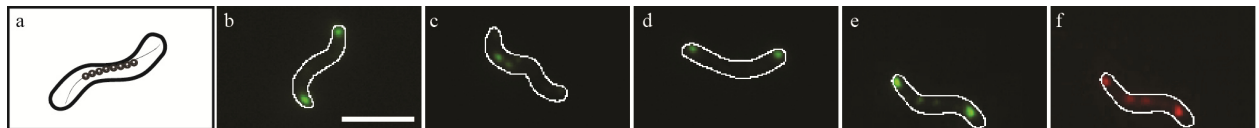
Author contributions: S.B., F.P., and D.S. designed research; S.B., F.P., and J.H. performed research; S.B., F.P., and D.S. analyzed data; S.B., F.P., and D.S. wrote the paper.

Competing financial interests: The authors declare no competing financial interests.

Supplementary material manuscript 1

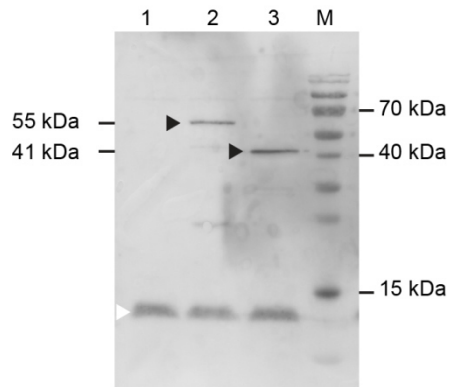


Supplementary Fig. S1: CheW₁-EGFP localization in a dividing cell. Representative DIC and fluorescence micrograph of a cell chromosomally expressing CheW₁-EGFP close to cell division. CheW₁-EGFP localizes distinctly at the cell poles and forms two new foci at mid-cell at the expected position of septum formation. Scale bar 2 μ m.

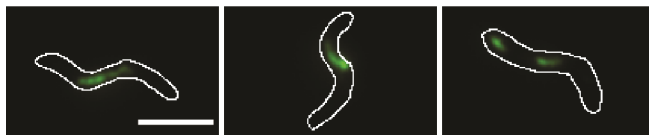


Supplementary Fig. S2: Schematics (a) and fluorescence micrograph of *M. gryphiswaldense* Δ *mamM* mutant cells expressing CheW₁-EGFP alone (b) or in combination with MamC-2xGBP (c) and wild type cells expressing chromosomal CheW₁-EGFP and cytoplasmic GBP (d), or CheW₁-EGFP and MamC-mCherry-GBP (e,f). Scale bar 2 μ m.

2. Publications and manuscripts



Supplementary Fig. S3: Western blot of *M. gryphiswaldense* cells expressing CheW₁-EGFP (1), CheW₁-EGFP MamC-mCherry-GBP (55.43 kDa) (2) and CheW₁-EGFP MamC-2xGBP (41.07 kDa), protein bands are indicated by black arrow heads (3). The native, unfused MamC (12.35 kDa) is present in all strains, indicated by white arrow head. Additional bands are visible for all strains expressing MamC fusions proving stable expression. MamC was detected using rabbit α MamC IgG as primary, and goat anti-rabbit IgG alkaline phosphatase antibodies as secondary antibody. PageRuler™ Prestained Protein Ladder from fermentas was used as a standard.

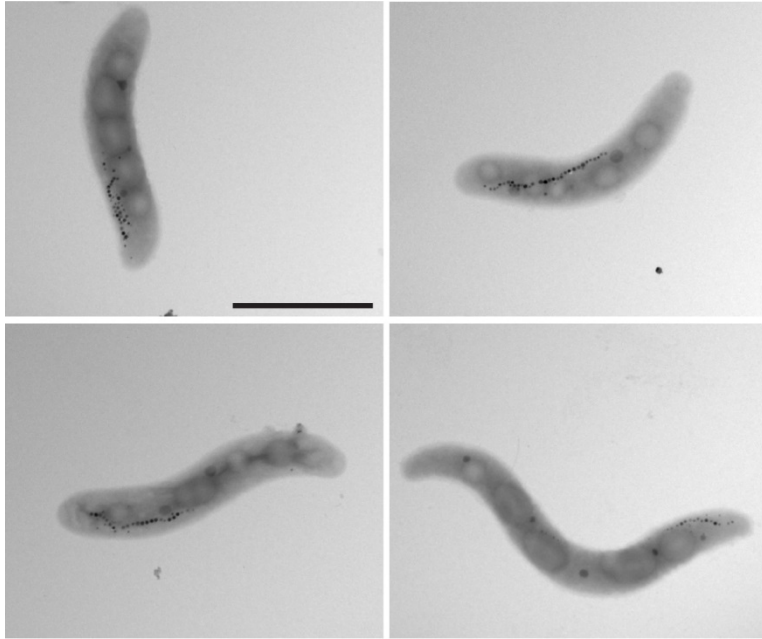


Supplementary Fig. S4: Fluorescence distribution in fluorescence micrographs of *M. gryphiswaldense* cells expressing chromosomal CheW₁-EGFP MamC-2xGBP. Scale bar 2 μ m.

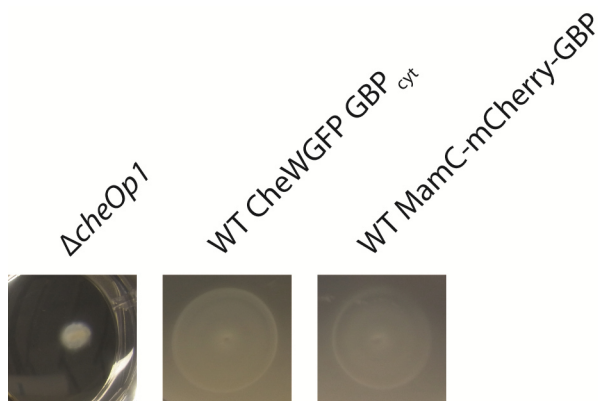


Supplementary Fig. S5: TEM micrographs of *M. gryphiswaldense* Δ cheW₁ (a) and cells expressing CheW₁-EGFP and cytoplasmic MagGBP (b) or CheW₁-EGFP and MamC-mCherry-GBP (c). Scale bar 1 μ m.

2. Publications and manuscripts



Supplementary Fig. S6: TEM micrographs of *M. gryphiswaldense* cells expressing CheW₁-EGFP and MamC-2xGBP. Scale bar 2 μ m.



Supplementary Fig. S7: Swim halos of *M. gryphiswaldense* Δ cheOp1 cells, wild type cells co-expressing either CheW₁-EGFP and MagGBP^{cyt} or CheW₁-EGFP and MamC-mCherry-GBP.

2. Publications and manuscripts

Supplementary Table S1: Plasmids used in this study

Plasmid name	Description	Source or reference
pJET1.2/blunt	Cloning vector; Amp ^R	Fermentas, Schwerte
pBBR-MCS2	Mobilizable broad-host-range vector; Km ^R	M. E. Kovach, <i>et al.</i> , 1995
pBAM1	Km ^R , Amp ^R , oriR6K, <i>tnpA</i>	E. Martinez-Garcia, <i>et al.</i> , 2011
pORFM	pK19mobGII, universal in-frame deletion/in-frame fusion vector with GalK-based counterselection and MCS	O. Raschdorf and F. Müller, 2014
pMA-T GBPOpt	Amp ^R , ColE1 ori, <i>maggbp</i>	GeneArt® (Invitrogen), life technologies, Darmstadt
pGH-Trpl GBP	Amp ^R , <i>maggbp-gbp-maggbp</i>	ATG:biosynthetics, Merzhausen
pSB6	pBAM1 with P _{mamDC45} , <i>magegfp</i> , Km ^R , Amp ^R	S. Borg, <i>et al.</i> , 2014
pSB7	pBAM1 with P _{tet} , <i>magegfp</i> , P _{Neo} -TetR, Km ^R , Amp ^R	S. Borg, <i>et al.</i> , 2014
pFP66	fusion of <i>cheW₁-egfp-cheW₁</i> downstream fragment inserted into pORFM	this study
pJH01	pAP150 with P _{mamDC45} , <i>cheW₁-egfp</i> , Km ^R	this study
pJH16	pBAM1 with P _{mamDC45} , <i>mamC-maggbp</i> , Km ^R , Amp ^R	this study
pJH17	pBAM1 with P _{tet} , <i>mamC-maggbp</i> , P _{Neo} -TetR, Km ^R , Amp ^R	this study
pJH39	pBAM1 with P _{mamDC45} , <i>mamC-maggbp-gbp</i> , Km ^R , Amp ^R	this study
pJH40	pBAM1 with P _{tet} , <i>mamC-maggbp-gbp</i> , P _{Neo} -TetR, Km ^R , Amp ^R	this study
pJH60	pBAM1 with P _{mamDC45} , <i>mamC-mCherry-maggbp</i> , Km ^R , Amp ^R	this study
pJH61	pBAM1 with P _{tet} , <i>mamC-mCherry-maggbp</i> , P _{Neo} -TetR, Km ^R , Amp ^R	this study
pJH97	pBAM1 with P _{mamDC45} , <i>mamC-maggbp-gbp-maggbp</i> , Km ^R , Amp ^R	this study
pJH100	pORFM with fused up- and downstream region of <i>cheW₁</i> for deletion of <i>cheW₁</i>	this study
pJH104	pBAM1 with P _{mamDC45} , <i>maggbp</i> , Km ^R , Amp ^R	this study

2. Publications and manuscripts

Supplementary Table S2: Strains used in this study

Strain	Description	Source or reference
<i>Escherichia coli</i>		
DH5 α	F ⁻ <i>supE44</i> Δ <i>lacU169</i> (Φ 80 <i>lacZDM15</i>) <i>hsdR17</i> <i>recA1</i> <i>endA1</i>	Invitrogen, life technologies, Darmstadt
WM3064	<i>gyrA96</i> <i>thi-1</i> <i>relA1</i> <i>thrB1004</i> <i>pro</i> <i>thi</i> <i>rpsL</i> <i>hsdS</i> <i>lacZ</i> Δ <i>M15</i> <i>RP4-1360</i> Δ (<i>araBAD</i>)567 Δ <i>dapA1341::[erm pir]</i>	W. Metcalf, unpublished
BW29427	DAP auxotroph derivative of <i>E. coli</i> strain B2155	K. Datsenko and B. L. Wanner, unpublished
<i>Magnetospirillum gryphiswaldense</i>		
<i>M. gryphiswaldense</i> MSR-1 R3/S1	Rif ^R , Sm ^R spontaneous mutant, lab strain	D. Schultheiss, <i>et al.</i> , 2003
<i>M. gryphiswaldense</i> Δ <i>mamJ</i>	Δ <i>mamJ</i>	A. Scheffel, <i>et al.</i> , 2006
<i>M. gryphiswaldense</i> Δ <i>mamM</i>	Δ <i>mamM</i>	R. Uebe, <i>et al.</i> , 2011
<i>M. gryphiswaldense</i> Δ <i>cheW</i> ₁	Δ <i>cheW</i> ₁	this study
<i>M. gryphiswaldense</i> MSR-1 FP66	in frame fusion of <i>egfp</i> to <i>cheW</i> ₁	this study
<i>M. gryphiswaldense</i> Δ <i>cheW</i> ₁ (pJH01)	Δ <i>cheW</i> ₁ complemented with p JH01	this study
<i>M. gryphiswaldense</i> MSR-1 JH5	FP66 transposon mutant with inserted <i>maggbp</i> from P _{mamDC45} , Km ^R	this study
<i>M. gryphiswaldense</i> MSR-1 JH6	FP66 transposon mutant with inserted <i>mamC-maggbp</i> from P _{mamDC45} , Km ^R	this study
<i>M. gryphiswaldense</i> MSR-1 JH7	FP66 transposon mutant with inserted <i>mamC-maggbp-gbp</i> from P _{mamDC45} , Km ^R	this study
<i>M. gryphiswaldense</i> MSR-1 JH8	FP66 transposon mutant with inserted <i>mamC-mCherry-maggbp</i> from P _{tet} , Km ^R	this study
<i>M. gryphiswaldense</i> MSR-1 JH9	FP66 transposon mutant with inserted <i>mamC-maggbp-gbp</i> from P _{tet} , Km ^R	this study

2. Publications and manuscripts

<i>M. gryphiswaldense</i> MSR-1 JH10	FP66 transposon mutant with inserted <i>mamC-maggbp-gbp-maggbp</i> from P _{tet} , Km ^R	this study
<i>M. gryphiswaldense</i> MSR-1 JH11	Δ <i>mamJ</i> with inframe fusion of <i>egfp</i> to <i>cheW_I</i>	this study
<i>M. gryphiswaldense</i> MSR-1 JH12	JH11 transposon mutant with inserted <i>mamC-maggbp</i> from P _{mamDC45} , Km ^R	this study
<i>M. gryphiswaldense</i> MSR-1 JH13	Δ <i>mamM</i> with inframe fusion of <i>egfp</i> to <i>cheW_I</i>	this study
<i>M. gryphiswaldense</i> MSR-1 JH14	JH13 transposon mutant with inserted <i>mamC-maggbp-gbp</i> from P _{mamDC45} , Km ^R	this study

Manuscript 2:

Generation of Multi-Shell Magnetic Hybrid Nanoparticles by Encapsulation of Genetically Engineered and Fluorescent Bacterial Magnetosomes with ZnO and SiO₂

Sarah Borg^a, Dirk Rothenstein^c, Joachim Bill^c and Dirk Schüler^{a,b}

in preparation

Sarah Borg and Dirk Rothenstein contributed equally to this work

Ludwig Maximilian University Munich, Dept. Biology I, LMU Biozentrum, Martinsried,
Germany^a

University of Bayreuth, Dept. Microbiology, Universitätsstraße 30, 95447 Bayreuth,
Germany^b

University of Stuttgart, Dept. of Material Science, Heisenbergstraße 3, 70569 Stuttgart,
Germany^c

Abstract

Magnetic nanoparticles (MNPs) have great potential in biomedical applications, but the chemical synthesis of size-controlled and functionalized core-shell MNPs has remained challenging. However, magnetosomes produced by the magnetotactic bacterium *Magnetospirillum gryphiswaldense* represent natural uniform and chemically pure magnetite MNPs, with superior magnetic characteristics. Here, we demonstrate that in addition to the naturally enveloping magnetosome membrane and biomolecules displayed on the surface of magnetosomes, further functionalities can be added by encapsulation with inorganic coatings. We generated novel multi-shell nanoparticles, consisting of the magnetosome core (magnetite crystal + magnetosome membrane + additional functional moieties, such as GFP and peptides) and an outer shell, consisting of either a silica or zinc oxide. Coating of functionalized magnetosomes with silica improved their colloidal stability and preserved the GFP fluorescence in the presence of proteases and detergents. In addition, the surface charge of magnetosomes could be adjusted by different coatings. This method will be useful for the versatile generation of new, multifunctional multi-shell and magnetic hybrid nanomaterials with potential for various biomedical applications, like magnetic resonance imaging, fluorescence imaging or drug delivery.

Introduction

Magnetic nanoparticles (MNPs) are typically between 5 and 100 nm in size [1] and most studies have been conducted with magnetite MNPs *inter alia* due to its proven biocompatibility [2]. However, it has remained difficult to produce particles with a narrow size distribution and to control the morphology of the particles in chemical synthesis routes. Additionally, chemical synthesis demands surface modification of the particles during or subsequent to the process [3]. Special types of MNPs are core-shell nanoparticles (CSNs). They are of particular interest because these particles consists of layers of different materials, which can add further functionalities, or passivate the core particle and thereby confer biocompatibility [4]. Magnetosomes are natural occurring CSNs, with a magnetic core enveloped by a magnetosome membrane, which consists of phospholipids and a set of magnetosome specific, membrane associated proteins [5,6]. *M. gryphiswaldense* magnetosomes have a cuboctahedral crystallographic orientation [7]. These special nanoparticles display exceptional properties like high uniformity, absolute purity and superior magnetic characteristics [7]. Therefore, they have attracted attention in various fields of applied science, such as in biotechnology and biomedicine [3,8]. The particles can be employed, for instance, as MRI contrast agents [8,9] and magnetic capturing of soluble proteins and drug targeting [8, 10]. One further key advantage of magnetosomes is that their functionalization with additional functional moieties, such as enzymes, antibodies or fluorophores, ca be achieved by genetic engineering and fusion of molecular tags to magnetosomal anchor proteins, such as MamC, which is highly constituent of the magnetosome membrane [11]. However, proteins and other biomolecules displayed on the magnetosome surface are sensitive against non-physiological conditions, detergents and proteolytic degradation. On the other hand, bacterial phospholipids and proteins might be highly immunogenic in *in vivo* applications, unless properly masked. Therefore, for many

2. Publications and manuscripts

biomedical applications, passivation of magnetosomes is be beneficial. This has been achieved by encapsulation with inert shells, as for instance consisting of an additional silica layer to impart wettability and biocompatibility [12]. Additionally, silica can be easily functionalized further by linking bioconjugates, such as avidin [13], to even expand multifunctionality of the CSNs. CSNs are generally classified in four main groups i) inorganic/inorganic; ii) inorganic/organic; iii) organic/inorganic and iv) organic/organic [4]. Magnetite-silica CSNs have been previously generated by various synthesis routs e. g. layer-by-layer assembly [14], co-precipitation [15], or reverse microemulsion approaches [16] with potential applications as e.g. biocatalyst [17], or drug delivery systems [18]. In contrast to synthetic MNP, the encapsulation of bacterial magnetosomes would allow for a single step generation of CSNs and the generation of highly versatile multi-shell MNPs with multiple functionalities.

In contrast, there is very little information available about Fe_3O_4 -ZnO CSNs, which would have potential application in biomedical approaches, as for example as alternative treatment against bacterial infections [19]. One of the few studies described seed-mediated grown Fe_3O_4 -ZnO CSNs where the core exists of 8-13 nm Fe_3O_4 nanoparticles encapsulated by a 4.45-5.15 nm ZnO layer [20]. In a similar approach Wan and co-workers generated Fe_3O_4 -ZnO nanoparticles of roughly the same size [21]. Most other studies describe Fe_3O_4 -ZnO hybrid composites of different sizes and morphologies, e. g. Fe_3O_4 -coated ZnO nanoflowers [22] or Fe_3O_4 -ZnO hybrid nanorods [23]. The doping of ZnO with Fe_3O_4 was also used to add magnetic properties to the semiconductive ZnO, therefore Fe_3O_4 was embedded in porous ZnO particles [24].

All of the studies described above rely first on the chemical synthesis of magnetite nanoparticles. In contrast, membrane enclosed core-shell magnetic nanoparticles, so called

2. Publications and manuscripts

magnetosomes, can be isolated from magnetotactic bacteria, such as *Magnetospirillum gryphiswaldense*, in a sustainable approach, with high yields of up to ~180 mg magnetite/liter/day [6, 25, 26]. The magnetite core exhibits exceptional magnetic properties, like an exceptionally high magnetic heat loss, high magnetization and uniformity [27]. In addition, the synthesis, and consequently the properties of the magnetic core can be genetically engineered [28].

Here, we report about the generation of hybrid CSNs consisting of (i) functionalized magnetosomes (displaying enhanced green fluorescent protein (EGFP), genetically fused to the magnetosome protein MamC), which are (ii) encapsulated by an additional coating consisting of either silica or ZnO (Figure 1). Fluorescent magnetosomes were isolated from bacteria and used as a template, on which the inorganic shell was directly mineralized using fast low-temperature synthesis approaches. This approach secured non-denaturing conditions to preserve integrity and fluorescence of encapsulated EGFP protein, which in addition exhibited highly increased resistance against proteases and detergents. Both types of passivated bacterial magnetic nanoparticles have potential in biomedical applications, biosensors or biocatalysts.

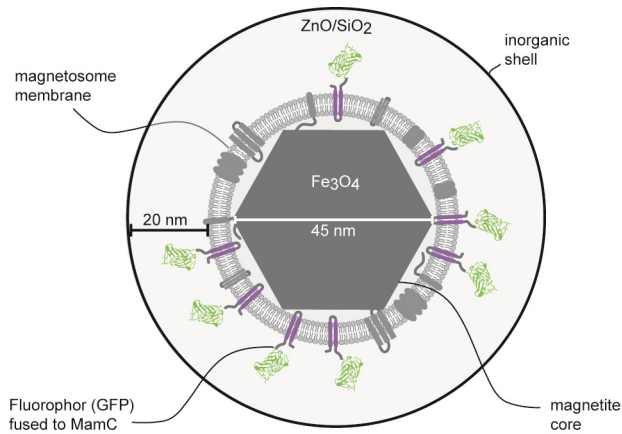


Figure 1: Scheme of multi-shell magnetic hybrid nanoparticles, consisting of the magnetite magnetosome core (45 nm) that is enveloped by the magnetosome membrane, with specific magnetosome membrane proteins (dark grey) and the anchor protein MamC (purple) that is fused to GFP (green). The functionalized magnetosome is encapsulated with a 20 nm layer of an inorganic silica or ZnO shell.

Results/Discussion

Magnetosomal expression of MagEGFP and ZnO-binding peptides by genetic fusion

In order to generate fluorescent magnetosomes, a *Magnetospirillum*-optimized derivative of the enhanced fluorescent protein (EGFP), so called MagEGFP [29], was fused to the magnetosome anchor protein MamC, as described before [29]. For the coating of magnetosomes with zinc oxide (ZnO), a second version of magnetosomes was produced, expressing the ZnO-binding peptide 31 (amino acid sequence HHGHSPTSPQVR), which was previously identified by phage display and showed a strong binding to ZnO with a dissociation constant in the nanomolar range (K_D 10 ± 3 nM) [30]. The peptide was expressed as fusion to the MagEGFP modification, resulting in MagEGFP-31 functionalized magnetosomes. Expression of MamC-MagEGFP as well as the MamC-MagEGFP-31 fusion proteins on magnetosomes and incorporation in the magnetosome membrane was verified by fluorescence microscopy. The functionalized magnetosomes were applied in the mineralization process with either silica or ZnO.

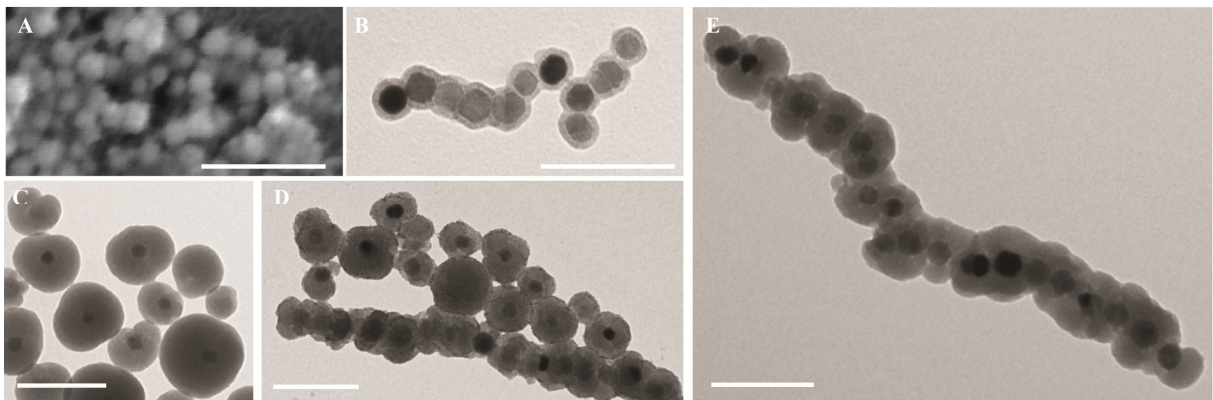


Figure 2: Silica-encapsulated magnetosomes. Scanning electron (A) and transmission electron micrographs of silica-encapsulated magnetosomes, with a silica layer thickness of ~20 nm (B). Representative transmission electron micrographs of magnetosomes encapsulated in the absence of an

external magnetic field (C), in the presence of a rotating magnetic field (D) and in a static magnetic field (E). The white scale bar represents 200 nm.

Silica encapsulation of magnetosomes

A modified Stöber reaction was used to encapsulate the MagEGFP functionalized magnetosomes with silica ^[31]. This experimental setup yielded magnetosomes coated with a homogenous and complete silica layer, as shown by TEM and SEM (Figure 2 A&B). The adjustment of the coating thickness and thus the entire particle size is of crucial interest for many biomedical applications. For instance, it is necessary to obtain particles with a defined thin silica layer, since large particles (>200 nm) are sequestered by phagocytotic cells and nanoparticles smaller than 5.5 nm are rapidly removed by renal clearance [8, 32]. To adjust the layer thickness of the silica coating various ratios of magnetosome and silica precursor were tested in the encapsulation reaction. Magnetosome concentrations between 0.4 and 2.0 $\mu\text{g iron}/\mu\text{l}$ (Figure 3) led to a decrease in silica layer thickness with increasing MNP concentration in the reaction. A magnetosome concentration of 0.4 $\mu\text{g}/\text{ml}$ in the reaction solution yielded encapsulated magnetosomes with an average silica layer thickness of about 20 nm. By increasing the magnetosome concentration to 0.8 $\mu\text{g}/\mu\text{l}$ the coating thickness slightly decreased to 17 nm. A more pronounced effect was found at magnetosome concentrations of 1.0 and 2.0 $\mu\text{g}/\mu\text{l}$, where the coating thickness of the particles was further decreased to 11 nm and ~ 3 nm, respectively (Figure 3). A similar inversely proportional relationship of the particle concentration and the coating thickness was also reported for the encapsulation of synthetic magnetic core nanoparticles [17]. The effect on layer thickness by varying the concentration of seed to reaction solution is presumably caused by free silanol groups surrounding the magnetic seed.

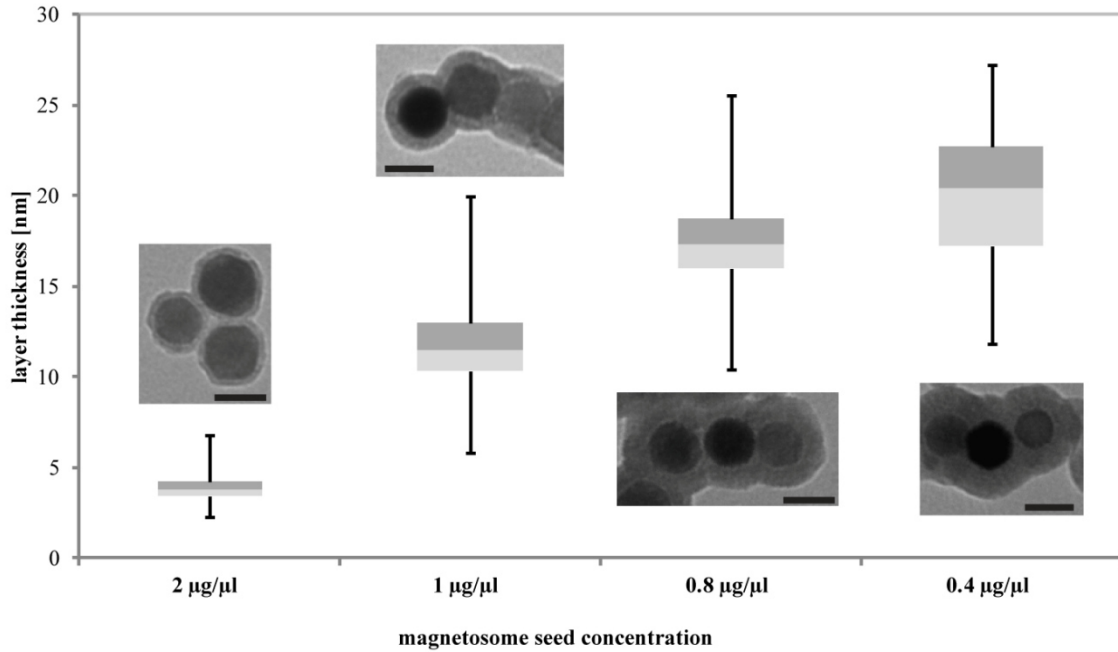


Figure 3: Layer thickness of silica precipitated on magnetosomes. Magnetosome seed concentrations from 0.4-2 µg/ml were applied to a silica precipitation solution and layer thickness was estimated using the software imageJ and by comparing pixel size to the scale bar. The scale bar represents 40 nm.

Next, we tested the effect of an external magnetic field on the mineralization characteristics of magnetosomes. To this end, magnetosomes were encapsulated with silica in the absence of an external magnetic field, in the presence of either a static magnetic field (between two bar magnets, magnetic field strength each = 70 mT), or in a rotating magnetic field (by placing the experimental set up on top of a conventional magnetic lab stirrer). Different types of encapsulated magnetosomes were obtained, depending on the experimental set up. The encapsulation in the absence of an external magnetic field predominantly resulted in separated encapsulated magnetosome particles (Figure 2C) and occasionally short chains of up to five magnetosomes adherent to each other, probably due to magnetostatic interactions between the ferrimagnetic magnetite cores. In contrast, in the presence of an static external magnetic field magnetosome particles preferentially assembled to sets of chains of

2. Publications and manuscripts

magnetosome (i.e. 5-20 particles, separated by ~10 nm) which aligned to the magnetic field and remained stable. Although not being entirely uniform, this prominently led to simultaneous encapsulation of many particles, resulting in chains of five to 20 particles, which remained attached to each other and aligned in a linear fashion extending over up to 800 nm (Figure 2E). Application of a rotating magnetic field yielded both chains and single particles encapsulated in silica (Figure 2D). Thus, by controlling the magnetic alignment of the particles during the mineralization process, either individual encapsulated particles or magnetic nanochains could be produced. The latter might be used in biosensors or bioassays, since the particles can be structured and aligned in a controlled fashion. For example, it was previously reported that magnetosome chains are taken up faster by cancer cells than single magnetosomes [33].



Figure 4: Colloidal stability of silica encapsulated magnetosomes. Silica encapsulated magnetosomes (left) and non-encapsulated magnetosomes (right) were dispersed in water by vortexing and incubated for 3 weeks, illustrating improved colloidal stability of silica encapsulated magnetosomes. Non-encapsulated magnetosomes agglomerated and sedimented faster (30 sec) than silica-encapsulated magnetosomes, which can be re-dispersed easily and remained suspended for at least 1 min.

2. Publications and manuscripts

Silica-encapsulated magnetosomes displayed higher colloidal stability than non-encapsulated magnetosomes after aging, as indicated by re-dispersion in water after two weeks of storage (Figure 4). Non-encapsulated magnetosomes tended to agglomerate after storage for several weeks and could be no more dispersed in aqueous solution anymore. In contrast, silica encapsulated magnetosomes could be re-dispersed after long time (> 3 weeks) of storage. This might be caused by repulsion of the silica shell due to its high negative zeta potential or due to shielding of the magnetic core by the silica layer, which would reduce the magnetic forces that are known to decrease in square of the particle size [34]. Improving the colloidal stability of magnetosomes in solution can be important for many applications to avoid agglomeration of the particles.

Silica encapsulation of MagEGFP-tagged magnetosomes increased resistance against proteases and detergents

Isolated GFP-functionalized magnetosomes displayed high fluorescence before encapsulation. The fluorescence of the magnetosomes was preserved after silica encapsulation, as the particles still exhibited a similarly bright fluorescence signal. Thus, the inorganic coating did not interfere with the MagEGFP (e.g. altering the conformation of the fluorescence protein or degrade the protein during mineralization), although magnetosomes were entirely silica coated. Next, the stability of the MagEGFP-tagged magnetosomes against detergent treatment, and proteolytic degradation was assessed. To this end, non-encapsulated and encapsulated particles were incubated at room temperature for one, two, and three weeks in buffer. The silica encapsulated MagEGFP-tagged magnetosomes showed fluorescence over the complete period of investigation. In contrast, non-encapsulated magnetosomes gradually lost the fluorescence, which became weaker in the time course until fluorescence was completely lost. Already after one week the fluorescence intensity was decreased, while after

2. Publications and manuscripts

three weeks fluorescence was no longer detectable within the sample of non-encapsulated magnetosomes. Thus, silica encapsulation drastically improved the thermal/aging stability of the fluorescence signal. The magnetosome membrane was completely passivated by a homogeneous silica coating, which assumedly protected the magnetosome integrity.

In addition, the resistance of encapsulated magnetosomes against proteolytic degradation or chemical denaturation of proteins and solubilization of phospholipids was tested. To this end, the magnetosomes were either exposed to a detergent treatment with 1% SDS, which was reported to lead to decreased fluorescence due to the degradation of EGFP [11], or the enzymatic digestion with proteinase K. Silica encapsulated magnetosomes remained fluorescent after the treatment with both 1% SDS and proteinase K. In contrast, non-encapsulated magnetosome particles showed a complete loss of the fluorescence after chemical and enzymatic treatment. As a possible explanation, encapsulation of the magnetosomes by the modified Stöber reaction led to a precipitation of an amorphous silica layer on the magnetosomes [31]. This is highly unstructured order of silica on the magnetosomes might shield the magnetosome core sufficiently from external factors such as proteases and detergents.

Encapsulation of magnetosomes with zinc oxide

Magnetosome displaying either MagEGFP or MagEGFP-31 were encapsulated with ZnO via a mineralization process which is compatible with fastidious biological templates [35]. The mineralization was performed in cycles, each mineralization cycle resulted in approximately 5 nm coating thickness. The mineralization (including 4 cycles) resulted in a ZnO coating thickness of ~20 nm estimated on TEM micrographs (Figure 5C). The surface of encapsulated magnetosomes appears rougher compared to non-encapsulated magnetosomes (Figure 5 A&D to B&E).

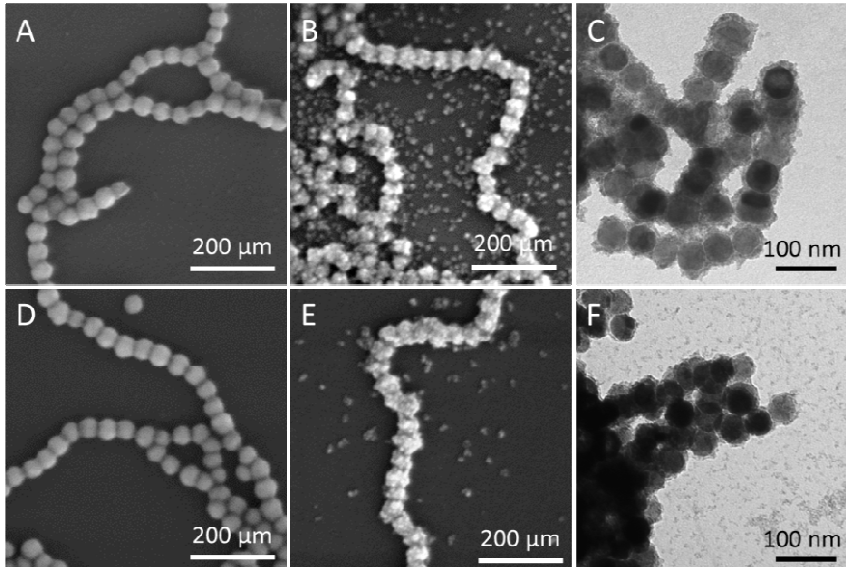


Figure 5: Zinc oxide mineralization of genetically engineered magnetosomes. MagEGFP (A-C) modified and MagEGFP-31 (D-F) modified magnetosomes were encapsulated with ZnO from a methanolic reaction solution. A) MagEGFP reference non-mineralized. B) SEM micrograph and C) TEM micrograph of ZnO mineralized MagEGFP magnetosomes. D) MagEGFP-31 reference non-mineralized. E) SEM micrograph and F) TEM micrograph of ZnO mineralized MagEGFP-31 magnetosomes.

Encapsulation of magnetosomes with ZnO might be beneficial, since zinc oxide was proven to exhibit strong antimicrobial activity [36,37], but pure ZnO nanoparticles tend to agglomerate to large agglomerates up to the size of several micrometers. Therefore, in recent attempts Fe₃O₄-ZnO hybrid nanoparticles were developed to benefit from the good colloidal stability of ferrofluids which remain in suspensions without significant agglomeration [21,38]. Biom mineralization processes leading to the generation of crystalline ZnO [35] allow the formation of ZnO coatings of bacterial magnetic nanoparticles for generation of ZnO hybrid CSNs. ZnO precipitation on magnetosomes was achieved in a defined manner and might provide additional functions to the magnetic nanoparticles, since ZnO exhibits piezoelectricity [39] and is a semiconducting material with antimicrobial activity [36, 37].

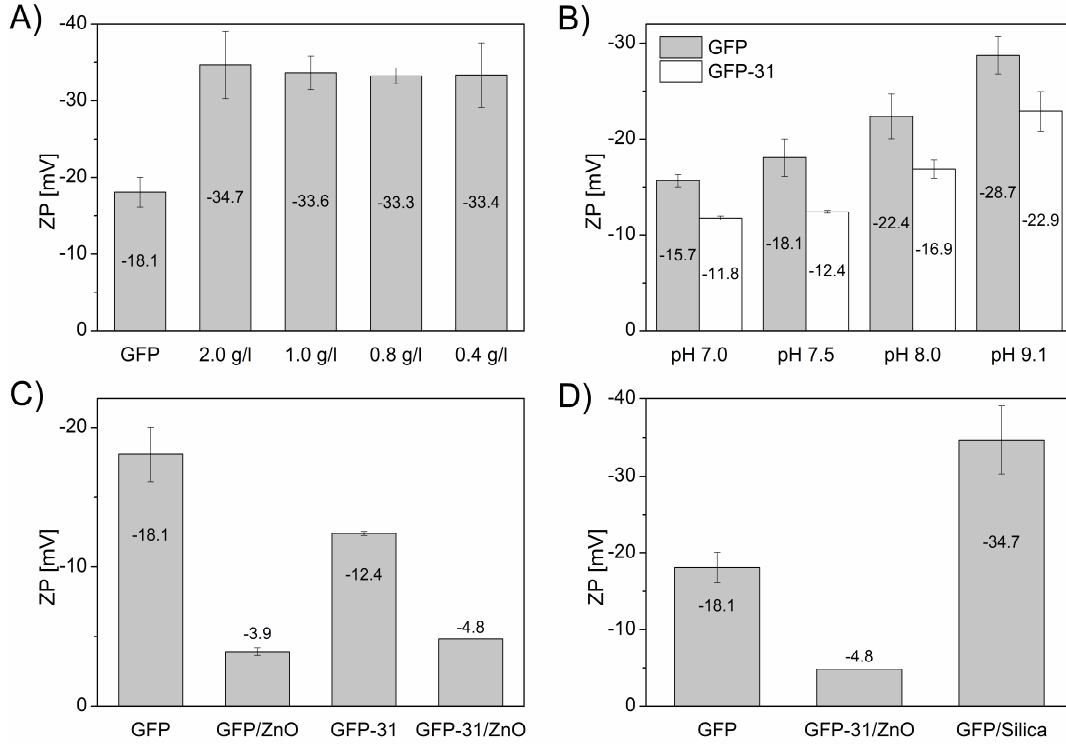
Zeta potential of mineralized magnetosomes

Figure 6: Zeta potentials of mineralized magnetosomes. A) ZP of silica encapsulated MagEGFP magnetosomes and non-mineralized reference magnetosomes. Non-mineralized MagEGFP magnetosomes exhibited a ZP of around -18 mV. This value shifted more negative after the encapsulation with silica. Layer thickness of silica did not significantly influence the ZP of the resultant hybrid particles. B) ZP of MagEGFP and MagEGFP-31 expressing magnetosomes. The ZP of the two magnetosome derivatives was determined under four different pH values. At higher pH values the magnetosomes exhibited a more negative ZP. In general, the ZP of MagEGFP-31 expressing magnetosomes was less negative compared to MagEGFP expressing magnetosomes. C) ZP of ZnO mineralized MagEGFP and MagEGFP-31 magnetosomes in comparison to their non-mineralized references. After encapsulation of magnetosomes the ZP of both derivatives became more positive. The ZP of ZnO encapsulated magnetosomes was similar to the ZP of ZnO nanoparticles (see supplementary information). D) Comparison of the ZP of ZnO and silica encapsulated magnetosomes. The encapsulation resulted in significant alteration of the ZP. While the ZP of ZnO mineralized

2. Publications and manuscripts

magnetosomes was more positive compared to the reference non-encapsulated magnetosomes, silica mineralization resulted in a more negative ZP.

Most interestingly was the zeta potential (ZP) at neutral pH (i.e., at physiological conditions), therefore silica mineralized magnetosome were measured at pH 7.5 (Figure 6A). The ZP of the silica encapsulated magnetosomes was measured in relation to the silica coating thickness. Regardless of the silica coating thickness the ZP was around -34 mV which indicates a complete coating of magnetosome particles also at the lowest silica thickness of below 5 nm. Pure silica nanoparticles also show a ZP of about -40 mV [15], which is in the same range as the silica coated magnetosomes. Due to the encapsulation, the ZP was more negative compared to non-encapsulated magnetosomes (Figure 6A, GFP) with a ZP of -18.1 mV.

The ZPs of non-mineralized MagEGFP and MagEGFP-31 magnetosomes were determined in 50 mM Tris buffer with a pH ranging between 7.0 and 9.1 (Figure 6B). The ZP of MagEGFP magnetosomes was in general more negative compared to MagEGFP-31 magnetosomes presenting the ZnO-binding peptide. The presence of expressed peptide 31, which has a calculated isoelectric point of 9.77, likely results in a positive net charge over the investigated pH range, and most likely accounts for the more positive ZP of MagEGFP-31 magnetosomes.

The ZnO coating of magnetosomes led to a drastic increase of the ZP. The zeta potentials of both types of ZnO encapsulated magnetosomes, MagEGFP and MagEGFP-31, were more positive compared to the non-mineralized references (Figure 6C). The ZPs of ZnO mineralized magnetosomes was slightly more positive compared to ZnO nanopowder which had a ZP of -8.8 mV at pH 7.5 (Figure S1). The silica and ZnO encapsulated magnetosomes showed, that the ZP of such particles can be adjusted to both more positive and more negative

2. Publications and manuscripts

values (Figure 6D). This allows the defined specification of the surface charge in regard to a potential application of such magnetic nanoparticles.

The surface charge of nanoparticles strongly affects their physical and biological properties. Strong negatively charged nanoparticles show low inclination for agglomeration due to the repulsion between single particles [40], which lead to homogeneously dispersed nanoparticle suspensions. Theoretically, the endocytosis of negatively charged particles should be decelerated due to repulsive forces between the particles and the negatively charged cell membrane. However, *in vitro* studies showed that endocytosis is minimized for coated iron oxide nanoparticles with a zeta potential close to 0 mV [41], but the particles are cleared more efficient from the body due to increased liver uptake [8,32].

Because of their improved colloidal stability, enhanced stability and shielding of the fluorescence marker it is conceivable to apply the silica encapsulated magnetosomes as contrast agent in fluorescence imaging. Optical fluorescence imaging comprises a wide variety of technologies that are being used in biological and medical applications, such as contrast agent and offer clear potential for *in vivo* applications [42]. The encapsulation with silica or ZnO would render them more resistant to extreme pH and proteolysis. In addition, the agglomeration behavior of the nanoparticles and thereby the stability of nanoparticles in suspension are affected [40].

With the two different inorganic coatings it is possible to adjust the ZP of magnetosomes both to more negative and more positive values which allows the tuning of the surface properties for various demands with regard to e.g. magnetosome-cell interaction. For instance, ZnO nanoparticles are known to possess biological functionality, such as antimicrobial activity against gram positive and gram negative bacteria and could therefore be applied as coatings to avoid spread of infectious diseases [36,43]. To date there are only few

2. Publications and manuscripts

reports on Fe₃O₄-ZnO hybrid CSNs. Kataoka and co-workers developed Fe-doped ZnO nanoparticles, where a room temperature ferromagnetism originated from unequal amounts of Fe³⁺ ions [24]. In a different study, Fe₃O₄-ZnO nanorods were developed as a new kind of electromagnetic wave absorptive material [23]. Wan and co-workers produced Fe₃O₄@ZnO core shell semiconductive hybrid materials that are similar to the hybrid nanoparticles in our study [21]. However, due to the absolute purity and strictly controlled morphology of the magnetosomes [7], uniform and well-defined Fe₃O₄-ZnO hybrid nanoparticles can be generated. The magnetosome based MNPs will be investigated in further studies with respect to biotechnological or biomedical applications.

Conclusion

In this study we generated two novel examples of magnetic multi-shell hybrid nanoparticles, consisting of the magnetite core, the magnetosome membrane with fused MagEGFP and the inorganic silica or ZnO layer. Coating of fluorescent magnetosomes with silica yielded particles with enhanced stability against proteases and detergents, which might have potential in biomedical applications, such as drug delivery agent or as contrast agent. In a second approach, we precipitated ZnO on the surface of EGFP-functionalized magnetosomes to generate well-defined Fe₃O₄-ZnO as semiconductive magnetic hybrid nanoparticles, which might be applicable in future approaches as sensors or biomedical approaches, as for instance in cancer treatment. This method will be useful for the versatile generation of new, multifunctional multi-shell and magnetic hybrid nanomaterials that can be investigated in future studies, for instance by applying silica encapsulated magnetosomes for *in vivo* assays or exploring the potential of ZnO mineralized magnetosomes in electronic devices.

Experimental Section

Bacterial strains, plasmids, and culture conditions

Bacterial strains and plasmids used for this study are listed in Table S1&2. *M. gryphiswaldense* strains were grown microaerobically with 1% oxygen in modified flask standard medium (FSM) at 30°C [25] and moderate shaking (120 rpm). *E. coli* strains were cultivated as previously described [44], for growth of *E. coli* MW3064 (W. Metcalf, unpublished) 1 mM DL- α , ϵ -diaminopimelic acid (DAP) was added to lysogeny broth media (LB). Strains were routinely cultured on plates solidified with 1.5% (w/v) agar. For strains carrying recombinant plasmids, media were supplemented with 25 $\mu\text{g ml}^{-1}$ kanamycin (Km) and 50 $\mu\text{g ml}^{-1}$ ampicilin (Amp) for *E. coli* strains, and 5 $\mu\text{g ml}^{-1}$ Km for *M. gryphiswaldense* strains, respectively.

Isolation of magnetosomes

The procedure for magnetosome isolation from *M. gryphiswaldense* cells was modified from Lang et al. (2008) [11]. *M. gryphiswaldense* strains were cultivated for 24 h at 30°C in 30 L FSM medium in a 50 L fermenter with 100 rpm stirrer speed and without airflow. The fermenter was inoculated with 3 L pre-culture. Stationary-phase cultures were harvested via centrifugation, washed with washing buffer (20 mM HEPES, 1 mM EDTA, pH 7.4), and finally resuspended in resuspension buffer (50 mM HEPES, 1 mM EDTA, 0.1 mM phenylmethylsulfonyl fluoride, pH 7.4). Cells were disrupted by three passages through a microfluidizer and cell debris was removed by centrifugation at 800 x g for 10 min. The cleared cell lysate was passed through a MACS magnetic-separation column (Miltenyi, Bergisch Gladbach, Germany) and placed between NdFeB magnets, to separate magnetosomes from the non-magnetic fraction. The column bound magnetosomes were washed with 10 column volumes (50 ml) of extratction buffer and high-salt buffer (10 mM

2. Publications and manuscripts

HEPES, 200 mM NaCl, 1 mM EDTA, pH 7.4). Residual salts were washed with extraction buffer and magnetosomes were eluted in extraction buffer by removal of the magnetic field. Finally, magnetosomes were purified by centrifugation through an 8-ml sucrose cushion (60% [wt/wt] in extraction buffer) at 200,000 x g for 90 min. Due to their high specific density magnetosomes are collected at the bottom of the tube, whereas residual cellular components are retained by the sucrose cushion. Finally, the magnetosomes were resuspended in 8 ml EP.

Analytical methods

Magnetic reaction of cells was validated by light microscopy applying a bar magnet. Optical density (OD) and magnetic response (C_{mag}) of exponentially growing cells were measured photometrically at 565 nm as previously reported [45]. For C_{mag} measurement a magnetic field of approximately 70 millitesla was used.

Biom mineralization of magnetosomes

Silica mineralization

Encapsulation of magnetosomes with silica was achieved using a modified version of the protocol from Barrado *et al.* (2005) [31]. An aliquot of isolated magnetosomes (100 μl \approx 0.8 mg/ml) was centrifuged and solvent was discarded, afterwards magnetosomes were mixed with 50, 100, 250 or 500 μl of a silica reaction solution for 3h at room temperature. The silica reaction solution (2 ml TEOS (tetraethylorthosilicate), 2.145 ml H_2O , 1.67 ml EtOH and 580 μl NH_3 (25%)) was freshly prepared for each experiment and stirred for 2 min before encapsulation of magnetosomes. Silica encapsulated particles were harvested via centrifugation (13.000 rpm, for 5 min), and washed 5 times with 250 μl H_2O to remove

2. Publications and manuscripts

residual silica particles. Encapsulation of magnetosomes with silica was tested in an external magnetic field, applying two bar magnets or on a magnetic stirrer creating a rotating magnetic field or without any external magnetic field present.

ZnO mineralization

The final concentrations in the ZnO deposition solution were 8.57 mM polyvinylpyrrolidone (PVP, MW 8000 Da), 11.34 mM zinc acetate dihydrate, and 25 mM tetraethylammonium hydroxide (TEAOH). For all components stock solutions in methanol were prepared. The PVP and zinc acetate dihydrate solutions were mixed and the TEAOH was added drop wise under constant stirring [35,46]. The mineralization solution was prepared freshly and used no longer than 24 h, to avoid adverse implications due to aging processes of the deposition solution. A Si-wafer substrate with the immobilized magnetosomes was placed in a glass vessel with deposition solution and incubated at 60°C for 1.5 hours. Afterwards, the substrate was washed in methanol to eliminate excess deposition solution and air dried at room temperature.

Stability assay

MagEGFP functionalized, non-encapsulated and silica-encapsulated magnetosomes were stored for up to three weeks at room temperature on the bench top and examined for decay of the fluorescence signal and colloidal stability. Additionally magnetosomes were treated with 1% SDS to test denaturation of proteins and solubilization phospholipids. Proteolytic degradation of proteins was tested by incubation of the particles with 40 µg proteinase K per ml for 5 min.

Fluorescence microscopy

2. Publications and manuscripts

Magnetosomes displaying MamC-GFP fusions encapsulated by silica were analyzed via fluorescence microscopy and imaged with an Olympus BX81 microscope equipped with an 100 UPLSAPO100XO objective (numerical aperture of 1.40) and a Hamamatsu Orca AG camera. The Olympus xcellence pro software was used to capture and analyze images.

Transmission electron microscopy (TEM) analysis

Silica and ZnO encapsulated magnetosomes were examined by transmission electron microscopy (TEM), for which hybrid particles were concentrated via centrifugation and adsorbed onto carbon-coated copper grids. Magnetosomes were imaged with a FEI Morgagni 268 (FEI, Eindhoven, Netherlands) electron microscope at an accelerating voltage of 80 kV.

Layer thickness of precipitation on magnetosomes was measured from TEM micrographs using the software ImageJ and comparing single pixel ratio to the scale bar. The distance from the magnetite core to the surface of the silica shell was defined as layer thickness.

Scanning electron microscopy (SEM) analysis

Mineralized magnetosomes and non-mineralized references were immobilized on cleaned Si-wafers. Therefore, Si-wafers (100) were cleaned by consecutive sonication in ddH₂O and a mixture of 1:1 acetone:ethanol each for 10 minutes followed by cleaning step with oxygen plasma (10 min, 30 Watt) and a final sonication step in ddH₂O water for 10 min each. If necessary, samples were sputtered with 0.5 nm platinum/palladium to enhance the contrast. SEM was performed with the Zeiss DSM 982 GEMINI scanning electron microscope, operated at 3 kV.

Zeta potential measurement

The ZP was determined with a Zetasizer Nano (Malvern, UK). Samples for silica and ZnO encapsulated magnetosomes were both mineralized in solution, washed, and re-

2. Publications and manuscripts

suspended in 50 mM Tris buffer, pH 7.5. Non-mineralized magnetosomes were measured at pH values of 7.0, 7.5, 8.0, and 9.1 in 50 mM Tris buffer. Measurements were made in duplicates, with two independent samples for each condition.

References:

1. Gupta, A.K. and M. Gupta, *Synthesis and surface engineering of iron oxide nanoparticles for biomedical applications*. Biomaterials, 2005. **26**(18): p. 3995-4021.
2. Schwertmann, U. and R.M. Cornell, *Iron oxides in the laboratory*. 2008: John Wiley & Sons.
3. Lu, A.-H., E.L. Salabas, and F. Schüth, *Magnetische Nanopartikel: Synthese, Stabilisierung, Funktionalisierung und Anwendung*. Angewandte Chemie, 2007. **119**(8): p. 1242-1266.
4. Ghosh Chaudhuri, R. and S. Paria, *Core/shell nanoparticles: classes, properties, synthesis mechanisms, characterization, and applications*. Chemical Reviews, 2011. **112**(4): p. 2373-2433.
5. Bazylinski, D.A. and R.B. Frankel, *Magnetosome formation in prokaryotes*. Nat Rev Micro, 2004. **2**(3): p. 217-230.
6. Grünberg, K., et al., *Biochemical and Proteomic Analysis of the Magnetosome Membrane in Magnetospirillum gryphiswaldense*. Applied and Environmental Microbiology, 2004. **70**(2): p. 1040-1050.
7. Faivre, D. and D. Schüler, *Magnetotactic bacteria and magnetosomes*. Chemical Reviews, 2008. **108**(11): p. 4875-4898.
8. Sun, C., J.S.H. Lee, and M. Zhang, *Magnetic nanoparticles in MR imaging and drug delivery*. Advanced Drug Delivery Reviews, 2008. **60**(11): p. 1252-1265.
9. Hartung, A., et al., *Labeling of macrophages using bacterial magnetosomes and their characterization by magnetic resonance imaging*. Journal of Magnetism and Magnetic Materials, 2007. **311**(1): p. 454-459.

2. Publications and manuscripts

10. Pollithy, A., et al., *Magnetosome Expression of Functional Camelid Antibody Fragments (Nanobodies) in Magnetospirillum gryphiswaldense*. Applied and Environmental Microbiology, 2011. **77**(17): p. 6165-6171.
11. Lang, C. and D. Schüler, *Expression of Green Fluorescent Protein Fused to Magnetosome Proteins in Microaerophilic Magnetotactic Bacteria*. Applied and Environmental Microbiology, 2008. **74**(15): p. 4944-4953.
12. Kim, J., et al., *Multifunctional Uniform Nanoparticles Composed of a Magnetite Nanocrystal Core and a Mesoporous Silica Shell for Magnetic Resonance and Fluorescence Imaging and for Drug Delivery*. Angewandte Chemie International Edition, 2008. **47**(44): p. 8438-8441.
13. Yi, D.K., et al., *Silica-coated nanocomposites of magnetic nanoparticles and quantum dots*. Journal of the American Chemical Society, 2005. **127**(14): p. 4990-4991.
14. Aliev, F.G., et al., *Layer-By-Layer Assembly of Core-Shell Magnetite Nanoparticles: Effect of Silica Coating on Interparticle Interactions and Magnetic Properties*. Advanced materials, 1999. **11**(12): p. 1006-1010.
15. Santra, S., et al., *Conjugation of Biomolecules with Luminophore-Doped Silica Nanoparticles for Photostable Biomarkers*. Analytical Chemistry, 2001. **73**(20): p. 4988-4993.
16. He, R., et al., *Core/shell fluorescent magnetic silica-coated composite nanoparticles for bioconjugation*. Nanotechnology, 2007. **18**(31): p. 315601.
17. Lee, J., et al., *Simple Synthesis of Functionalized Superparamagnetic Magnetite/Silica Core/Shell Nanoparticles and their Application as Magnetically Separable High-Performance Biocatalysts*. Small, 2008. **4**(1): p. 143-152.

2. Publications and manuscripts

18. Lien, Y.-H. and T.-M. Wu, *Preparation and characterization of thermosensitive polymers grafted onto silica-coated iron oxide nanoparticles*. Journal of Colloid and Interface Science, 2008. **326**(2): p. 517-521.
19. Tran, N. and T.J. Webster, *Magnetic nanoparticles: biomedical applications and challenges*. Journal of Materials Chemistry, 2010. **20**(40): p. 8760-8767.
20. Chiu, W., et al., *Heterogeneous Seeded Growth: Synthesis and Characterization of Bifunctional Fe₃O₄/ZnO Core/Shell Nanocrystals*. The Journal of Physical Chemistry C, 2010. **114**(18): p. 8212-8218.
21. Wan, J., H. Li, and K. Chen, *Synthesis and characterization of Fe₃O₄@ZnO core-shell structured nanoparticles*. Materials Chemistry and Physics, 2009. **114**(1): p. 30-32.
22. Cao, J., et al., *Fabrication, characterization and application in electromagnetic wave absorption of flower-like ZnO/Fe₃O₄ nanocomposites*. Materials Science and Engineering: B, 2010. **175**(1): p. 56-59.
23. Chen, Y.-J., et al., *Synthesis, Multi-Nonlinear Dielectric Resonance, and Excellent Electromagnetic Absorption Characteristics of Fe₃O₄/ZnO Core/Shell Nanorods*. The Journal of Physical Chemistry C, 2010. **114**(20): p. 9239-9244.
24. Kataoka, T., et al., *Electronic structure and magnetism of the diluted magnetic semiconductor Fe-doped ZnO nanoparticles*. Journal of Applied Physics, 2010. **107**(3).
25. Heyen, U. and D. Schüler, *Growth and magnetosome formation by microaerophilic Magnetospirillum strains in an oxygen-controlled fermentor*. Applied microbiology and biotechnology, 2003. **61**(5-6): p. 536-544.

2. Publications and manuscripts

26. Zhang, X., et al., *Chitosan-Coated Octadecyl-Functionalized Magnetite Nanoparticles: Preparation and Application in Extraction of Trace Pollutants from Environmental Water Samples*. Analytical Chemistry, 2010. **82**(6): p. 2363-2371.
27. Hergt, R., et al., *Magnetic properties of bacterial magnetosomes as potential diagnostic and therapeutic tools*. Journal of Magnetism and Magnetic Materials, 2005. **293**(1): p. 80-86.
28. Lohße, A., et al., *Functional Analysis of the Magnetosome Island in Magnetospirillum gryphiswaldense: The mamAB Operon Is Sufficient for Magnetite Biomineralization*. PLoS ONE, 2011. **6**(10): p. e25561.
29. Borg, S., et al., *New Vectors for Chromosomal Integration Enable High-Level Constitutive or Inducible Magnetosome Expression of Fusion Proteins in Magnetospirillum gryphiswaldense*. Applied and Environmental Microbiology, 2014. **80**(8): p. 2609-2616.
30. Rothenstein, D., et al., *Isolation of ZnO-Binding 12-mer Peptides and Determination of Their Binding Epitopes by NMR Spectroscopy*. Journal of the American Chemical Society, 2012. **134**(30): p. 12547-12556.
31. Barrado, E., et al., *Characterization of iron oxides embedded in silica gel obtained by two different methods*. Journal of Non-Crystalline Solids, 2005. **351**(10–11): p. 906-914.
32. Chouly, C., et al., *Development of superparamagnetic nanoparticles for MRI: effect of particle size, charge and surface nature on biodistribution*. Journal of Microencapsulation, 1996. **13**(3): p. 245-255.
33. Alphandéry, E., F. Guyot, and I. Chebbi, *Preparation of chains of magnetosomes, isolated from Magnetospirillum magneticum strain AMB-1 magnetotactic bacteria,*

2. Publications and manuscripts

- yielding efficient treatment of tumors using magnetic hyperthermia. International Journal of Pharmaceutics*, 2012. **434**(1–2): p. 444-452.
34. Philipse, A.P. and D. Maas, *Magnetic Colloids from Magnetotactic Bacteria: Chain Formation and Colloidal Stability*. *Langmuir*, 2002. **18**(25): p. 9977-9984.
35. Atanasova, P., et al., *Virus-Templated Synthesis of ZnO Nanostructures and Formation of Field-Effect Transistors*. *Advanced materials*, 2011. **23**(42): p. 4918-4922.
36. Adams, L.K., D.Y. Lyon, and P.J.J. Alvarez, *Comparative eco-toxicity of nanoscale TiO₂, SiO₂, and ZnO water suspensions*. *Water Research*, 2006. **40**(19): p. 3527-3532.
37. Jones, N., et al., *Antibacterial activity of ZnO nanoparticle suspensions on a broad spectrum of microorganisms*. *FEMS Microbiology Letters*, 2008. **279**(1): p. 71-76.
38. Gordon, T., et al., *Synthesis and characterization of zinc/iron oxide composite nanoparticles and their antibacterial properties*. *Colloids and Surfaces A: Physicochemical and Engineering Aspects*, 2011. **374**(1–3): p. 1-8.
39. Gao, P.X. and Z.L. Wang, *Nanoarchitectures of semiconducting and piezoelectric zinc oxide*. *Journal of Applied Physics*, 2005. **97**(4): p. 044304.
40. Berg, J.M., et al., *The relationship between pH and zeta potential of ~ 30 nm metal oxide nanoparticle suspensions relevant to in vitro toxicological evaluations*. *Nanotoxicology*, 2009. **3**(4): p. 276-283.
41. Neuberger, T., et al., *Superparamagnetic nanoparticles for biomedical applications: Possibilities and limitations of a new drug delivery system*. *Journal of Magnetism and Magnetic Materials*, 2005. **293**(1): p. 483-496.
42. Bridot, J.-L., et al., *Hybrid gadolinium oxide nanoparticles: multimodal contrast agents for in vivo imaging*. *Journal of the American Chemical Society*, 2007. **129**(16): p. 5076-5084.

2. Publications and manuscripts

43. Zhang, L., et al., *Investigation into the antibacterial behaviour of suspensions of ZnO nanoparticles (ZnO nanofluids)*. Journal of Nanoparticle Research, 2007. **9**(3): p. 479-489.
44. Sambrook, J. and D.W. Russell, *Molecular cloning: a laboratory manual (3-volume set)*. Vol. 999. 2001: Cold spring harbor laboratory press Cold Spring Harbor, New York:.
45. Schüler, D., R. Uhl, and E. Bäuerlein, *A simple light scattering method to assay magnetism in Magnetospirillum gryphiswaldense*. FEMS microbiology letters, 1995. **132**(1-2): p. 139-145.
46. Lipowsky, P., et al., *Controlling the assembly of nanocrystalline ZnO films by a transient amorphous phase in solution*. The Journal of Physical Chemistry C, 2008. **112**(14): p. 5373-5383.

Acknowledgment:

Financial support from the Deutsche Forschungsgemeinschaft (grants BI 469/24-1 to J.B. and SCHU 1080/15-1 to D.S.) in the scope of DFG-SPP 1569 is greatly acknowledged. The authors DR and JB are grateful to Dr. Alexander Southan and the Institute of Interfacial Process Engineering and Plasma Technology, University of Stuttgart as well as the MPI for Intelligent Systems / Stuttgart Center for Electron Microscopy (StEM) for the access to measuring instruments. The help and advice of Prof. Dr. Nils Kröger, Technical University of Dresden, with silica encapsulation experiments is greatly acknowledged.

Supporting information manuscript 2

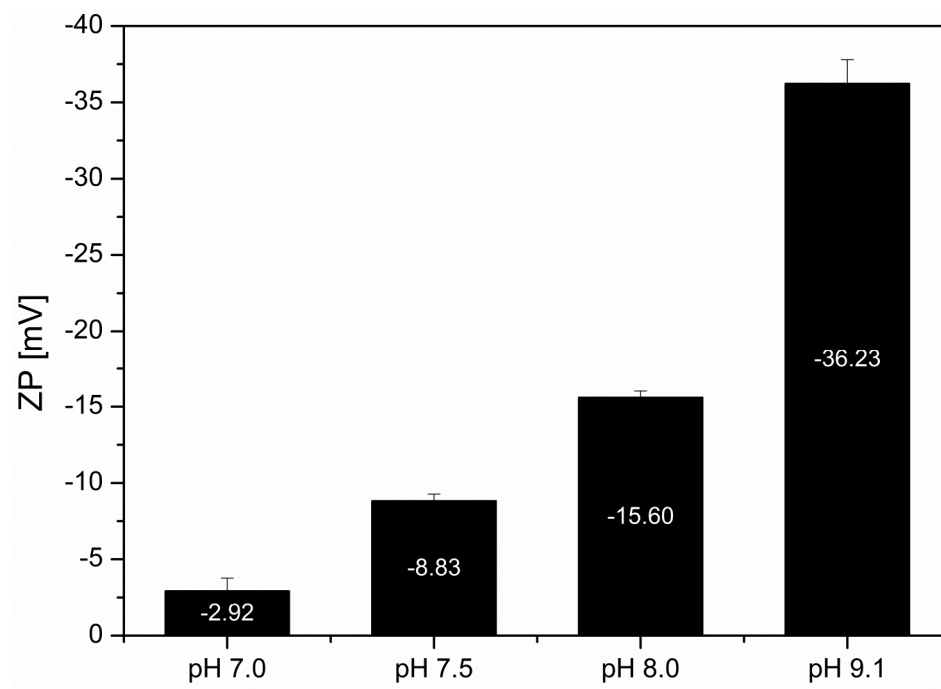


Figure S1: Zeta potential (ZP) of ZnO nanoparticles.

2. Publications and manuscripts

Table S1: Plasmids used in this study

Plasmid name	Description	Source or reference
pJET1.2/blunt	Cloning vector; Amp ^R	Fermentas, Schwerte
pBBR-MCS2	Mobilizable broad-host-range vector; Km ^R	M. E. Kovach, <i>et al.</i> , 1995
pBAM1	Km ^R , Amp ^R , oriR6K, <i>tnpA</i>	E. Martinez-Garcia, <i>et al.</i> , 2011
pJH1	pBAM1 with P _{mamDC45} , <i>mamC</i> - <i>magegfp</i> , Km ^R , Amp ^R	S. Borg, <i>et al.</i> , 2014

Table S2: Strains used in this study

Strain	Description	Source or reference
<i>Escherichia coli</i> strains		
DH5α	F ⁻ <i>supE44 ΔlacU169 (Φ80 lacZDM15) hsdR17 recA1 endA1 gyrA96 thi-1 relA1</i>	Invitrogen, life technologies, Darmstadt
WM3064	<i>thrB1004 pro thi rpsL hsdS lacZΔM15 RP4-1360 Δ(araBAD)567 ΔdapA1341::[erm pir]</i>	W. Metcalf, unpublished

2. Publications and manuscripts

Magnetospirillum

gryphiswaldense strains

M. gryphiswaldense MSR-1 R3/S1	<i>Rif^R, Sm^R spontaneous mutant, lab strain</i>	D. Schultheiss, et al., 2003
M. gryphiswaldense MSR-1 JH1	<i>Km^R, transposon mutant with inserted mamC- magegfp from PmamDC45</i>	S. Borg et al., 2014

3. Discussion

3.1 Expression of genetic fusions in *M. gryphiswaldense*

In this study systematic approaches combining following improvements (summarized in Figure 6) were used to optimize expression of heterologous genetic fusions for magnetosome display in *M. gryphiswaldense*. Production of fusion proteins was previously achieved by expression of genetic fusions from medium copy number plasmids under the control of the P_{mamDC} promoter [57, 118]. The promoter of the *mamGFDC* operon proved to be more efficient than other operon promoters or even ribosomal promoters in *M. gryphiswaldense*. P_{mamDC} exhibited also stronger expression of reporter genes than the homologous of the P_{msp3} and P_{mms16} promoters, which were reported to exhibit strong expression in *M. magneticum* [116-118]. The strong P_{mamDC} promoter was optimized and introduced into a versatile expression cassette (Figure 6a). For instance truncation of P_{mamDC} from 325 to 45 bp led to a 3-fold increase in fluorescence of the reporter EGFP. The increase of expression of *egfp* by truncation might be due to exclusion of regulatory elements from the promoter region [130]. Moreover, truncation of the promoter yielded a compact, easy-to-clone gene cassette, whose extension of 58 bp is within the typical range of other prokaryotic promoters (40–65 bp) [131]. In addition to promoter length, the spacing between Shine-Dalgarno sequence and the start codon was adjusted and the codon usage of the reporter gene *egfp* was optimized based on the average codon usage of *M. gryphiswaldense* (62.2% G+C) (Figure 6b&c). Already minor optimization of the codon usage (the sequence identity of the genes after optimization was 89 %) increased fluorescence of the transcribed synthetic “*magegfp*” (*Magnetospirillum*-optimized *egfp*) by 30%, providing a fluorescence reporter with increased sensitivity for future tagging and localization studies. Therefore, adjusting the codon usage of genes that differ more significantly might boost gene expression enormously. Codon optimization proved to be powerful also for boosting expression of a variety of foreign genes, similar as demonstrated in various hosts [105, 132]. Combination of all optimization steps led to an 8-fold increase of constitutive expression of the cytoplasmic *mag-egfp* reporter in comparison to previously available systems. Thus, the new optimized expression cassette allows high constitutive expression of foreign genes in *M. gryphiswaldense* and expression of heterologous genes can be increased even further by adapting the codon usage to the host organism.

3. Discussion

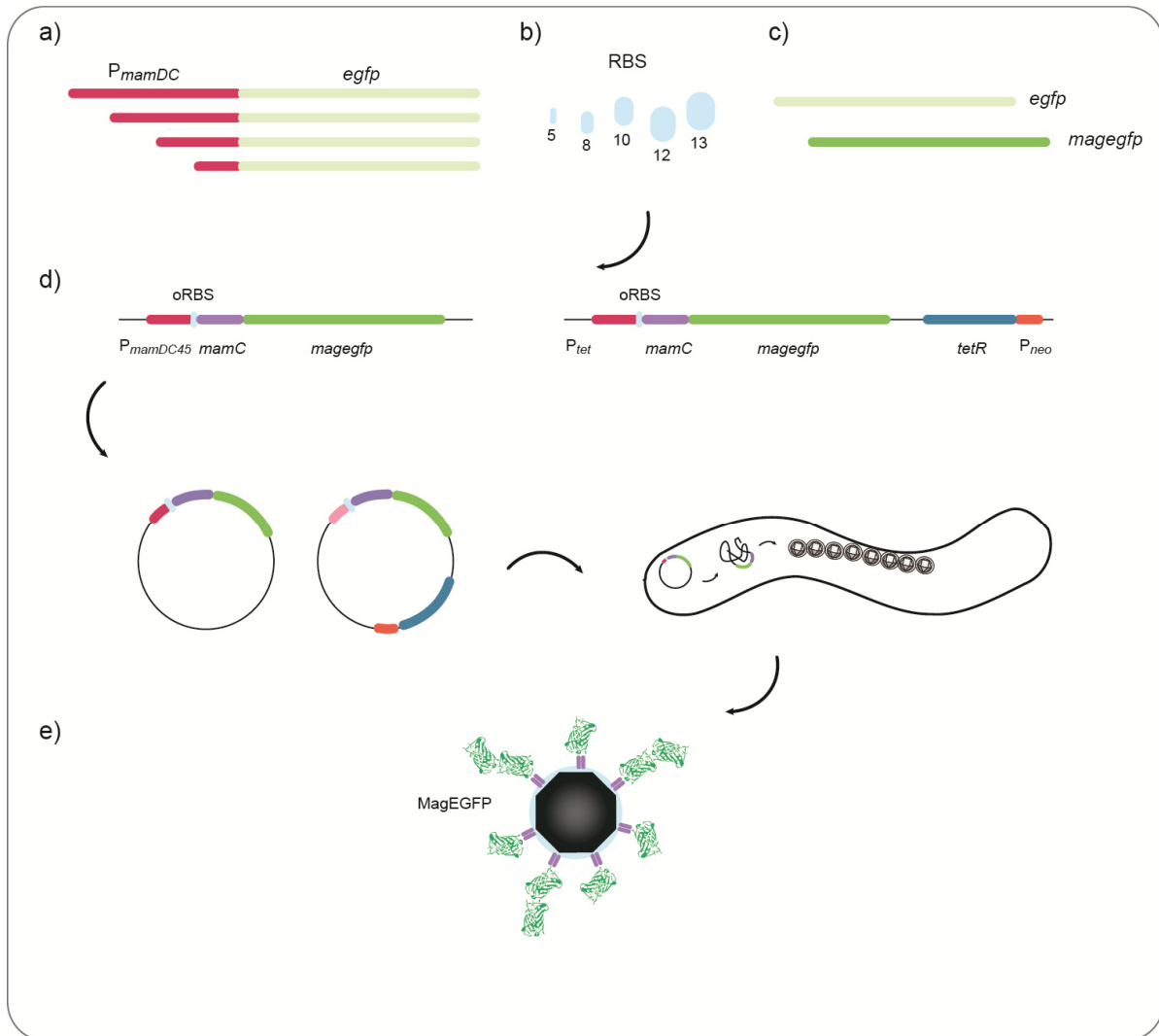


Figure 6: Strategy of approaches for optimized gene expression in *M. gryphiswaldense*. Truncation of the P_{mamDC} promoter of the *mamGFDC* operon from 325 to 45 bp with *egfp* as reporter gene resulted in 3-fold increased fluorescence; b) Optimization of the RBS, varying the spacing between Shine-Dalgarno sequence and start codon, yielded 2.8-fold higher fluorescence with the reporter *egfp*; c) Codon optimization of the reporter gene *egfp* by adjusting the codon usage to *M. gryphiswaldense* (*magegfp*) led to 30% stronger fluorescence than with native *egfp*; d) Integration of the optimized expression cassettes into transposable vectors and insertion into the host chromosome; e) Multi-copy display of the fluorescence (Mag)EGFP marker on single magnetosomes.

*Construction of an inducible expression system in *M. gryphiswaldense**

For the production of toxic fusion proteins an inducible expression system in *M. gryphiswaldense* would be a valuable tool. The construction of several hybrid promoters

3. Discussion

consisting of the optimized $P_{mamDC45}$ promoter or the P_{nirS} promoter, regulating the expression of a homodimeric cytochrome cd1 nitrite reductase [133], and operator sequences from the *tet* [112] and the *lac* system [107] failed. The first construct containing the $P_{mamDC45}$ promoter followed by a tetracycline operator (*tetO*) sequence and the reporter gene *egfp*, was repressed under non-inducing conditions, but did not exhibit high fluorescence after induction even with elevated inducer concentrations. Changing the orientation of the operator sequence resulted in *egfp* expression under non-inducing conditions and recreation of a similarly constructed hybrid promoter published by Yoshino (2010) [119] was not reproducible in *M. gryphiswaldense*. A hybrid promoter harboring *lac* operator (*lacO*) sequences replacing *tetO* was not also repressed under non-inducing conditions. A combination of the P_{nirS} promoter and *tetO* was tested in addition to the hybrid promoters based on $P_{mamDC45}$, but exhibited only basal levels of expression and was not inducible. Generation of functional hybrid promoters failed possibly due to the absence of further regulatory elements in the genetic neighborhood of $P_{mamDC45}$, required for inducible expression [134]. Since it was not possible to generate a functional inducible hybrid promoter, several different systems known to be functional in other alphaproteobacteria were tested for high and inducible expression in *M. gryphiswaldense*. The pIND4 plasmid used in *Rhodobacter sphaeroides*, which is carrying the *lac* promoter [135] showed no induction of the reporter gene *egfp*. A second IPTG inducible expression plasmid containing the P_{lacZ} promoter and *lacO* sequences, tested positive in diverse bacteria [136], did not exhibit high levels of *gfp* expression in *M. gryphiswaldense* either. Broadening the search for functional expression plasmids, a taurine inducible promoter from *Sinorhizobium meliloti* was tested, which was functional in several different alphaproteobacteria [137], but proved to be not working in *M. gryphiswaldense*. The vanillate and xylose inducible systems from *C. crescentus* [111] showed very low levels of expression and no detectable repression in our host organism. Also, reconstruction of a riboswitch, that was functional in the closely related magnetotactic bacterium *M. magneticum* [120] showed high fluorescence levels even in absence of the inducer theophylline in *M. gryphiswaldense*. These approaches might not function in *M. gryphiswaldense* possibly due to lack of specialized uptake systems for the different inducers. Another reason might be that repressor genes are not efficiently transcribed and therefore transcription of the reporter genes might not be suppressed. Adapting the promoters of the repressor genes might increase efficiency of these systems in *M. gryphiswaldense*.

3. Discussion

Finally, the original *Tn10* P_{tet} promoter from *E. coli* was found to be tightly repressed in *M. gryphiswaldense* [129], and could also be induced to reasonably high expression levels (about 30% of constitutive $P_{mamDC45}$ driven expression) in the presence of saturating Atet concentrations as low as 2.5 ng ml⁻¹. Saturating inducer concentration in *M. gryphiswaldense* was 40, 80, 160 and even 200-fold lower than in *Helicobacter pylori* [138], *E. coli* [113], *Bacillus subtilis* [139] and *M. magneticum* [119], respectively, while the regulatory range (up to 12-fold with the reporter GusA) is comparable to *tet*-responsive systems in other bacteria (*Staphylococcus aureus*: 50-100-fold, *Streptococcus pneumoniae*: 5-fold [140, 141]).

The inducible expression system was then used for protein display on magnetosomes. Expression of *mamC-magegfp* under the control of P_{tet} was tightly repressed under non-inducing conditions, while induction in magnetosome-containing wild type cells caused expression of *magegfp* on magnetosomes after only six hours. This implies that newly synthesized MamC-MagEGFP can be inserted into and targeted specifically to the MM of pre-existing magnetosome particles. In addition to magnetosome display, the TetR controlled expression system could also be used for the generation of conditional knockouts and gene depletion studies.

Chromosomal insertion of expression systems for display of single and multiple genetic fusions on magnetosomes results in super-fluorescent magnetic nanoparticles

Inhomogeneous expression of reporter genes from plasmids in isogenic cultures is frequently observed in bacteria [127, 142]. Chromosomal insertion of gene fusions into the genome of *M. gryphiswaldense* led to more homogenous expression, compared to multi-copy expression from plasmids [57, 76]. This was achieved via *Tn5*-mediated transposition, which allows straightforward, single-site integration into the host chromosome (Figure 6d). One caveat of *Tn5*-mediated transposition is random integration of the expression cassette into genomic loci of unknown function, which possibly causes unwanted second site mutations. However, no mutants with obvious growth and magnetosome formation defects could be identified, indicating the absence of effects on host metabolism. Additionally, expression of the reporter genes in absence or presence of the inducer, were similar in all insertants, suggesting that no interference such as read-through from external promoters occurred (compare publication 1).

Expression of foreign proteins can be enhanced further by increasing their copy number. Choi and co-workers integrated double copies of the *cym* repressor into

3. Discussion

Methylobacterium extorquens, thereby increasing repression of an inducible promoter [143]. Expression of five chromosomal copies of *gfp* resulted in 20-fold higher expression in the same organism [144]. Multicopy insertion of whole recombinant pathways can increase gene expression by 60% in contrast to plasmidal expression in *E. coli* [145]. Similarly, duplication of *(mag)egfp* fused to *mamC* resulted in stronger fluorescence and 2.5-fold increased expression of the *(mag)egfp* reporter on magnetosomes in comparison to single *mamC-magegfp* fusion. MamC-MagEGFP-EGFP on magnetosomes displayed proteolytic stability, as no cleavage products could be detected via Western blot. Engineered magnetosomes, displaying tandem EGFP proteins represent magnetic nanoparticles with greatly enhanced fluorescence, which could be used in a number of applications, for instance as bimodal contrast agents for both magnetic resonance imaging (MRI) and near-infrared fluorescence (NIRF) optical imaging [146]. Additionally, functionalized magnetosomes with enhanced fluorescence intensity and uniformity can be used as fluorescent tags to follow intracellular protein localization or to study the intricate cell biology of *M. gryphiswaldense* and other magnetic bacteria.

The number of proteins displayed on a single magnetosome is of interest e. g. for applications such as drug delivery. But the amount of proteins on a single magnetosome might be limited by the strength of the available expression system, as well as the restricted surface area of the MM. Over 30 proteins are inserted into or associated with the MM [50,60], therefore it might not be possible to express unlimited amounts of *mamC* fusions on magnetosomes. To estimate the amount of MagEGFP displayed on magnetosomes quantitative Western blot was performed. Expression of *mamC-magegfp* driven by $P_{mamDC45}$ resulted in 3.6-fold higher MagEGFP concentration than directed by expression of the *magegfp* gene from P_{tet} . The amount of (Mag)EGFP obtained with tandem constructs of the fluorescent protein and MamC was 2.5-fold higher compared to constitutively expressed *mamC-magegfp*. Based on these results, the copy number of *egfp* expressed on single magnetosome particles was estimated. The density of magnetite is 5.24 g/cm³ and for simplicity an approximately spherical shape for magnetosomes was assumed, which would result in a volume of 2.76×10^{-17} cm³ and mass of 1.45×10^{-16} g for an average single magnetosome crystal, with an averaged diameter of 37.5 nm for magnetosomes. On the basis of these estimations and the results of the quantitative Western blot, expression of single *mamC-magegfp* fusions under the control of $P_{mamDC45}$, resulted in about 100 MagEGFP copies per single magnetosome, while only ~30 copies were present if the same construct was

3. Discussion

expressed from P_{tet} . Calculations for the tandem *mamC-magegfp-egfp* fusion expressed under the control of $P_{mamDC45}$ resulted in 250 (Mag)EGFP copies per particle. The tandem fusion of *magegfp-egfp* yielded twice as many copies of the proteins on the magnetosome surface, which might be due to increased stability of the tandem protein, or alternatively, to variability of magnetosome sizes, which to some extent depends on the growth stage of the cells. Therefore calculations were repeated for smaller (35 nm) and larger (48 nm) magnetosome, which yielded GFP copy numbers of 80 to 210 for single, and 200 to 520 for tandem (Mag)EGFP respectively. Assuming a MamC to MagEGFP ratio of 1:1 for the single, and 1:2 for the tandem MagEGFP-EGFP, the number of MamC copies per magnetosome particle is most likely within the range of 80 to 260. An average magnetosome would have a surface area of 4417 nm² and with an approximated diameter of 3.45 nm for the 12.5 kDa MamC protein [57], the theoretical number of MamC covering the entire particle surface would amount to 1280. Previous estimations revealed a relative abundance of 16.3% of MamC in the MM [54], which contains about 30 different proteins [54]. The estimated 80–250 copies would occupy about 6-20% of the surface of a magnetosomes, which seems to be within a realistic range. Therefore, the number of MamC molecules that can serve as anchors can unlikely be further increased without disturbing MM function. Instead, increasing the number of gene copies fused to a single *mamC* anchor seems to be a more favorable approach to increase yields of heterologous genes expressed per particle (Figure 6e). These calculations are based on the diameter of the magnetosome particles, therefore it is estimated that smaller magnetosomes would display less fusion proteins. To test whether it is possible to increase the amount of protein displayed on a single magnetosome by increasing its size, it would be necessary to repeat the experiment with mutant strains producing smaller and larger magnetosomes. It is reasonable to assume that significantly bigger magnetosome particles can display more MamC coupled proteins without disturbing membrane function.

Construction of luciferase producing M. gryphiswaldense cells for application in biosensors

Apart from expression of fusion proteins to magnetosomes, the optimized constitutive expression cassette was also used to generate *M. gryphiswaldense* cells producing red-emitting click beetle luciferase. Luciferase expressing cells were used to design a portable toxicity detector, since the bioluminescent signal is directly proportional to viability of the

3. Discussion

cells. *M. gryphiswaldense* cells are perfectly suitable for application in biosensors, because they can be manipulated magnetically and trapped in reaction and detection areas of the sensor with bar magnets.

For generation of the biosensor a charge-coupled device (CCD) was placed in contact with the detection chamber of a microfluidic chip, consisting of multilayered polydimethylsiloxane (PDMS), to assess the bioluminescent signal. The chip contains three diamond-shaped reaction chambers, which are connected to the detection areas. *M. gryphiswaldense* cells expressing the luciferase were applied to the reaction chambers and incubated with samples of dimethyl sulfoxide (DMSO) and a bile acid as model toxic compounds. Both DMSO and the bile acid had a cytotoxic effect on *M. gryphiswaldense* cells as indicated by reduced bioluminescence of the cells. Due to magnetic concentration of the cells the sample volume can be decreased, which increases the light output and sensitivity of the sensor. The sensitivity of the system could be also further increased by adapting the codon usage of the luciferase to *M. gryphiswaldense*, which would improve expression of the reporter, as shown for *magegfp* in manuscript 1.

3.2 Construction of a nanotrap by display of nanobodies on magnetosomes

The optimized chromosomally insertable expression system was then used for functionalization of magnetosomes with nanobodies. Genes encoding nanobodies can be expressed in various host organisms [147] and *rbp* was recently expressed on the magnetosome surface in *M. gryphiswaldense* for capturing of cytoplasmic mCherry [77]. With the use of the constitutive expression system mono- and bivalent nanobodies, consisting of *gbp* and a synthetic *Magnetospirillum*-optimized version (*maggbp*) fused to *mamC*, were stably expressed in *M. gryphiswaldense*. The inducible tetracycline promoter facilitated modulation of the expression levels of *gbp* by expression of up to three copies of (*mag*)*gbp* as *mamC*-fusion.

3. Discussion

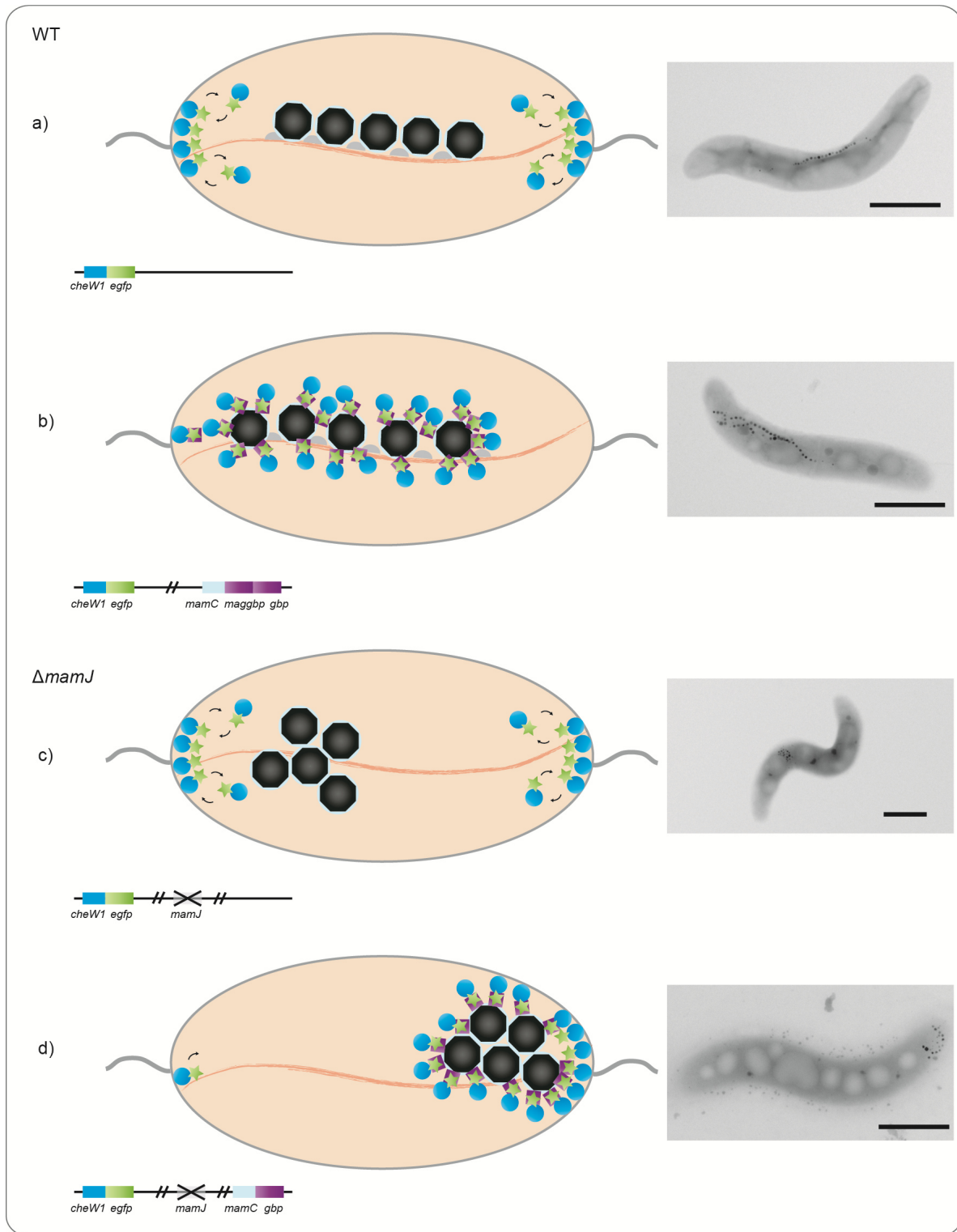


Figure 7: Rearrangement of cellular components by nanobody recruitment. a) Expression of *cheW₁-egfp* fusion in *M. gryphiswaldense* wild type cells; b) Co-expression of *cheW₁-egfp* and bivalent MamC-nanobody fusion in *M. gryphiswaldense* wild type cells causes depletion of CheW₁ from the pole and concurrent tethering of magnetosome chains to chemotaxis receptors; c) Expression of *cheW₁-egfp* fusion in *M. gryphiswaldense* Δ *mamJ* cells; d) Co-expression of *cheW₁-egfp* and

3. Discussion

monovalent MamC-nanobody fusion in *M. gryphiswaldense* $\Delta mamJ$ cells already causes depletion of CheW₁ from one pole and concurrent recruitment of magnetosome clusters to the opposite pole. Left panel TEM micrographs display the associated strain abstracted and described in a-d.

3.3 Nanobodies as nanotrap for rearrangement of cellular structures and resulting chemotaxis knockdown

Nanobodies on magnetosomes were then used to create a nanotrap and capture intracellular EGFP-tagged proteins and redirect whole organelles within the cell. As proof of principle an *egfp*-tagged version of the chemotaxis adaptor *cheW*₁ was co-expressed with the *mamC-gbp* fusions on the magnetosomes, to investigate if membrane bound proteins can be recruited to the magnetosome organelles of *M. gryphiswaldense*. Localization of the tagged protein and behavioral effects due to artificial recruitment can be followed by TEM and FM imaging, and by video microscopy at the single cell level. Co-expression of *mamC-gbp* and *cheW*_{1-egfp} lead to a fluorescence shift from the poles to midcell, indicating that the membrane bound protein is artificially recruited to the nanotrap on the magnetosome chain. This could be caused by depletion of CheW₁-EGFP from a cytoplasmic pool or, alternatively, membrane bound CheW₁ could forcefully be subtracted from polar chemotaxis clusters (Figure 7a&b). The chemotaxis signaling complexes are weakly dynamic *in vivo* and fluorescence recovery after photobleaching (FRAP) of fluorescence tagged chemotaxis proteins revealed slow turnover rates for CheA and CheW constructs [148]. The stoichiometry of all cluster components is tightly controlled and over-expression of single genes like *cheW* leads to impairment of chemotaxis [149], therefore the pool of free cytoplasmic CheW is supposedly rather small. Thus, recruitment and depletion of free CheW₁ from the cytoplasm to magnetosome-bound GBP seems probable. Additionally, CheW₁ initially bound to chemotaxis receptors and gradually released to the cytoplasm could be trapped ectopically by nanobodies over time.

To investigate if the special magnetosome organelles are required for recruitment of EGFP-tagged proteins or if nanobodies can be attached to any distinctly localized structure in the cell, the nanotrap was tested in $\Delta mamM$ cells. This mutant lacks the cation diffusion facilitator MamM that is essential for magnetosome biomineralization but not for vesicle formation [63]. Here, the CheW₁-GFP fusions are localized at cell poles but shift towards midcell upon expression of *mamC* fused to bivalent *gbp*. Obviously, recruitment and

3. Discussion

retargeting of CheW₁-GFP is sufficiently effective with GBP fixed to membrane vesicles and independent from magnetosome synthesis and can therefore be adapted to any organism with any membrane structures.

In cells producing mature magnetosomes, recruitment of CheW₁-EGFP was strongly affected by magnetosome chain configuration. In wild type cells the expression of monovalent *gbp* caused only partial depletion of the polar localized CheW₁-EGFP, while fluorescence patterns in the Δ *mamJ* strain was surprisingly different. Cells of Δ *mamJ* are lacking the acidic MamJ protein, which is assumed responsible for attachment of magnetosomes to the MamK filament, and contain magnetosome clusters instead of magnetosome chains [72]. In this strain virtually no fluorescence could be detected at midcell or the opposite pole upon expression of *mamC-1xgbp* in addition to *cheW₁-egfp*, which argues for full recruitment of EGFP-tagged chemotaxis proteins to the magnetosome clusters. This effect might be due to increased avidity of concentrated nanobodies at clustered magnetosomes, or is caused by the concentration of two sinks at a single pole, as the native chemoreceptor cluster and the artificial magnetosome-nanobody cluster are in close proximity, which might shift the CheW₁ diffusion equilibrium from chemoreceptor bound to nanobody bound state (Figure 7c&d).

The configuration and positioning of the magnetosome chain as well as localization of the chemotaxis proteins were affected by interaction of MamC-GBP and CheW₁-GFP reciprocally. Recruitment of CheW₁-GFP to the magnetosomes disturbed proper alignment into regular, densely spaced chains, with increasing nanobody concentration. Coverage of the magnetosome surface with the nanotrap possibly increased inter-particle spacing, which weakens magnetostatic interactions between the particles. This effect was prominent in the wild type background expressing *mamC-2xgbp* and *cheW₁-gfp*, where magnetosome chains were nearly completely shifted and anchored to polar or sub-polar positions. The localization of magnetosome chains at midcell is not fixed and mobility of chains is observed during cell division when chains are split and re-positioned by the cytoskeletal magnetosome filament dynamics of the actin-like MamK, to midcell of daughter cells [73]. This might support the rearrangement and recruitment of magnetosomes chains in strains harboring the nanotrap. The impact of the nanotrap on chain localization was most severe in Δ *mamJ* cells. Expression of the monovalent *gbp* was sufficient to rearrange and recruit magnetosome clusters to one of the cell poles, which might be facilitated due to lack of MamK-mediated interaction to divisome

3. Discussion

constituents [73]. In wild type cells MamK-magnetosome interactions need to be overcome by recruitment to membrane bound CheW₁-GFP, while detached magnetosome in $\Delta mamJ$ can be rearranged rather easily.

Redirection of CheW₁-GFP in wild type cells clearly depended on gene dosage of the nanotrapp, since the observed fluorescence shift was only partial upon expression of *mamC-1xgfp*, while over-expression of *mamC-2xgfp* caused a complete loss of CheW₁-GFP fluorescence at the cell poles. Avidity of nanobodies can be significantly increased (500x) if two identical copies are expressed as fusion in comparison to a monovalent nanobody [150]. Similar, in our approach monovalent GBP recruited CheW₁-GFP apparently in lower rates than the bivalent nanobody, since CheW₁-GFP could be detected at midcell as well as at the cell poles. Expression of the gene encoding the bivalent nanobody increased avidity to the extent that CheW₁-GFP was completely captured at magnetosome-bound GBP. Co-expression of *cheW₁-gfp* and the nanotrapp did not only redirect entire organelles to distinct localizations, but also diminished chemotactic efficiency of *M. gryphiswaldense* cells. Although chemoreceptors form complexes in the absence of CheA or CheW, the adaptor protein CheW is needed to stabilize CheA-receptor interaction and lattice formation [151, 152]. Partial depletion of CheW₁-GFP gradually reduced chemotactic efficiency, while expression of the bivalent nanobody essentially phenocopied the deletion of *cheW₁*. It was shown that the effect on aerotaxis was not due to inactivation of CheW₁-GFP, as GBP expressed in the cytoplasm showed no measurable phenotype. Therefore redirection and depletion of the chemotaxis protein from its native polar environment must disrupt the chemotaxis cascade and cause the behavioral effect. Similar to eukaryotes, function of bacterial proteins depends on a distinct localization despite the lack of superior compartmentalization. Manipulation of protein function by depletion of its subcellular localization has already been applied in eukaryotic systems [99, 153] and was now established for bacterial cells, which are only the size of a couple of hundred nanometers. Several approaches for silencing or manipulating the expression of genes on the transcriptional level already exist [154, 155], but one of the biggest advantages of regulating gene expression at the protein level is that mRNA transcripts or protein expression levels are not disturbed [156]. Important bacterial genes are often organized in operon structures. Therefore it might be favorable to knockdown individual proteins with the use of nanotrapps to avoid polar effects on transcription of downstream genes. Inducible expression genes encoding multivalent nanobodies was shown in *M. gryphiswaldense*, but had no strong behavioral effect due to lack of promoter strength (P_{tet}

3. Discussion

shows 30% of $P_{mamDC45}$ transcriptional activity), chemotaxis effects were only visible after prolonged incubation in comparison to constitutive expression of the nanotrap. Nevertheless, this approach can be optimized and extended, e. g. to gradually control *in vivo* stoichiometry of proteins in larger clusters. Controlled expression of varying copy numbers of nanobodies might be used for studying complex processes as cell division or differentiation in other bacteria, for instance by depletion of essential proteins. Nanobodies are commonly used in eukaryotes as well established tools to trap soluble proteins [92, 98, 99] or inhibit proteins function [96]. Use of nanobodies in bacteria is limited to only a few studies to date, although *E. coli* cells function as an effective production host [91]. Single-chain Fv of conventional antibodies, the equivalent to the VHH (nanobody) in HCABs, was expressed in bacteria to block transcriptional activity [157, 158]. However, applications of nanobodies in bacteria are limited to a study focused on inhibit enzyme activity [102] and another, reporting the display of RBP on magnetosomes to capture cytoplasmic RFP [77]. In contrast to the studies where enzyme inhibition was achieved by neutralization, depletion of CheW₁-GFP was done by anchoring nanobodies to defined positions, thereby creating a nanotrap, and redirecting of trapped proteins to entirely different compartments of *M. gryphiswaldense*. The universal GFP-tag used for recruitment of CheW₁ allows expanding this approach to other bacteria and investigating various pathways. Even though compartmentalization as found in eukaryotes is missing in most bacteria, nanobodies could be fixed to other membrane structures (e. g. at the cell pole or at midcell), specific protein complexes or organelles. With the GFP-GBP system as nanotrap many proteins can be targeted, avoiding the laborious process of camelid immunization and isolation of specific nanobodies. Another potential application would be the creation of artificial compartmentalization of biosynthetic pathways. This could be achieved by restricting reaction partners to subcellular compartments which could dramatically increase product yields [159, 160], by arranging biosynthetic enzymes in artificial scaffolds for control of metabolic flux by fusing reaction partners to different magnetosome anchor proteins (MamG, MamF, MamD, MamC) [161-164], or by construction of membrane enclosed reaction compartments in minimal cells [165].

3.4 First attempts for the generation of magnetic hybrid nanoparticles

In the final part of this thesis, magnetosomes were applied for the attempt to create inorganic-organic-inorganic, magnetic hybrid materials. Two interesting materials for the generation of magnetic CSNs are silica and zinc oxide (ZnO). Silica is an inert material which decreases the bulk conductivity of a sample [11], while ZnO is a good semiconductor with a

3. Discussion

wide band gap (3.37 eV) [166]. MNPs were encapsulated with these inorganic materials to provide additional functionalization or passivation of the material for biomedical applications.

Passivation was achieved by silica precipitation on magnetosomes, since it is an inert material which decreases the bulk conductivity of a sample [11]. Additionally, the silica layer can easily be functionalized due to the existence of abundant silanol groups [167]. For use of iron oxide silica CSNs in biomedical applications, such as biolabelling, imaging, drug targeting, bioseparation and bioassays [14], it is desirable to gain tight size control during synthesis of the particles, since larger particles (> 200 nm) are sequestered easily by phagocytotic cells, while smaller nanoparticles (< 5.5 nm) are rapidly removed by renal clearance [168, 169]. Initially, I attempted to functionalize magnetosomes with silica precipitating peptides, so called silaffins (Sil) that are derived from diatoms [170]. Silaffins displayed on the magnetosome surface should initiate formation of silica spheres surrounding the magnetosomes. Expression of silaffins on magnetosomes was not successful from the constitutive or the inducible expression cassette, possibly due to the polycationic character of the peptides. Expression of *mamC-sil-magegfp* under the control of $P_{mamDC45}$ caused cell death, while inducible expression resulted in diffuse fluorescence patterns, which did not correlate with magnetosome chain position. Assumedly, polycationic silaffins destroy the inner membrane and the MM if expressed as *mamC*-fusion (compare manuscript 2).

To display silaffins on the magnetosome surface, without expressing genes of the polycationic peptides in *M. gryphiswaldense*, isolated, GBP displaying magnetosomes were incubated with recombinant GFP-tagged Sil. Binding of the GFP-conjugated silaffins to GBP covered magnetosomes was successful, since magnetosomes were still fluorescent after several washing steps as shown by fluorescence microscopy. However, no silica precipitates could be observed on the particles by TEM analysis. Taken together it is not possible to express silaffins on the magnetosome surface, but peptides can be displayed on magnetosomes with the GBP-GFP nanotrap. Peptide mediated silica precipitation, however, was not possible on magnetosomes of *M. gryphiswaldense*, possibly because silaffins could not be attached to the magnetosomes in sufficient yields. Therefore MagEGFP functionalized magnetosomes were encapsulated in first attempts with silica, applying a chemical approach by modified Stöber reaction [171]. In fact, magnetosome silica CSNs could be generated with silica layer thicknesses of 3.84 to 20.15 nm, depending on reaction conditions. Increasing the ratio of magnetic seed nanoparticles to silica solution was previously reported to diminish the

3. Discussion

layer thickness of silica [172]. Silica encapsulated, fluorescent magnetosomes with the thinnest layer thickness of 3.84 nm, were incubated with proteinase K and SDS to test whether passivation of the particles would enhance stability of the immobilized EGFP. Indeed, encapsulation of functionalized magnetosomes led to increased stability against proteases and detergents in comparison to magnetosomes displaying EGFP without an additional outer layer of silica. Therefore fluorescent magnetic silica CSNs could have potential in biomedical applications such as fluorescence imaging [173], as contrast agents in MRI or for drug delivery [169]. For biomedical applications it is necessary to obtain uniform encapsulated magnetic particles, which are exclusively present as single magnetosomes or whole chains. With our approach it is not yet possible to generate a complete uniform distribution of single encapsulated magnetosomes due to magnetic attraction of the particles, but could be achieved by adjusting reaction conditions like synthesis of the particles in a magnetic field or separating particles after synthesis by density gradient centrifugation. Additionally, it would be interesting to use smaller particles from mutant strains, lacking operons responsible for magnetosome size, and test whether encapsulation of exclusively single particles could be produced. The zeta potential characterizes the surface charge of particles and can be used as indicator for dispersion and agglomeration of particles in suspension. Silica encapsulation of magnetosomes decreases the zeta potential of the particles significantly (-34.7 mV in contrast to -18.1 mV for non-encapsulated magnetosomes). The surface charge of nanoparticles has a direct effect on endocytosis, negatively charged particles should be taken up slower due to negative repulsion of the negatively charged cell membrane [174]. Additionally, strong negatively charged nanoparticles tend to agglomerate less due to repulsion between the particles [175], but are usually cleared more rapidly from the body because of increased liver uptake [168, 169].

The second pilot approach aimed to generate magnetic CSNs of magnetosomes and zinc oxide because it is a good semiconductor with a wide band gap (3.37 eV) [166]. Pure ZnO nanoparticles proved to have strong antimicrobial activity and might have potential as surface coating to prevent spreading of bacterial infections [176, 177]. The disadvantage of pure ZnO nanoparticles is strong agglomeration [181]. Therefore Fe₃O₄-ZnO hybrid materials were generated in previous studies because ferrofluids are expected to exhibit strong colloidal stability [18, 178]. Most studies describe Fe₃O₄-ZnO hybrid composites of different sizes and morphologies, e. g. Cao and co-workers synthesized Fe₃O₄-coated ZnO “nanoflowers” [179]. Other example are Fe₃O₄-ZnO hybrid nanorods [180] or doping of ZnO with Fe₃O₄ to add

3. Discussion

magnetic properties to the semiconductive ZnO. In this approach Fe₃O₄ was embedded in porous ZnO particles, the material can be used for removal of toxic metal ions, organic dyes or bacterial pathogens [181, 182].

In contrast to the silica encapsulation approach, ZnO-binding peptides, identified by Rothenstein and co-workers [183], could successfully be expressed as ZnO-MagEGFP tandem fusion on magnetosomes and were thought to be used for ZnO precipitation. Magnetosomes displaying only MagEGFP but not the ZnO-binding peptide were used as a negative control. In preliminary experiments it could be shown that ZnO was precipitated equally on magnetosomes displaying the ZnO-binder or just MagEGFP. Precipitation of ZnO was performed in methanol solution that strongly facilitates production of ZnO particles on any surface, it might be possible that the effect of the immobilized ZnO-binder is masked by rapid reaction conditions and precipitation of ZnO by the ZnO-binding peptide might be visible only under ambient reaction conditions. Since no difference could be detected under the tested conditions, further experiments were performed with MagEGFP functionalized magnetosomes, coated with an approximately 20 nm thick layer of ZnO. The zeta potential of hybrid particles was -2.5 mV and therefore drastically increased in comparison to non-coated EGFP-functionalized magnetosomes (-18.1 mV), and correlates well with the zeta potential of pure ZnO (-2.9 mV). Reduced surface charge could increase retention time within the human body [174], which would make magnetosome-ZnO hybrid nanoparticles an interesting tool in biomedical applications. Hanley and co-workers discovered that ZnO nanoparticles exhibit enhanced cytotoxicity against cancer cells in comparison to normal cells [184], the magnetic core of magnetosome-ZnO CSNs would allow for targeting the particles specifically to tumors within the body without the need of specific tags for recognition of tumor cells. Additionally the cytotoxic effect of ZnO could be supported by hyperthermia treatment as suggested for magnetosomes before [185]. The ZnO shell surrounding magnetosomes is a biocompatible material which might be dissolved into Zn ions after remaining for a few hours in the body, without having a toxic effect to the organism [186]. Magnetosomes devoid of the ZnO shell could then be recognized and eliminated by immune cells.

In summary, in this thesis an optimized expression system, containing a constitutive or an inducible expression cassette, for chromosomal insertion of any heterologous fusion gene was developed, extending the genetic toolbar for *M. gryphiswaldense*. Applying these new integrative expression vectors, magnetosomes were functionalized with multivalent

3. Discussion

nanobodies as nanotrap that specifically recognize fluorescently tagged proteins, and can be used for retargeting and depletion of chemotaxis proteins and re-direction of entire organelles. Finally, magnetosomes displaying *Magnetospirillum*-optimized *egfp* were encapsulated with inorganic materials such as silica and zinc oxide for generation of innovative hybrid materials.

3.5 Open questions and future directions

The expression systems developed in this thesis can now be used for the display of various fusion proteins, such as novel fluorescence markers, different nanobodies or enzymes on magnetosomes. Moreover, the inducible expression system could also be applied for studies on essential genes and regulatory pathways by depletion of targeted genes. Although the optimized expression system is efficient for constitutive expression of heterologous genes, the relatively weak strength of the inducible promoter requires improvement. For example, with only 30% strength of the constitutive expression system it is not possible to express genes of toxic fusion proteins in high yields. For identification of strong native inducible promoters microarrays could be used to map promoters responding to specific stimuli [187]. Additionally, construction of hybrid promoters consisting of different promoter operator elements should be re-assessed by broader systematic approaches, using the non-truncated P_{mamDC} and other promoters that possibly still contain regulatory elements.

Genes of nanobodies were expressed to create nanotraps on magnetosomes for re-direction of fluorescent proteins in *M. gryphiswaldense*. This led to recruitment and depletion of the chemotaxis protein CheW from the poles, resulting in chemotaxis knock down. The inducible expression system could now be used to gradually knockdown chemotaxis and eventually discover a link between chemotaxis and polarity in *M. gryphiswaldense*. Moreover, the nanotrap system could be used to deplete essential proteins and study behavioral effects by retargeting in magnetotactic or other bacteria, since it was previously shown that nanobodies can be functionally expressed in other bacteria [102]. The use of both GBP and RBP would allow trapping different enzymes to the same compartment constructing artificial scaffolds as reaction vessels. Display of different nanobodies in the mono- to trivalent state would supply tight control over stoichiometry and metabolic flux of the artificial pathway [164]. Nanotrap technology could possibly be extended to naturally existing anchor points in non-magnetotactic bacteria, such as spores in *B. subtilis*, or other spatial determinants like MreB.

New hybrid MNPs with extended function could be generated using magnetosomes as seed and applying further chemical approaches for coating with e. g. titanium dioxide, silver or gold. Iron doped TiO_2 was reported to exhibit increased photocatalytical activity [188], while silver nanoparticles exhibit strong antimicrobial activity [189] and gold nanoparticles are commonly used as catalysts or in sensors [190]. Coating of magnetosomes with these

3. Discussion

materials would add new properties coupled with the ability of magnetic manipulation. Concurrently, peptide directed precipitation of silica and zinc oxide should be investigated in more detail. ZnO-binding peptides should be considered in more ambient approaches, such as Tris-HCl buffered reaction conditions. It is most probable that precipitation of ZnO could be facilitated by peptides under these conditions. Immobilization of silaffins on magnetosomes is not possible assumedly due to the polycationic character of the peptides, but silaffins are well characterized and the silica binding motif was previously identified [170]. Therefore, it might be possible to express only the silica binding motif as fusion to *mamC*, to avoid disturbance of the MM and to sequester silica. If expression of modified silaffin genes targeted to magnetosomes would be successful, functionalized magnetosomes could also be used to precipitate TiO₂, as demonstrated previously with silaffins [191]. Newly generated magnetic hybrid MNPs, generated by those approaches could have great potential in biomedical applications as in drug delivery, bioimaging, cell labeling or in biosensors [192].

4. References

1. Gupta, A.K. and M. Gupta, *Synthesis and surface engineering of iron oxide nanoparticles for biomedical applications*. *Biomaterials*, 2005. **26**(18): p. 3995-4021.
2. Faivre, D. and D. Schüler, *Magnetotactic bacteria and magnetosomes*. *Chem. Rev.*, 2008. **108**(11): p. 4875-4898.
3. Schwertmann, U. and R.M. Cornell, *Iron oxides in the laboratory*. 2008: John Wiley & Sons.
4. Cornell, R. and U. Schwertmann, *The Iron Oxides: Structure, Properties, Reactions, Occurrence and Uses* 1996, New York: VCH. 167-168.
5. Verwey, E., *Electronic conduction of magnetite (Fe_3O_4) and its transition point at low temperatures*. *Nature*, 1939. **144**(3642): p. 327-328.
6. Si, S., et al., *Magnetic monodisperse Fe_3O_4 nanoparticles*. *Crystal Growth & Design*, 2005. **5**(2): p. 391-393.
7. Ma, M., et al., *Preparation and characterization of magnetite nanoparticles coated by amino silane*. *Coll. Surf. A: Physicochemical and Engineering Aspects*, 2003. **212**(2-3): p. 219-226.
8. Maity, D., et al., *Studies of magnetite nanoparticles synthesized by thermal decomposition of iron (III) acetylacetonate in tri(ethylene glycol)*. *J. Magn. Magn. Mater.*, 2009. **321**(19): p. 3093-3098.
9. Suslick, K.S., M. Fang, and T. Hyeon, *Sonochemical synthesis of iron colloids*. *JACS*, 1996. **118**(47): p. 11960-11961.
10. Lu, A.-H., E.L. Salabas, and F. Schüth, *Magnetische Nanopartikel: Synthese, Stabilisierung, Funktionalisierung und Anwendung*. *Angew. Chem.*, 2007. **119**(8): p. 1242-1266.
11. Ghosh Chaudhuri, R. and S. Paria, *Core/shell nanoparticles: classes, properties, synthesis mechanisms, characterization, and applications*. *Chem. Rev.*, 2011. **112**(4): p. 2373-2433.
12. Aliev, F.G., et al., *Layer-by-layer assembly of core-shell magnetite nanoparticles: Effect of silica coating on interparticle interactions and magnetic properties*. *Adv. Mater.*, 1999. **11**(12): p. 1006-1010.
13. Santra, S., et al., *Conjugation of biomolecules with luminophore-doped silica nanoparticles for photostable biomarkers*. *Anal. Chem.*, 2001. **73**(20): p. 4988-4993.

4. References

14. He, R., et al., *Core/shell fluorescent magnetic silica-coated composite nanoparticles for bioconjugation*. *Nanotechnology*, 2007. **18**(31): p. 315601.
15. Lee, J., et al., *Simple synthesis of functionalized superparamagnetic magnetite/silica core/shell nanoparticles and their application as magnetically separable high-performance biocatalysts*. *Small*, 2008. **4**(1): p. 143-152.
16. Lien, Y.-H. and T.-M. Wu, *Preparation and characterization of thermosensitive polymers grafted onto silica-coated iron oxide nanoparticles*. *J. Colloid Interface Sci.*, 2008. **326**(2): p. 517-521.
17. Chiu, W., et al., *Heterogeneous seeded growth: synthesis and characterization of bifunctional Fe₃O₄/ZnO core/shell nanocrystals*. *J. Phys. Chem. C*, 2010. **114**(18): p. 8212-8218.
18. Wan, J., H. Li, and K. Chen, *Synthesis and characterization of Fe₃O₄@ZnO core-shell structured nanoparticles*. *Mater. Chem. Phys.*, 2009. **114**(1): p. 30-32.
19. Kim, D.K., et al., *Protective coating of superparamagnetic iron oxide nanoparticles*. *Chem. Mater.*, 2003. **15**(8): p. 1617-1627.
20. Berry, C.C. and A.S.G. Curtis, *Functionalisation of magnetic nanoparticles for applications in biomedicine*. *J. Phys. D: Appl. Phys.*, 2003. **36**(13): p. R198.
21. D'Souza, A.J.M., R.L. Schowen, and E.M. Topp, *Polyvinylpyrrolidone-drug conjugate: synthesis and release mechanism*. *J. Controlled Release*, 2004. **94**(1): p. 91-100.
22. Zhang, Y., N. Kohler, and M. Zhang, *Surface modification of superparamagnetic magnetite nanoparticles and their intracellular uptake*. *Biomaterials*, 2002. **23**(7): p. 1553-1561.
23. Sahoo, Y., et al., *Alkyl phosphonate/phosphate coating on magnetite nanoparticles: A comparison with fatty acids*. *Langmuir*, 2001. **17**(25): p. 7907-7911.
24. Lewin, M., et al., *Tat peptide-derivatized magnetic nanoparticles allow in vivo tracking and recovery of progenitor cells*. *Nat. Biotech.*, 2000. **18**(4): p. 410-414.
25. Sahoo, Y., et al., *Aqueous Ferrofluid of Magnetite Nanoparticles: Fluorescence Labeling and Magnetophoretic Control*. *J. Phys. Chem. B*, 2005. **109**(9): p. 3879-3885.
26. Berry, C.C., et al., *The influence of transferrin stabilised magnetic nanoparticles on human dermal fibroblasts in culture*. *Int. J. Pharm.*, 2004. **269**(1): p. 211-225.

4. References

27. Zhang, X., et al., *Chitosan-Coated Octadecyl-Functionalized Magnetite Nanoparticles: Preparation and Application in Extraction of Trace Pollutants from Environmental Water Samples*. Anal. Chem., 2010. **82**(6): p. 2363-2371.
28. Jogler, C. and D. Schüler, *Genetic and Biochemical Analysis of Magnetosome Formation in Magnetospirillum gryphiswaldense*, in *Handbook of Biomineralization*. 2008, Wiley-VCH Verlag GmbH. p. 145-161.
29. Bellini, S., *On a unique behavior of freshwater bacteria*. Chin. J. Oceanol. Limnol., 2009. **27**(1): p. 3-5.
30. Blakemore, R., *Magnetotactic bacteria*. Science, 1975. **190**(4212): p. 377-379.
31. Matsunaga, T., T. Sakaguchi, and F. Tadakoro, *Magnetite formation by a magnetic bacterium capable of growing aerobically*. Appl. Microbiol. Biotechnol., 1991. **35**(5): p. 651-655.
32. Schleifer, K.H., et al., *The genus Magnetospirillum gen. nov. description of Magnetospirillum gryphiswaldense sp. nov. and transfer of Aquaspirillum magnetotacticum to Magnetospirillum magnetotacticum comb. nov.* Syst. Appl. Microbiol., 1991. **14**(4): p. 379-385.
33. Schüler, D. and M. Köhler, *The isolation of a new magnetic spirillum*. Zentralblatt für Mikrobiologie, 1992. **147**(1-2): p. 150-151.
34. Bazylinski, D.A. and R.B. Frankel, *Magnetosome formation in prokaryotes*. Nat Rev Micro, 2004. **2**(3): p. 217-230.
35. Blakemore, R.P., R.B. Frankel, and A.J. Kalmijn, *South-seeking magnetotactic bacteria in the Southern Hemisphere*. Physics, 1980: p. 159.
36. Popp, F., J.P. Armitage, and D. Schüler, *Polarity of bacterial magnetotaxis is controlled by aerotaxis through a common sensory pathway*. Nat. Commun., 2014. **5**(5398).
37. Schüler, D., *Genetics and cell biology of magnetosome formation in magnetotactic bacteria*. FEMS Microbiol. Rev., 2008. **32**(4): p. 654-672.
38. Farina, M., D.M.S. Esquivel, and H.G.P.L. de Barros, *Magnetic iron-sulphur crystals from a magnetotactic microorganism*. Nature, 1990. **343**(6255): p. 256-258.
39. Mann, S., et al., *Biomineralization of ferrimagnetic greigite (Fe₃S₄) and iron pyrite (FeS₂) in a magnetotactic bacterium*. Nature, 1990. **343**(6255): p. 258-261.
40. Han, L., et al., *Comparison of magnetite nanocrystal formed by biomineralization and chemosynthesis*. J. Magn. Magn. Mater., 2007. **313**(1): p. 236-242.

4. References

41. Staniland, S., et al., *Controlled cobalt doping of magnetosomes in vivo*. Nat Nano, 2008. **3**(3): p. 158-162.
42. Coker, V.S., et al., *Cation site occupancy of biogenic magnetite compared to polygenic ferrite spinels determined by X-ray magnetic circular dichroism*. Eur. J. Mineral., 2007. **19**(5): p. 707-716.
43. Kopp, R.E., et al., *Ferromagnetic resonance spectroscopy for assessment of magnetic anisotropy and magnetostatic interactions: A case study of mutant magnetotactic bacteria*. J. Geophys. Res. B: Solid Earth, 2006. **111**(B12).
44. Arató, B., et al., *Crystal-size and shape distributions of magnetite from uncultured magnetotactic bacteria as a potential biomarker*. Am. Mineral., 2005. **90**(8-9): p. 1233-1240.
45. Bazylinski, D.A., A.J. Garratt-Reed, and R.B. Frankel, *Electron microscopic studies of magnetosomes in magnetotactic bacteria*. Microsc. Res. Tech., 1994. **27**(5): p. 389-401.
46. Sparks, N.H.C., et al., *Magnetotactic bacteria are widely distributed in sediments in the U.K.* FEMS Microbiol. Lett., 1986. **37**(3): p. 305-308.
47. Faivre, D., et al., *Environmental parameters affect the physical properties of fast-growing magnetosomes*. Am. Mineral., 2008. **93**(2-3): p. 463-469.
48. Scheffel, A., et al., *The major magnetosome proteins MamGFDC are not essential for magnetite biomineralization in Magnetospirillum gryphiswaldense but regulate the size of magnetosome crystals*. J. Bacteriol., 2008. **190**(1): p. 377-386.
49. Schüller, D. and E. Baeuerlein, *Dynamics of iron uptake and Fe₃O₄ biomineralization during aerobic and microaerobic growth of Magnetospirillum gryphiswaldense*. J. Bacteriol., 1998. **180**(1): p. 159-162.
50. Lohße, A., et al., *Functional analysis of the magnetosome island in Magnetospirillum gryphiswaldense: The mamAB operon is sufficient for magnetite biomineralization*. PLoS ONE, 2011. **6**(10): p. e25561.
51. Devouard, B., et al., *Magnetite from magnetotactic bacteria: Size distributions and twinning*. Am. Mineral., 1998. **83**: p. 1387-1398.
52. Lins, U. and M. Farina, *Magnetosome size distribution in uncultured rod-shaped bacteria as determined by electron microscopy and electron spectroscopic imaging*. Microsc. Res. Tech., 1998. **42**(6): p. 459-464.

4. References

53. Moskowitz, B.M., et al., *Magnetic properties of magnetotactic bacteria*. J. Magn. Magn. Mater., 1988. **73**(3): p. 273-288.
54. Grünberg, K., et al., *Biochemical and proteomic analysis of the magnetosome membrane in Magnetospirillum gryphiswaldense*. Appl. Environ. Microbiol., 2004. **70**(2): p. 1040-1050.
55. Komeili, A., et al., *Magnetosomes are cell membrane invaginations organized by the actin-like protein MamK*. Science, 2006. **311**(5758): p. 242-245.
56. Murat, D., et al., *Comprehensive genetic dissection of the magnetosome gene island reveals the step-wise assembly of a prokaryotic organelle*. Proc. Natl. Acad. Sci. U.S.A., 2010. **107**(12): p. 5593-5598.
57. Lang, C. and D. Schüler, *Expression of green fluorescent protein fused to magnetosome proteins in microaerophilic magnetotactic bacteria*. Appl. Environ. Microbiol., 2008. **74**(15): p. 4944-4953.
58. Schüler, D., *Molecular analysis of a subcellular compartment: the magnetosome membrane in Magnetospirillum gryphiswaldense*. Arch. Microbiol., 2004. **181**(1): p. 1-7.
59. Richter, M., et al., *Comparative genome analysis of four magnetotactic bacteria reveals a complex set of group-specific genes implicated in magnetosome biomineralization and function*. J. Bacteriol., 2007. **189**(13): p. 4899-4910.
60. Grünberg, K., et al., *A large gene cluster encoding several magnetosome proteins is conserved in different species of magnetotactic bacteria*. Appl. Environ. Microbiol., 2001. **67**(10): p. 4573-4582.
61. Katzmann, E., et al., *Loss of the actin-like protein MamK has pleiotropic effects on magnetosome formation and chain assembly in Magnetospirillum gryphiswaldense*. Mol. Microbiol., 2010. **77**(1): p. 208-224.
62. Lohße, A., et al., *Genetic dissection of the mamAB and mms6 operons reveals a gene set essential for magnetosome biogenesis in Magnetospirillum gryphiswaldense*. J. Bacteriol., 2014.
63. Uebe, R., et al., *The cation diffusion facilitator proteins MamB and MamM of Magnetospirillum gryphiswaldense have distinct and complex functions, and are involved in magnetite biomineralization and magnetosome membrane assembly*. Mol. Microbiol., 2011. **82**(4): p. 818-835.

4. References

64. Zeytuni, N., et al., *Self-recognition mechanism of MamA, a magnetosome-associated TPR-containing protein, promotes complex assembly*. Proc. Natl. Acad. Sci. U.S.A., 2011. **108**(33): p. E480-E487.
65. Quinlan, A., et al., *The HtrA/DegP family protease MamE is a bifunctional protein with roles in magnetosome protein localization and magnetite biomineralization*. Mol. Microbiol., 2011. **80**(4): p. 1075-1087.
66. Raschdorf, O., et al., *The magnetosome proteins MamX, MamZ and MamH are involved in redox control of magnetite biomineralization in Magnetospirillum gryphiswaldense*. Mol. Microbiol., 2013. **89**(5): p. 872-886.
67. Baumgartner, J., et al., *Magnetotactic bacteria form magnetite from a phosphate-rich ferric hydroxide via nanometric ferric (oxyhydr)oxide intermediates*. Proc. Natl. Acad. Sci. U.S.A., 2013. **110**(37): p. 14883-14888.
68. Siponen, M.I., et al., *Magnetochrome: a c-type cytochrome domain specific to magnetotactic bacteria*. Biochem. Soc. Trans., 2012. **40**(6): p. 1319-1323.
69. Arakaki, A., et al., *Control of the morphology and size of magnetite particles with peptides mimicking the Mms6 protein from magnetotactic bacteria*. J. Colloid Interface Sci., 2010. **343**(1): p. 65-70.
70. Oestreicher, Z., et al., *Magnetosomes and magnetite crystals produced by magnetotactic bacteria as resolved by atomic force microscopy and transmission electron microscopy*. Micron, 2012. **43**(12): p. 1331-1335.
71. Wang, W., et al., *Interfacial properties and iron binding to bacterial proteins that promote the growth of magnetite nanocrystals: X-ray reflectivity and surface spectroscopy studies*. Langmuir, 2012. **28**(9): p. 4274-4282.
72. Scheffel, A., et al., *An acidic protein aligns magnetosomes along a filamentous structure in magnetotactic bacteria*. Nature, 2006. **440**(7080): p. 110-114.
73. Katzmann, E., et al., *Magnetosome chains are recruited to cellular division sites and split by asymmetric septation*. Mol. Microbiol., 2011. **82**(6): p. 1316-1329.
74. Ullrich, S., et al., *A hypervariable 130-kilobase genomic region of Magnetospirillum gryphiswaldense comprises a magnetosome island which undergoes frequent rearrangements during stationary growth*. J. Bacteriol., 2005. **187**(21): p. 7176-7184.
75. Ullrich, S. and D. Schüler, *Cre-lox-based method for generation of large deletions within the genomic magnetosome island of Magnetospirillum gryphiswaldense*. Appl. Environ. Microbiol., 2010. **76**(8): p. 2439-2444.

4. References

76. Ohuchi, S. and D. Schüler, *In vivo display of a multisubunit enzyme complex on biogenic magnetic nanoparticles*. Appl. Environ. Microbiol., 2009. **75**(24): p. 7734-7738.
77. Pollithy, A., et al., *Magnetosome expression of functional camelid antibody fragments (nanobodies) in Magnetospirillum gryphiswaldense*. Appl. Environ. Microbiol., 2011. **77**(17): p. 6165-6171.
78. Matsunaga, T. and A. Arakaki, *Molecular bioengineering of bacterial magnetic particles for biotechnological applications*, in *Magnetoreception and Magnetosomes in Bacteria*, D. Schüler, Editor. 2007, Springer Berlin Heidelberg. p. 227-254.
79. Lang, C., D. Schüler, and D. Faivre, *Synthesis of magnetite nanoparticles for bio- and nanotechnology: Genetic engineering and biomimetics of bacterial magnetosomes*. Macromol. Biosci., 2007. **7**(2): p. 144-151.
80. Matsunaga, T. and S. Kamiya, *Use of magnetic particles isolated from magnetotactic bacteria for enzyme immobilization*. Appl. Microbiol. Biotechnol., 1987. **26**(4): p. 328-332.
81. Matsunaga, T., et al., *Chemiluminescence enzyme immunoassay using bacterial magnetic particles*. Anal. Chem., 1996. **68**(20): p. 3551-3554.
82. Amemiya, Y., et al., *Novel detection system for biomolecules using nano-sized bacterial magnetic particles and magnetic force microscopy*. J. Biotechnol., 2005. **120**(3): p. 308-314.
83. Ceyhan, B., et al., *Semisynthetic Biogenic Magnetosome Nanoparticles for the Detection of Proteins and Nucleic Acids*. Small, 2006. **2**(11): p. 1251-1255.
84. Wacker, R., et al., *Magneto Immuno-PCR: A novel immunoassay based on biogenic magnetosome nanoparticles*. Biochem. Biophys. Res. Commun., 2007. **357**(2): p. 391-396.
85. Maeda, Y., et al., *Noncovalent immobilization of streptavidin on in vitro- and in vivo-biotinylated bacterial magnetic particles*. Appl. Environ. Microbiol., 2008. **74**(16): p. 5139-5145.
86. Ginet, N., et al., *Single-step production of a recyclable nanobiocatalyst for organophosphate pesticides biodegradation using functionalized bacterial magnetosomes*. PLoS ONE, 2011. **6**(6): p. e21442.

4. References

87. Yoshino, T. and T. Matsunaga, *Efficient and stable display of functional proteins on bacterial magnetic particles using Mms13 as a novel anchor molecule*. Appl. Environ. Microbiol., 2006. **72**(1): p. 465-471.
88. Kanetsuki, Y., et al., *Effective expression of human proteins on bacterial magnetic particles in an anchor gene deletion mutant of Magnetospirillum magneticum AMB-1*. Biochem. Biophys. Res. Commun., 2012. **426**(1): p. 7-11.
89. Waugh, D.S. and N.R. Pace, *Complementation of an RNase P RNA (rnpB) gene deletion in Escherichia coli by homologous genes from distantly related eubacteria*. J. Bacteriol., 1990. **172**(11): p. 6316-6322.
90. Xu, J., et al., *Surface expression of protein A on magnetosomes and capture of pathogenic bacteria by magnetosome/antibody complexes*. Front. Microbiol., 2014. **5**.
91. Muyldermans, S., *Nanobodies: Natural single-domain antibodies*. Annu. Rev. Biochem., 2013. **82**(1): p. 775-797.
92. Rothbauer, U., et al., *A versatile nanotrapp for biochemical and functional studies with fluorescent fusion proteins*. Mol. Cell. Proteomics, 2008. **7**(2): p. 282-289.
93. Harmsen, M.M. and H.J. De Haard, *Properties, production, and applications of camelid single-domain antibody fragments*. Appl. Microbiol. Biotechnol., 2007. **77**(1): p. 13-22.
94. De Genst, E., et al., *Molecular basis for the preferential cleft recognition by dromedary heavy-chain antibodies*. Proc. Natl. Acad. Sci. U.S.A. of the United States of America, 2006. **103**(12): p. 4586-4591.
95. Lauwereys, M., et al., *Potent enzyme inhibitors derived from dromedary heavy-chain antibodies*. EMBO J., 1998. **17**(13): p. 3512-3520.
96. Jobling, S.A., et al., *Immunomodulation of enzyme function in plants by single-domain antibody fragments*. Nat Biotech, 2003. **21**(1): p. 77-80.
97. Caussin, E., O. Kanca, and M. Affolter, *Fluorescent fusion protein knockout mediated by anti-GFP nanobody*. Nat Struct Mol Biol, 2012. **19**(1): p. 117-121.
98. Herce, H.D., et al., *Visualization and targeted disruption of protein interactions in living cells*. Nat Commun, 2013. **4**.
99. Schornack, S., et al., *Protein mislocalization in plant cells using a GFP-binding chromobody*. Plant J., 2009. **60**(4): p. 744-754.
100. Rothbauer, U., et al., *Targeting and tracing antigens in live cells with fluorescent nanobodies*. Nat Meth, 2006. **3**(11): p. 887-889.

4. References

101. Miller, T.W. and A. Messer, *Intrabody applications in neurological disorders: progress and future prospects*. Mol Ther, 2005. **12**(3): p. 394-401.
102. Zafra, O., et al., *Monitoring biodegradative enzymes with nanobodies raised in Camelus dromedarius with mixtures of catabolic proteins*. Environ. Microbiol., 2011. **13**(4): p. 960-974.
103. Hannig, G. and S.C. Makrides, *Strategies for optimizing heterologous protein expression in Escherichia coli*. Trends Biotechnol., 1998. **16**(2): p. 54-60.
104. Glick, B.R., *Metabolic load and heterologous gene expression*. Biotechnol. Adv., 1995. **13**(2): p. 247-261.
105. Gustafsson, C., S. Govindarajan, and J. Minshull, *Codon bias and heterologous protein expression*. Trends Biotechnol., 2004. **22**(7): p. 346-353.
106. Terpe, K., *Overview of bacterial expression systems for heterologous protein production: from molecular and biochemical fundamentals to commercial systems*. Appl. Microbiol. Biotechnol., 2006. **72**(2): p. 211-222.
107. Polisky, B., R.J. Bishop, and D.H. Gelfand, *A plasmid cloning vehicle allowing regulated expression of eukaryotic DNA in bacteria*. Proc. Natl. Acad. Sci. U.S.A., 1976. **73**(11): p. 3900-3904.
108. de Boer, H.A., L.J. Comstock, and M. Vasser, *The tac promoter: a functional hybrid derived from the trp and lac promoters*. Proc. Natl. Acad. Sci. U.S.A., 1983. **80**(1): p. 21-25.
109. Brosius, J., M. Erfle, and J. Storella, *Spacing of the -10 and -35 regions in the tac promoter. Effect on its in vivo activity*. J. Biol. Chem., 1985. **260**(6): p. 3539-3541.
110. Meisenzahl, A.C., L. Shapiro, and U. Jenal, *Isolation and characterization of a xylose-dependent promoter from Caulobacter crescentus*. J. Bacteriol., 1997. **179**(3): p. 592-600.
111. Thanbichler, M., A.A. Iniesta, and L. Shapiro, *A comprehensive set of plasmids for vanillate- and xylose-inducible gene expression in Caulobacter crescentus*. Nucleic Acids Res., 2007. **35**(20): p. e137.
112. Hillen, W. and C. Berens, *Mechanisms underlying expression of Tn10 encoded tetracycline resistance*. Annu Rev Microbiol, 1994. **48**(1): p. 345-369.
113. Skerra, A., *Use of the tetracycline promoter for the tightly regulated production of a murine antibody fragment in Escherichia coli*. Gene, 1994. **151**(1-2): p. 131-135.

4. References

114. Degenkolb, J., et al., *Structural requirements of tetracycline-Tet repressor interaction: determination of equilibrium binding constants for tetracycline analogs with the Tet repressor*. *Antimicrob. Agents Chemother.*, 1991. **35**(8): p. 1591-1595.
115. Thanbichler, M. and L. Shapiro, *MipZ, a spatial regulator coordinating chromosome segregation with cell division in Caulobacter*. *Cell*, 2006. **126**(1): p. 147-162.
116. Yoshino, T. and T. Matsunaga, *Development of efficient expression system for protein display on bacterial magnetic particles*. *Biochem. Biophys. Res. Commun.*, 2005. **338**(4): p. 1678-1681.
117. Yoshino, T., et al., *Assembly of G protein-coupled receptors onto nanosized bacterial magnetic particles using Mms16 as an anchor molecule*. *Appl. Environ. Microbiol.*, 2004. **70**(5): p. 2880-2885.
118. Lang, C., A. Pollithy, and D. Schüler, *Identification of promoters for efficient gene expression in Magnetospirillum gryphiswaldense*. *Appl. Environ. Microbiol.*, 2009. **75**(12): p. 4206-4210.
119. Yoshino, T., et al., *Inducible expression of transmembrane proteins on bacterial magnetic particles in Magnetospirillum magneticum AMB-1*. *Appl. Environ. Microbiol.*, 2010. **76**(4): p. 1152-1157.
120. Topp, S., et al., *Synthetic riboswitches that induce gene expression in diverse bacterial species*. *Appl. Environ. Microbiol.*, 2010. **76**(23): p. 7881-7884.
121. Schultheiss, D. and D. Schüler, *Development of a genetic system for Magnetospirillum gryphiswaldense*. *Arch. Microbiol.* , 2003. **179**(2): p. 89-94.
122. Matsunaga, T., et al., *Gene transfer in magnetic bacteria: transposon mutagenesis and cloning of genomic DNA fragments required for magnetosome synthesis*. *J. Bacteriol.*, 1992. **174**(9): p. 2748-2753.
123. Kolinko, I., et al., *Frequent mutations within the genomic magnetosome island of Magnetospirillum gryphiswaldense are mediated by RecA*. *J. Bacteriol.*, 2011. **193**(19): p. 5328-5334.
124. Raschdorf, O., et al., *A tailored galK counterselection system for efficient markerless gene deletion and chromosomal tagging in Magnetospirillum gryphiswaldense*. *Appl. Environ. Microbiol.*, 2014.
125. Schübbe, S., et al., *Transcriptional organization and regulation of magnetosome operons in Magnetospirillum gryphiswaldense*. *Appl. Environ. Microbiol.*, 2006. **72**(9): p. 5757-5765.

4. References

126. Pollithy, A., *Optimierung von Expressionssystemen und magnetosomenspezifische Expression von Nanobodies in Magnetospirillum gryphiswaldense*. 2009, Ludwig-Maximilians Universität, Mikrobiologie: München.
127. Davidson, C.J. and M.G. Surette, *Individuality in bacteria*. *Annu Rev Genet*, 2008. **42**(1): p. 253-268.
128. D'Orazio, S.E. and C.M. Collins, *The plasmid-encoded urease gene cluster of the family Enterobacteriaceae is positively regulated by UreR, a member of the AraC family of transcriptional activators*. *J. Bacteriol.*, 1993. **175**(11): p. 3459-3467.
129. Lang, C., *Magnetosome-specific expression of chimeric proteins in Magnetospirillum gryphiswaldense for applications in cell biology and biotechnology*. 2009, Ludwig Maximilian University, Microbiology: Munich.
130. Haugen, S.P., W. Ross, and R.L. Gourse, *Advances in bacterial promoter recognition and its control by factors that do not bind DNA*. *Nat Rev Micro*, 2008. **6**(7): p. 507-519.
131. Hawley, D.K. and W.R. McClure, *Compilation and analysis of Escherichia coli promoter DNA sequences*. *Nucleic Acids Res.*, 1983. **11**(8): p. 2237-2255.
132. Grosjean, H. and W. Fiers, *Preferential codon usage in prokaryotic genes: the optimal codon-anticodon interaction energy and the selective codon usage in efficiently expressed genes*. *Gene*, 1982. **18**(3): p. 199-209.
133. Li, Y., et al., *The periplasmic nitrate reductase Nap is required for anaerobic growth and involved in redox control of magnetite biomineralization in Magnetospirillum gryphiswaldense*. *J. Bacteriol.*, 2012. **194**(18): p. 4847-4856.
134. Guss, A.M., et al., *New methods for tightly regulated gene expression and highly efficient chromosomal integration of cloned genes for Methanosarcina species*. *Archaea*, 2008. **2**(3).
135. Ind, A.C., et al., *Inducible-expression plasmid for Rhodobacter sphaeroides and Paracoccus denitrificans*. *Appl. Environ. Microbiol.*, 2009. **75**(20): p. 6613-6615.
136. Khan, S.R., et al., *Broad-host-range expression vectors with tightly regulated promoters and their use to examine the influence of TraR and TraM expression on Ti plasmid quorum sensing*. *Appl. Environ. Microbiol.*, 2008. **74**(16): p. 5053-5062.
137. Tett, A.J., et al., *Regulatable vectors for environmental gene expression in Alphaproteobacteria*. *Appl. Environ. Microbiol.*, 2012. **78**(19): p. 7137-7140.

4. References

138. Debowski, A.W., et al., *Development of a tetracycline-inducible gene expression system for the study of Helicobacter pylori pathogenesis*. Appl. Environ. Microbiol., 2013. **79**(23): p. 7351-7359.
139. Geissendörfer, M. and W. Hillen, *Regulated expression of heterologous genes in Bacillus subtilis using the Tn10 encoded tet regulatory elements*. Appl. Microbiol. Biotechnol., 1990. **33**(6): p. 657-663.
140. Ji, Y., et al., *Regulated antisense RNA eliminates alpha-toxin virulence in Staphylococcus aureus infection*. J. Bacteriol., 1999. **181**(21): p. 6585-6590.
141. Stieger, M., et al., *Integrational plasmids for the tetracycline-regulated expression of genes in Streptococcus pneumoniae*. Gene, 1999. **226**(2): p. 243-251.
142. Siegele, D.A. and J.C. Hu, *Gene expression from plasmids containing the araBAD promoter at subsaturating inducer concentrations represents mixed populations*. Proc. Natl. Acad. Sci. U.S.A., 1997. **94**(15): p. 8168-8172.
143. Choi, Y.J., et al., *Bestowing inducibility on the cloned methanol dehydrogenase promoter (Pmx_AF) of Methylobacterium extorquens by applying regulatory elements of Pseudomonas putida F1*. Appl. Environ. Microbiol., 2006. **72**(12): p. 7723-7729.
144. Choi, Y.J., et al., *Multicopy integration and expression of heterologous genes in Methylobacterium extorquens ATCC 55366*. Appl. Environ. Microbiol., 2006. **72**(1): p. 753-759.
145. Tyo, K.E.J., P.K. Ajikumar, and G. Stephanopoulos, *Stabilized gene duplication enables long-term selection-free heterologous pathway expression*. Nat Biotech, 2009. **27**(8): p. 760-765.
146. Lisy, M.-R., et al., *Fluorescent bacterial magnetic nanoparticles as bimodal contrast agents*. Invest Radiol, 2007. **42**(4): p. 235-241 10.1097/01.rli.0000255832.44443.e7.
147. Vanlandschoot, P., et al., *Nanobodies®: New ammunition to battle viruses*. Antiviral Res, 2011. **92**(3): p. 389-407.
148. Schulmeister, S., et al., *Protein exchange dynamics at chemoreceptor clusters in Escherichia coli*. Proc. Natl. Acad. Sci. U.S.A., 2008. **105**(17): p. 6403-6408.
149. Erbse, A.H. and J.J. Falke, *The core signaling proteins of bacterial chemotaxis assemble to form an ultrastable complex*. Biochemistry, 2009. **48**(29): p. 6975-6987.
150. Coppieters, K., et al., *Formatted anti-tumor necrosis factor α VHH proteins derived from camelids show superior potency and targeting to inflamed joints in a murine model of collagen-induced arthritis*. Arthritis Rheum., 2006. **54**(6): p. 1856-1866.

4. References

151. Briegel, A., et al., *New insights into bacterial chemoreceptor array structure and assembly from electron cryotomography*. *Biochemistry*, 2014. **53**(10): p. 1575-1585.
152. Kentner, D., et al., *Determinants of chemoreceptor cluster formation in Escherichia coli*. *Mol. Microbiol.*, 2006. **61**(2): p. 407-417.
153. Kaiser, P.D., et al., *Recent progress in generating intracellular functional antibody fragments to target and trace cellular components in living cells*. *BBA - Proteins and Proteomics*.
154. Man, S., et al., *Artificial trans-encoded small non-coding RNAs specifically silence the selected gene expression in bacteria*. *Nucleic Acids Res.*, 2011. **39**(8): p. e50.
155. Na, D., et al., *Metabolic engineering of Escherichia coli using synthetic small regulatory RNAs*. *Nat Biotech*, 2013. **31**(2): p. 170-174.
156. Melchionna, T. and A. Cattaneo, *A protein silencing switch by ligand-induced proteasome-targeting intrabodies*. *J. Mol. Biol.*, 2007. **374**(3): p. 641-654.
157. Garcillán-Barcia, M.P., et al., *Conjugative transfer can be inhibited by blocking relaxase activity within recipient cells with intrabodies*. *Mol. Microbiol.*, 2007. **63**(2): p. 404-416.
158. Jurado, P., L.A. Fernández, and V. De Lorenzo, *In vivo drafting of single-chain antibodies for regulatory duty on the σ_{54} -promoter Pu of the TOL plasmid*. *Mol. Microbiol.*, 2006. **60**(5): p. 1218-1227.
159. Avalos, J.L., G.R. Fink, and G. Stephanopoulos, *Compartmentalization of metabolic pathways in yeast mitochondria improves the production of branched-chain alcohols*. *Nat Biotech*, 2013. **31**(4): p. 335-341.
160. DeLoache, W.C. and J.E. Dueber, *Compartmentalizing metabolic pathways in organelles*. *Nat Biotech*, 2013. **31**(4): p. 320-321.
161. Bashor, C.J., et al., *Rewiring cells: synthetic biology as a tool to interrogate the organizational principles of living systems*. *Annu. Rev. Biophys.*, 2010. **39**: p. 515.
162. Chen, A.H. and P.A. Silver, *Designing biological compartmentalization*. *Trends Cell Biol.*, 2012. **22**(12): p. 662-670.
163. Choudhary, S., et al., *Engineered protein nano-compartments for targeted enzyme localization*. *PLoS ONE*, 2012. **7**(3): p. e33342.
164. Dueber, J.E., et al., *Synthetic protein scaffolds provide modular control over metabolic flux*. *Nat Biotech*, 2009. **27**(8): p. 753-759.

4. References

165. Schwille, P. and S. Diez, *Synthetic biology of minimal systems*. Crit. Rev. Biochem. Mol. Biol., 2009. **44**(4): p. 223-242.
166. Tan, S.T., et al., *Blueshift of optical band gap in ZnO thin films grown by metal-organic chemical-vapor deposition*. J. Appl. Phys., 2005. **98**(1): p. 013505-013505-5.
167. Deng, Y.-H., et al., *Investigation of formation of silica-coated magnetite nanoparticles via sol-gel approach*. Coll. Surf. A: Physicochemical and Engineering Aspects, 2005. **262**(1-3): p. 87-93.
168. Chouly, C., et al., *Development of superparamagnetic nanoparticles for MRI: effect of particle size, charge and surface nature on biodistribution*. J. Microencapsulation, 1996. **13**(3): p. 245-255.
169. Sun, C., J.S.H. Lee, and M. Zhang, *Magnetic nanoparticles in MR imaging and drug delivery*. Adv. Drug Delivery Rev., 2008. **60**(11): p. 1252-1265.
170. Kröger, N., R. Deutzmann, and M. Sumper, *Polycationic peptides from diatom biosilica that direct silica nanosphere formation*. Science, 1999. **286**(5442): p. 1129-1132.
171. Barrado, E., et al., *Characterization of iron oxides embedded in silica gel obtained by two different methods*. Chem. Rev., 2005. **351**(10-11): p. 906-914.
172. Kim, J., et al., *Multifunctional uniform nanoparticles composed of a magnetite nanocrystal core and a mesoporous silica shell for magnetic resonance and fluorescence imaging and for drug delivery*. Angew. Chem. Int. Ed., 2008. **47**(44): p. 8438-8441.
173. Frangioni, J.V., *In vivo near-infrared fluorescence imaging*. Curr. Opin. Chem. Biol., 2003. **7**(5): p. 626-634.
174. Neuberger, T., et al., *Superparamagnetic nanoparticles for biomedical applications: Possibilities and limitations of a new drug delivery system*. J. Magn. Magn. Mater., 2005. **293**(1): p. 483-496.
175. Berg, J.M., et al., *The relationship between pH and zeta potential of ~ 30 nm metal oxide nanoparticle suspensions relevant to in vitro toxicological evaluations*. Nanotoxicology, 2009. **3**(4): p. 276-283.
176. Adams, L.K., D.Y. Lyon, and P.J.J. Alvarez, *Comparative eco-toxicity of nanoscale TiO₂, SiO₂, and ZnO water suspensions*. Water Research, 2006. **40**(19): p. 3527-3532.
177. Jones, N., et al., *Antibacterial activity of ZnO nanoparticle suspensions on a broad spectrum of microorganisms*. FEMS Microbiol. Lett., 2008. **279**(1): p. 71-76.

4. References

178. Gordon, T., et al., *Synthesis and characterization of zinc/iron oxide composite nanoparticles and their antibacterial properties*. Coll. Surf. A: Physicochemical and Engineering Aspects, 2011. **374**(1–3): p. 1-8.
179. Cao, J., et al., *Fabrication, characterization and application in electromagnetic wave absorption of flower-like ZnO/Fe₃O₄ nanocomposites*. Mater. Sci. Eng., B, 2010. **175**(1): p. 56-59.
180. Chen, Y.-J., et al., *Synthesis, multi-nonlinear dielectric resonance, and excellent electromagnetic absorption characteristics of Fe₃O₄/ZnO core/shell nanorods*. J. Phys. Chem. C, 2010. **114**(20): p. 9239-9244.
181. Kataoka, T., et al., *Electronic structure and magnetism of the diluted magnetic semiconductor Fe-doped ZnO nanoparticles*. J. Appl. Phys., 2010. **107**(3).
182. Singh, S., K. Barick, and D. Bahadur, *Fe₃O₄ embedded ZnO nanocomposites for the removal of toxic metal ions, organic dyes and bacterial pathogens*. J. Mater. Chem. A, 2013. **1**(10): p. 3325-3333.
183. Rothenstein, D., et al., *Isolation of ZnO-binding 12-mer peptides and determination of their binding epitopes by NMR spectroscopy*. JACS, 2012. **134**(30): p. 12547-12556.
184. Hanley, C., et al., *Preferential killing of cancer cells and activated human T cells using ZnO nanoparticles*. Nanotechnology, 2008. **19**(29): p. 295103.
185. Hergt, R., et al., *Magnetic properties of bacterial magnetosomes as potential diagnostic and therapeutic tools*. J. Magn. Magn. Mater., 2005. **293**(1): p. 80-86.
186. Zhou, J., N.S. Xu, and Z.L. Wang, *Dissolving behavior and stability of ZnO wires in biofluids: A study on biodegradability and biocompatibility of ZnO nanostructures*. Adv. Mater., 2006. **18**(18): p. 2432-2435.
187. Conway, T. and G. K., *Microarray expression profiling: capturing a genome-wide portrait of the transcriptome*. Mol. Microbiol., 2003. **47**(4): p. 879-889.
188. Wang, C.-y., D.W. Bahnemann, and J.K. Dohrmann, *A novel preparation of iron-doped TiO₂ nanoparticles with enhanced photocatalytic activity*. Chem. Commun., 2000(16): p. 1539-1540.
189. Rai, M., A. Yadav, and A. Gade, *Silver nanoparticles as a new generation of antimicrobials*. Biotechnol. Adv., 2009. **27**(1): p. 76-83.
190. Daniel, M.-C. and D. Astruc, *Gold nanoparticles: assembly, supramolecular chemistry, quantum-size-related properties, and applications toward biology, catalysis, and nanotechnology*. Chem. Rev., 2004. **104**(1): p. 293-346.

4. References

191. Kröger, N., et al., *Bioenabled synthesis of rutile (TiO₂) at ambient temperature and neutral pH*. *Angew. Chem.*, 2006. **118**(43): p. 7397-7401.
192. Laurent, S., et al., *Magnetic iron oxide nanoparticles: synthesis, stabilization, vectorization, physicochemical characterizations, and biological applications*. *Chem. Rev.*, 2008. **108**(6): p. 2064-2110.

Danksagung

Zunächst möchte ich Prof. Schüler für seine Betreuung und Unterstützung während dieser Doktorarbeit danken. Es war eine herausfordernde Zeit, in der ich viele neue Aufgaben übernehmen durfte, vielen Dank.

Außerdem möchte ich PD Dr. Ralf Heermann für die Übernahme der Zweitkorrektur und das Interesse an meiner Arbeit danken.

Dirk Rothenstein und Prof. Joachim Bill von der Universität Stuttgart möchte ich für die gute und erfolgreiche Zusammenarbeit danken. Ebenso Prof. Nils Kröger für eine lehrreiche Kooperation mit der TU Dresden.

Natürlich gebührt besonderer Dank meinen Kollegen im "Magnetolab" für eine angenehme Zusammenarbeit, ein nettes Arbeitsklima und gute (auch nicht-wissenschaftliche) Unterhaltungen. Besonders möchte ich Karen Tavares danken, dass sie Annas Platz eingenommen hat und mir den Arbeitsalltag durch viel Humor erleichtert hat. Vielen Dank auch an Julia Hofmann, die beste Masterstudentin die man sich wünschen kann.

Anna Lohße gebührt besonderer Dank, da sie mir den Einstieg ins Magnetolab von Tag eins erleichtert hat und mit viel Pizza und Ablenkung dafür gesorgt hat, dass ich bei Verstand bleibe - you can get it if you really want.

Meiner kleinen "Ersatzfamilie" danke ich sehr für die eine oder andere Ablenkung von der Arbeit, die ständige Verpflegung und dafür dass sie mir die Berge näher gebracht haben (ich hasse wandern ehrlich gesagt gar nicht mehr).

Allen meinen Freunden, die nicht im Magnetolab sind, danke ich für die konstante Unterstützung und Ablenkung und vor allem dafür dass sie mich immer in "die richtige Welt" zurückholen. Besonders Anna Heins möchte ich dafür danken dass sie immer da ist und schnell angefliegen kommt, wenn der Wahnsinn überhandnimmt.

Am wichtigsten ist es mir meiner Familie zu danken. Der Rückhalt und die Unterstützung die ich von meinen Eltern erfahre, ist außergewöhnlich und nicht selbstverständlich und dafür bin ich sehr dankbar, da ich immer das Gefühl habe von ihnen aufgefangen zu werden. Das gleiche gilt für meine Geschwister Nadine, Verena und Christian. Danke fürs Zuhören, Dasein und Rumlernen.

Eidesstattliche Erklärung

Ich erkläre hiermit an Eides statt, dass die vorgelegte Dissertation von mir selbständig und ohne unerlaubte Hilfe angefertigt ist. Des Weiteren erkläre ich, dass ich nicht anderweitig ohne Erfolg versucht habe, eine Dissertation einzureichen oder mich der Doktorprüfung zu unterziehen. Die vorliegende Dissertation liegt weder ganz, noch in wesentlichen Teilen einer anderen Prüfungskommission vor.

Sarah Borg, München